MECHATRONIC DESIGN OF FLEXIBLE MANIPULATORS

by

Pixuan Zhou

A Dissertation Submitted to the Faculty of the

DEPARTMENT OF SYSTEMS AND INDUSTRIAL ENGINEERING

In Partial Fulfillment of the Requirements
For the Degree of

DOCTOR OF PHILOSOPHY

In the Graduate College

THE UNIVERSITY OF ARIZONA

1 9 9 9

INFORMATION TO USERS

This manuscript has been reproduced from the microfilm master. UMI films the text directly from the original or copy submitted. Thus, some thesis and dissertation copies are in typewriter face, while others may be from any type of computer printer.

The quality of this reproduction is dependent upon the quality of the copy submitted. Broken or indistinct print, colored or poor quality illustrations and photographs, print bleedthrough, substandard margins, and improper alignment can adversely affect reproduction.

In the unlikely event that the author did not send UMI a complete manuscript and there are missing pages, these will be noted. Also, if unauthorized copyright material had to be removed, a note will indicate the deletion.

Oversize materials (e.g., maps, drawings, charts) are reproduced by sectioning the original, beginning at the upper left-hand corner and continuing from left to right in equal sections with small overlaps. Each original is also photographed in one exposure and is included in reduced form at the back of the book.

Photographs included in the original manuscript have been reproduced xerographically in this copy. Higher quality 6" x 9" black and white photographic prints are available for any photographs or illustrations appearing in this copy for an additional charge. Contact UMI directly to order.

UMI

A Bell & Howell Information Company
300 North Zeeb Road, Ann Arbor MI 48106-1346 USA
313/761-4700 800/521-0600

MECHATRONIC DESIGN OF FLEXIBLE MANIPULATORS

by

Pixuan Zhou

A Dissertation Submitted to the Faculty of the

DEPARTMENT OF SYSTEMS AND INDUSTRIAL ENGINEERING

In Partial Fulfillment of the Requirements
For the Degree of

DOCTOR OF PHILOSOPHY

In the Graduate College

THE UNIVERSITY OF ARIZONA

1 9 9 9

THE UNIVERSITY OF ARIZONA ®
GRADUATE COLLEGE

As members of the Final Examination Committee, we certify that we have read the dissertation prepared by Pixuan Zhou

entitled MECHATRONIC DESIGN OF FLEXIBLE MANIPULATORS

and recommend that it be accepted as fulfilling the dissertation requirement for the Degree of Doctor of Philosophy

Dr. Fei-Yue Wang	4/29/1999 Date
Dr. Sidney Yakowitz	4/29/99 Date
Dr. Duane Dietrich	4/30/99 Date
Dr. Paul Lever	4/29/99 Date
	Date

Final approval and acceptance of this dissertation is contingent upon the candidate's submission of the final copy of the dissertation to the Graduate College.

I hereby certify that I have read this dissertation prepared under my direction and recommend that it be accepted as fulfilling the dissertation requirement.

Dissertation Director Dr. Fei-Yue Wang — 4/29/99 Date

STATEMENT BY AUTHOR

This dissertation has been submitted in partial fulfillment of requirements for an advanced degree at The University of Arizona and is deposited in the University Library to be made available to borrowers under rules of the Library.

Brief quotations from this dissertation are allowable without special permission, provided that accurate acknowledgment of source is made. Requests for permission for extended quotation from or reproduction of this manuscript in whole or in part may be granted by the head of the major department or the Dean of the Graduate College when in his or her judgment the proposed use of the material is in the interests of scholarship. In all other instances, however, permission must be obtained from the author.

SIGNED: 

ACKNOWLEDGMENTS

I would like to thank my advisor, Dr. Fei-Yue Wang, who introduced me to this exciting field, for his constant support and invaluable guidance through out my Ph.D. program and this research.

I am also very grateful to Dr. Sidney Yakowitz, Dr. Duane Dietrich and Dr. Hill Frederick for their time in reviewing this dissertation, and their willingness to serve on this committee. My appreciation, especially, goes to Dr. Paul Lever, my co-advisor for his support.

My colleagues in the Laboratory of Robotics and Automation and other groups gave me their genuine help and assistance. They are: Dr. Jeff Russell, Dr. Hung-man Kim, Dr. Xiabo Shi, Mr. David Chen, Dr. Bing Pu, Mr. Xiaoyan Fan, Lin, Mr. William 'Remo', Mr. Ray Chen, Mr. Simom Shan, Ms. Dongfeng Ge, Mr. Ouyang Shaofang, Mr. Hua Tian, Dr. Ling Shen, Mr. Frank K. Zhou, Dr. Jie Ming Li, Dr. T. K. Wong, Dr. Y. J. Wong, Dr. X. Q. Chen, Dr. W. Y. Li, Mr. W. Song. They all deserve to be mentioned here.

DEDICATION

To my parents and parents -in-law

To my brothers and sisters and sister-in-law

To my wife Lin, and son Zhenglong

For their understanding, faith and love

TABLE OF CONTENTS

LIST OF FIGURES

LIST OF TABLES

ABSTRACT

The construction of lightweight manipulators with a larger speed range is one of the major goals in the design of well-behaving industrial robotic arms. Their use will lead to higher productivity and less energy consumption than is common with heavier, rigid arms. However, due to the flexibility involved with link deformation and the complexity of distributed parameter systems, modeling and control of flexible manipulators still remain a major challenge to robotic research. A compromise between modeling costs and control efficiency for real-time implementation is inevitable. The interdependency of subsystems results in a local optimal performance in the traditional design scheme. An important research topic in flexible manipulator design is the pursuit of better system performance while avoiding model-intensive or control-intensive work. This problem can be solved using the proposed mechatronic design approach. It treats the mechanical, electrical and control components of a flexible manipulator concurrently. The result is an improved design with an explicit link shape and controller parameters which result in the control problem and modeling accuracy no longer being critical for obtaining desired performance. Dynamics of flexible manipulators with rotatory inertia are derived, and state-space equations with the integration of DC motor dynamics are developed as a theoretical base for mechatronic designs. Two case studies based on LQR formula and H_∞ control are considered. The beam shape and controller parameters are obtained using an adaptive iterative algorithm with the accommodation of various geometrical constraints. Also, different output feedback strategies are investigated to evaluate the impacts of various controller structures. Finally, a sensitivity analysis in terms of parameter variations and model uncertainties is conducted to reveal the robustness of this mechatronic design.

CHAPTER 1

INTRODUCTION

1.1 Motivation

A manipulator becomes flexible when its link deformation cannot be ignored in the analysis of its performance. A manipulator which has large dimensions, is lightweight, fast, or handles a heavy load exhibits flexibility. Flexible manipulators utilize less energy due to their lightweight, higher productivity achieved through fast motion. They are safer to operate due to good damping behavior and the less pronounced interconnections between the different segments for multiple-link manipulators. These manipulators are found in space explorations (NASA Remote Manipulator System) because of the constraints on arm length, weight and 'gravity-loss'; in mining applications (Robotics Excavators) because of their heavy payload; in construction applications (Robotics Crane Systems) because of the length and heavy tip load; and where dexterous manipulators are required such as in medical operations or chip placement performed pick-and-place manipulators in electronic assembly manufacture. Even through, the NASA Remote Manipulator System [10] has very low natural frequencies ($0.04HZ$ to $0.35HZ$) and consequently has to move slowly (0.5 deg/sec) in order to avoid vibrations because of its beam mass (450 kilograms) and

its heavy payload (27,200 kilograms). Similar examples of problems are also reported in literature [63].

In contrast, a micro-arm [6] needs a counterbalance to suppress vibration due to fast motion. The link flexibility of manipulators must be taken into account in modeling and control. However, due to the complexity of deformation and the characteristics of distributed parameter systems, and also due to the real-time requirement, modeling and control of flexible manipulators still remain major challenges in robotic research in general.

Modeling efficiency of flexible manipulators: Flexible manipulators are distributed systems described by partial-differential equations, therefore, their dynamic behavior is of infinite degrees of freedom [93]. From the perspective of control theory, it is impossible to design an infinite dimensional controller. The controlled plant must have a finite dimension, thereby requiring less significant terms in the model to be omitted. This causes model uncertainties since those terms generally are time-variable and system dependent. The boundary conditions set by tip-load, hub inertia, friction, rotatory inertia, and shear force also impact beam dynamics, which make the model implementation more complicated for the purpose of real-time control.

Precise end-point motion control of flexible manipulators: In most cases, the control point is the beam tip, but for convenience in operation, the actuator is generally installed on the hub side, which creates a noncollocated control problem.

The payload conditions can have a substantial effect on the beam dynamics. For example, a large tip-load will reduce the natural frequencies significantly. This strong dependency on the beam conditions governs the efficiency of a controller.

Interrelation and interdependency of subsystems of manipulator systems: The complexity of manipulator systems is also due to the interrelation and interdependency of their subsystems as in Fig. (1.1).

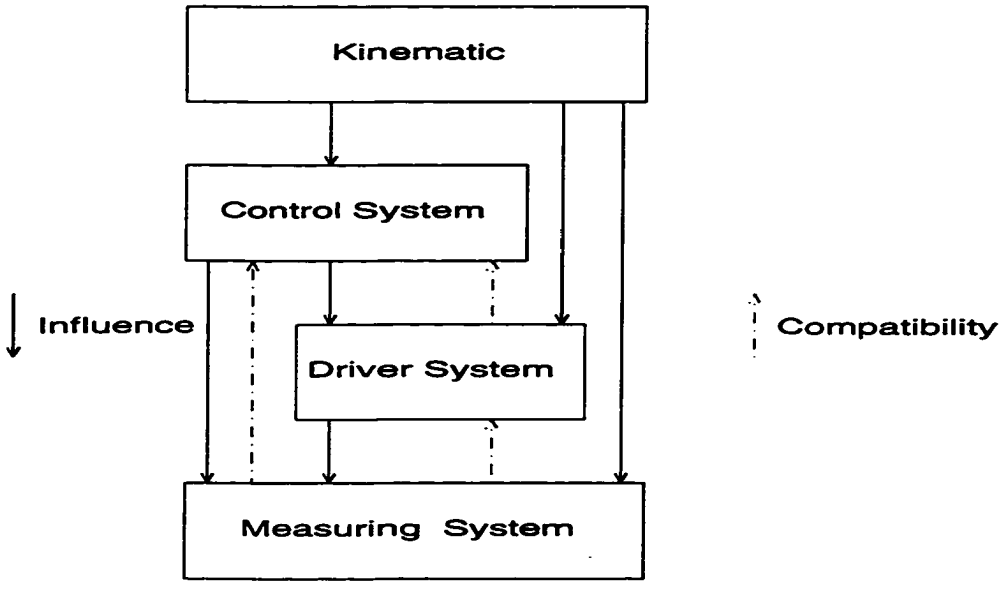

Figure 1.1: Interrelation and Interdependency of Subsystems of Manipulator Systems

A manipulator system consists of different subsystems, which are:

- a kinematic system, mainly related to the beam structure,

- a control system,

- a driver system, or actuator,

- a measuring system, or sensors.

Some subsystems exert influence over others whereas some subsystems are only influenced by others, meaning that interdependency is hierarchical. The kinematics of a manipulator would obviously influence the driver system, the control system as well as the measuring system. In a similar way, the control system influences the design of the driver system and the measuring system whereas the driver system only influences the measuring system.

If a flexible manipulator system can be designed taking the interrelationships between subsystems into account while avoiding control-intensive or model-intensive work, the control and modeling problems will no longer be critical, thus improving productivity and reducing energy consumption. In a word, there is still a lot of room for improvement on flexible manipulator system design.

1.2 Problem Statement

If we consider these issues and their interrelations from the perspective of system design and implementation, the following problem areas can be identified:

- **The tradeoff between the real-time control and modeling efficiency.** For real-time control applications, complicated dynamic models cannot be implemented. However, the model must be accurate enough to take controller efficiency into account, resulting in a more complicated model than necessary for general cases. As illustrated in Fig. (1.2) [1], a computed torque model

is used to obtain curve I. The tracking is perfect when there is no model uncertainty, but the performance degrades as uncertainty increases. Finally, the system becomes unstable. When the robust controller based on a simplified model is used, the performance becomes worse as model uncertainty increases as shown by curve II. The efficiency of modeling and the precision of control of flexible manipulators are contradictory and a compromise between them for real-time implementation is inevitable.

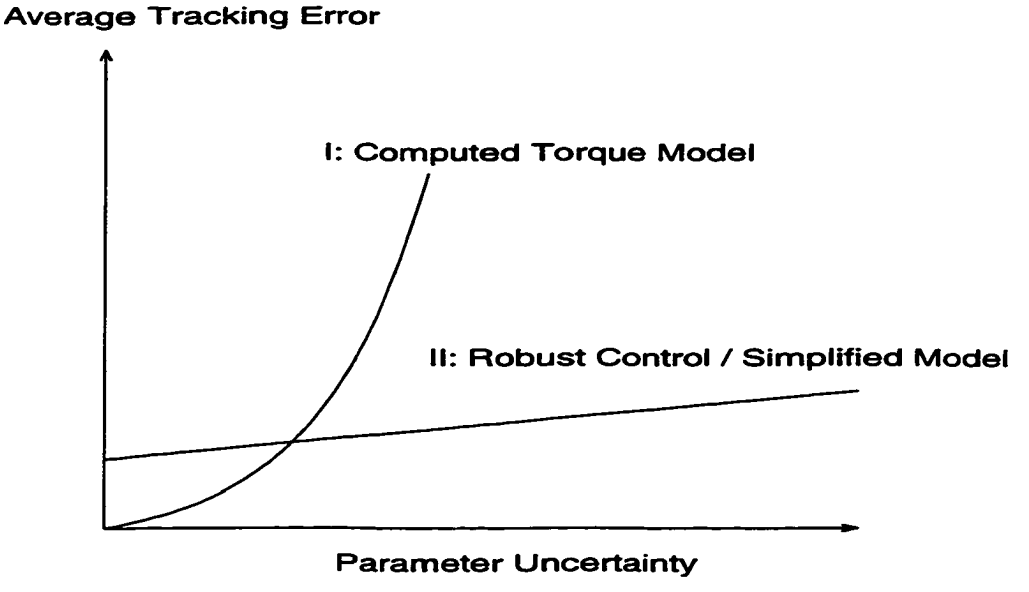

Figure 1.2: The Effect of Model Uncertainty on Control Performance

- **The coupling effects between the controller design and the modeling resulting from the interdependency of subsystems.** Over the last decade, significant efforts have been put into the modeling or the control of flexible manipulators. Most researchers have addressed the coupling of the two issues

as irrelevant. Thus the coupling effects between these components have not been considered in the system design process.

- **Drawbacks of the traditional design approach.** In traditional design, a manipulator linkage is designed first, followed by a driver system, a measuring system, and then a control system as in Fig. (1.3). As a result, this traditional design scheme leads only to a locally optimal solution. The potential performance of a flexible manipulator is rarely fully realized.

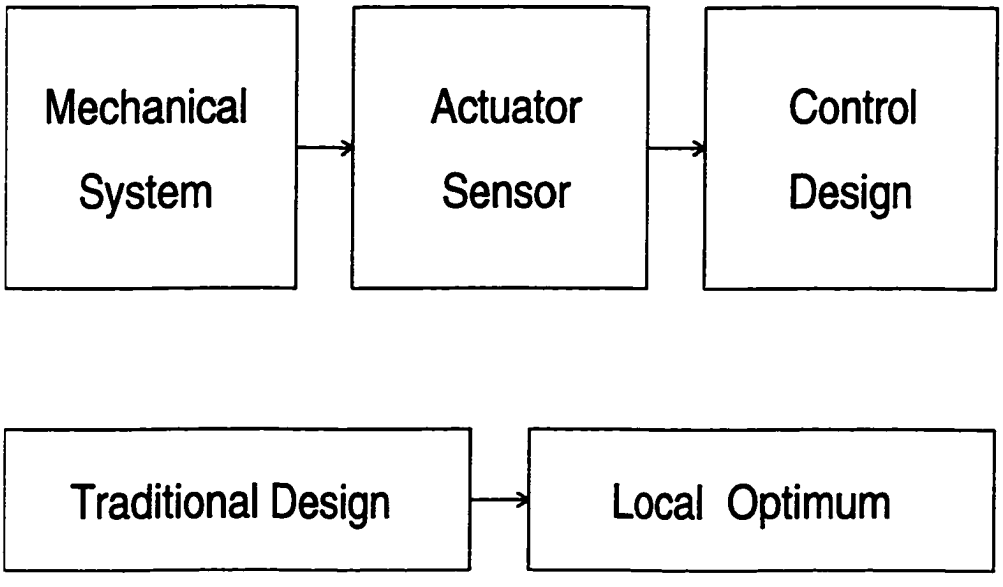

Figure 1.3: Traditional Design Procedure

What considerations are required to design flexible manipulator systems that achieve the full potential performance? First, the model-intensive and/or control-intensive approaches must be avoided to meet the real-time requirement. Second, the proposed method must take advantages of the coupling effects. And finally, a

better result must be obtained for the manipulator systems. A "Mechatronic Design Methodology" (MDM) to be described herein fits these requirements exactly.

1.3 Contributions: Mechatronic Design Methodology

For applications in manipulator systems, the MDM is *a system optimization through the integration of actuator, controller, system dynamics and sensor specifications.* It has the following features, compared with traditional design approaches:

Different methodology: As described above, the traditional design of the system results only in a local optimal performance as shown in Fig. (1.3).

By contrast, *Mechatronic design treats the mechanical, electrical, and control components of a flexible manipulator concurrently, instead of sequentially from the very beginning of the design process.* This in turn results in better objective functions in the system. This new procedure is shown in Fig. (1.4). Objective functions can be comprised of the best beam motion, the least beam mass, the least beam power consumption, or even combinations of these parameters required by some special perspectives such as quadratic functions.

Different direction: In order to make real-time control feasible, most researchers simplify the beam model complexity by neglecting some less significant terms, such as shear force, rotary inertia, viscous and Coulomb friction or by linearizing at some particular operating point. High performance control system requirements usually

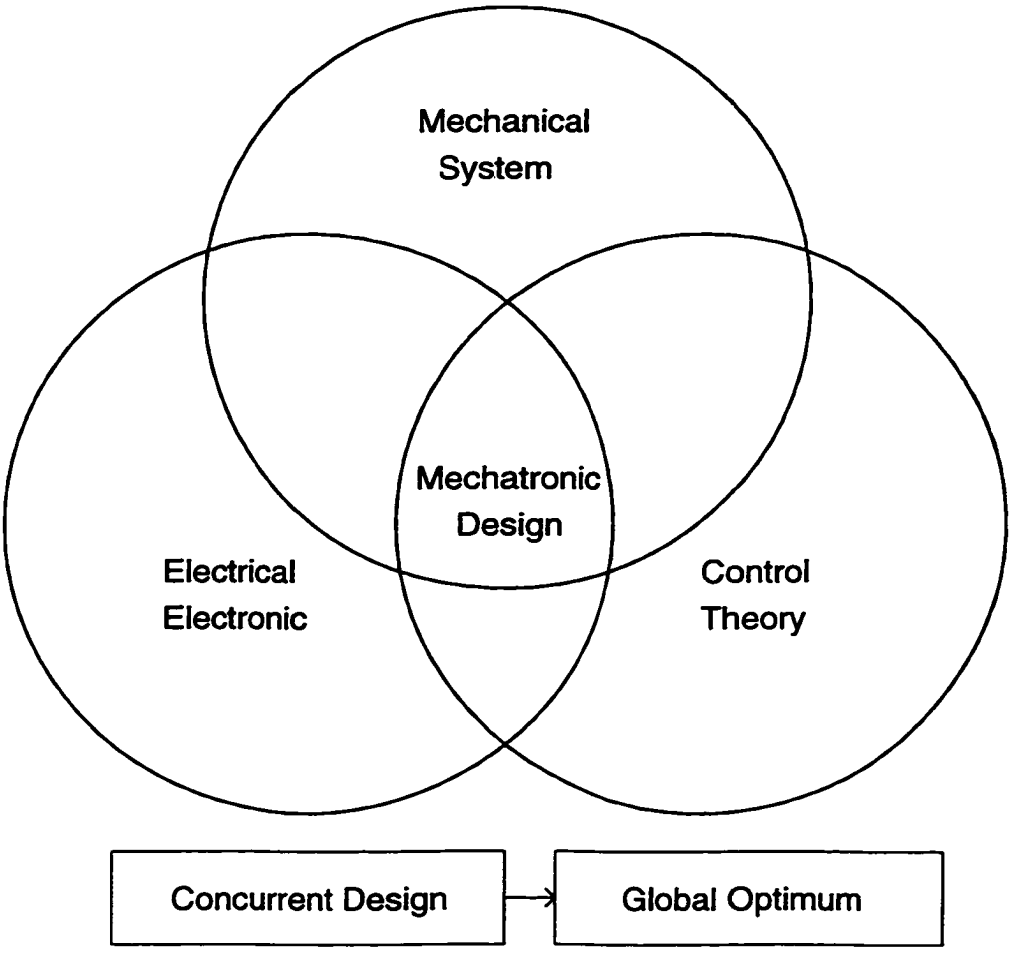

Figure 1.4: Mechatronic Design Procedure

necessitate significant deviation from these normal values, thereby resulting in degraded stability and performance.

Mechatronic design focuses on system overall design instead of modeling or control. That is, the objective is to design a better manipulator system so its control problem and dynamics accuracy will not be very critical for its performance. In other words, the result from this mechatronic design is better than what is obtained from model-intensive work or control-intensive work.

To achieve such results, an analytic model is obtained by variational methods to obtain a concrete dynamic, while a state-space model is developed to describe the linearized model for the actual system. This yields a simplified state-space equation in which the geometric parameters of the beam are the variables of optimization.

As a result of this methodology, extensive analyses of the concurrent design approaches based on LQR and H_∞ formulae and related dynamics are investigated after indicating model uncertainties, which result in an improved solution for both the beam construction and the controller. The optimization results pertaining to the optimum shape and system performance index are discussed and compared to the corresponding uniform beam with various assumed initial conditions. In a case study, the performance index for the uniform beam was reduced from 4342.569 in a traditional system to 4176.437 in an improved system. The results indicated that the mechatronic design system can improve productivity. Furthermore a dual problem can be solved because the beam mass can also be reduced to get the same performance for the optimal shape beam compared to the uniform beam, thus reducing the power consumption as well.

1.4 Dissertation Organization

Chapter 2 of this dissertation examines the previous work of optimum design and control in flexible manipulators. In Chapter 3, a pick-and-place manipulator-like system is considered. The model derivation proceeds step-by-step from calculation of

energies through a dynamic equation and constraints. Several representative formulae are given. Chapter 4 continues with an extensive analysis of the resonant frequencies and modal shapes developed for the governing equations. Chapter 5 discusses the segmentized model of flexible link, and a state space equation is formulated in which the beam geometric distribution is the variable. Several feasible output specifications are presented. Chapter 6 investigates the mechatronic design based on the LQR formula. Regarding the concurrent optimum performance problem, a heuristic iterative programming algorithm and a global adaptive random searching algorithm are integrated. In devising a practicable solution to this problem, structural constraints for the link geometrics are introduced into the problem solving process. Numerical results pertaining to various test cases are presented. Chapter 7 is parallel to Chapter 6, where the H_∞ controller is addressed, based on the state-space equation for the generalized plant derived from equations in Chapter 5. An H_∞ controller is described that internally stabilizes the close-loop system, but minimizes all impacts from system uncertainties and disturbances. Chapter 7 concludes with responses for step-type disturbance and step input which were carried out to show the system robustness. Finally, Chapter 8 gives a system robustness analysis by means of a numerical computation approach from the perspective of system parameter variations. A discussion of research and conclusion are contained in Chapter 9 to end this dissertation, as well as suggestions for future work in the field of mechatronic design.

CHAPTER 2

LITERATURE REVIEW

2.1 Research on Structural Optimal Design

Since Timoshenko beam theory [93] [20] [46] was formulated, a great many specialized treatments of beam vibrations have been presented. The first approach was to design a beam which had a high first mode natural frequency. Niordson [62] demonstrated an iteration scheme to improve the fundamental frequency. While Brach [12] formulated the moment-area relationship $I = r_p A^p$ with $p = 1, 2, 3$ and Sheu [84] considered a non-transverse frequency method to do that. In 1973, Karihaloo and Niordson [41] demonstrated by analysis as did by Niordson in [62] that an optimal beam could increase the natural frequency up to 678%.

Similar analysis and results of the determination of natural frequencies of a beam with varying thickness can be found in Chehil and Jategaonkar [18], Jategaonkar and Chehil [38] and references therein. A review paper by Laura *et al* [45] has commented on the dynamic stiffening of beams. Roy and Ganesan [78] conducted a series of studies on the amplitude of deflection and the dynamic bending stress behavior of cantilevers with varying thickness based on the responses corresponding to the first three natural frequencies. It was observed in all above studies that proper selection of thickness variation could reduce vibration amplitude considerably.

A number of papers investigated a beam constructed of multiple materials for the purpose of increasing dynamic rigidity, and the results were the optimal shape and material length ratio. These early studies were conducted by Rivin [75] (1983), Rivin and Kang [76](1983) and Takeyama [90] (1984). Further work was undertaken by Khorrami and Ümit Özgöner [43], who successfully used a variational scheme to solve the optimum tapering of a cantilever. In 1983, Elwany and Barr [22] developed a method utilizing rectangular cross-section beams to maximize fundamental bending frequency. This was taken further by Liao [50], who developed a generalized method for circular cross-section beams under flexural vibration which employed beams composed of two materials at different ends. All shapes and length ratios are outlined by a Two-Point Shooting algorithm devised by Robert and Shipman [77]. From another perspective, Ma and We [55] and Makowski [61] addressed place-grids methods for lightweight structures.

All show that proper selection of beam shape or/and beam material can increase beam natural frequency, thus the beam moves faster but experiences good damping behavior.

2.2 Control of Flexible Manipulators

Numerous papers have addressed the control of flexible manipulators. Initial studies concentrated on the state space model. Cannon and Schmitz [15] first investigated the Linear Quadratic Gaussian (LQG) controller assuming that the states were

available. However, the states were not available, and they had to be reconstructed by optimal estimators. In 1993, Lin and Lewis [52] studied the Kalman filter for the estimation of the rigid and flexible modes for control purposes. Sakawa [81] applied a Linear Quadratic (LQ) control to track hub reference by damping the flexible modes. The states were obtained by means of an observer. Geniele *et al* [29] used an inner loop to stablize the flexible system and an outer loop to track the desired trajectory. Luca and Sicilino [53] defined two controllers to track the joint angle and one point along the arm respectively using input-output inversion. The same approach was used by Madhavan and Singh in their study [56]. They also used a sliding mode control to design a controller that could tolerate a wide range of uncertainties, thus enhancing the robustness in [57].

Other studies used the transfer function approach. Wang *et al* [111] used tip deflection as output and devised an output feedback based on passivity of the model's transfer function. Siciliano and Book decomposed the flexible manipulator dynamics into two subsystems: fast and slow systems, by applying singular perturbation theory. They showed that the fast system was linear, but that the slow one was nonlinear. Furthermore linear state controller and nonlinear controller were designed for the two systems respectively to track hub angle. Similar research was found in [3] by Aoustin and co-authors. Corrected slow and fast subsystems were used in [59] (1997) by Moallem, Khorasani and Patel.

Recently Gutiérrez, *et al* [33] extended this approach by conducting a neural network (NN) tracking controller. The outer NN proportional derivator (PD) tracking loop was used to stabilize the fast mode, while the inner feedback loop was used to linearize the slow mode dynamics. The results were compared between PD and proportional integral derivative (PID). Lenz and Özbay [47] derived the robust control for a flexible beam subjected to perturbations and delays by using H_∞ theory. Tchernychev *et al* [91] (1997) developed a constrained H^∞ controller in which time-domain constraints are treated directly without translation to frequency-domain. Zhu *et al* [118] (1997) investigated a backstepping approach for tip tracking by lumping the beam to spring-mass system to develop a robust controller in the presence of system disturbances/uncertainties. Jnifene and Fahim (1997) [39] dealt with non-minimum phase characteristics by introducing active damping into the system, and proposed a computed torque/delayed deflection approach. The torque was calculated from joint angle and a delayed deflection, while the delay time depended on the point where the deflection was measured.

Ghanekar *et al* [30] examined the large robotic manipulator scaling laws for linear controllers by nondimensional groups, thus allowing a small-scale prototype to be used to perform the design work. Liang *et al* [49] (1998) discussed the problem of a free floating space manipulator, and mapped it to a conventional, fixed-base manipulator. This allowed well-understood methods to be used to build the manipulator system. Simulation work was also presented, as Tang and Lu [94] used a video

system to estimate modal shapes and vibration states. Strain gauges were used by Fukuda in [28], and by Hastings in [36] to measure the deflection. Photosensors were also used for detecting the displacement in [15] [96] [89]. Chalhoub, *et al* used an accelerometer to measure the beam vibration in [17]. The state of vibration could be obtained indirectly by combining some strain gauges and/ or displacement in [88] by Sundararajan and co-authors.

These studies did control-intensive work to improve beam performance. But they ignored the impact applied from the beam mechanic shape. The couplings between the controller and construction was not considered in the design. The resulting system was only local optimal.

2.3 Shape Optimization of Flexible Manipulators

Recently researches on flexible manipulators have increased dramatically since flexible beams move faster and consume less energy. One of the first papers on optimal shape for flexible manipulators is [41] by Karihaloo and Niordson. Extensive studies in optimal shape design have been conducted recently by Wang's group. Wang (1991) [97] simplified substantially the scheme presented in [41]. In 1991, this group [98] examined the external fundamental frequencies and developed an iterative scheme, producing the first one-link optimum manipulator shape. It was shown that by the proper selection of hub, the optimal link could improve the first natural frequency by 600%. Wang and Guan (1992) [99] showed that the effects from rotatory

inertia and shear force are very small and neglectable on the effect of tip-load on the fundamental frequencies using modal shape approach. A minimum weight design of flexible manipulators was developed by Wang and Russell (1992, 1993) [100] [102]. In 1995, they constructed a scheme under constraints of total beam weight [103]. In that year, they also investigated a new approach [106], the segmentized scheme of optimal design, which treats the flexible beam as a collection of small lengths of rigid beam constrained by each other's interfacial conditions. The new technique converts the optimal shape design problem into a matrix determinant problem. A great number of details pertaining to this can be found in [80]. It shows an increase of 625% in frequency and a reduction of 48.59% in mass due to optimal shape design. In 1996, a new computing method for optimum mass and rigidity distribution was formulated by Wang, Zhou and Lever (1996) [105] for a flexible manipulator with a tip-load. The robustness with respect to design specification and appropriate constraints was considered. Practical issues were addressed also.

These studies focused on open-loop design, that is, they only concerned the beam mechanic construction. From these studies, proper design the flexible beam shape can make it suffering less vibration. But in reality, all manipulators must be in closed-loop to get high performance, how to design the flexible beam shape from the control perspective still remains a challenge.

2.4 Recent Trends

Recently, well-behaved flexible manipulators for the purpose of control design from the perspective of plant characteristic have been pursued through system optimization. This method was discussed in the field of flexible spacecrafts as described early in [35]. The same philosophy has been applied to flexible manipulators [2] [66]. Lim [51] (1987) developed robustness optimization of structural and controller parameters, in which three different cost functions were optimized. Miller and Shim [58] (1987) minimized the structural mass and system energy using a gradient search method to suppress structural vibration. Moallem, Patel and Khorasani [60] (1998) investigated optimization based on the sensitivity of system eigenvalues. In these papers, beam shear force and inertia moment were neglected with simplified boundary conditions. Wang and Zhou (1995) [110], Zhou et al (1996) [116] formulated various optimizations for link shape problems with explicit objective functions based on closed transfer functions. Zhou, Wang and Lever (1998) [117] conducted an optimal construction and control integration algorithm based on segmentized solution. This study shows a new research direction for system optimization to design overall system, not only designing a controller or beam shape.

CHAPTER 3

DYNAMICS OF FLEXIBLE MANIPULATORS

In this chapter, the model for flexible manipulators is defined and employed in a derivation of variational methods based on the calculation of energies. The dynamic equations with all boundary conditions are derived and utilized to specify the state-space equations. Several representations of dynamic equations are presented.

3.1 Model of Flexible Manipulators

The flexible manipulator system is illustrated as Fig. (3.1). The hub has a rotational inertia I_h. The link length is L. The tip load M_p, has a moment of inertia I_p. A torque τ is actuated to the link at the hub side. In order to model the motion of the manipulator, three coordinates are applied here as:

1. (X_0, Y_0), stationary coordinates;

2. (X_1, Y_1), link coordinates, X_1 is the neutral axis of the link;

3. (X_2, Y_2), tip load coordinates.

The angular displacement of the link axis x_1 is θ, which is measured from the coordinates frame (x_0, y_0) as shown in the figure. The transverse displacement of the link from its equilibrium position, or the distance from the point at the neutral axis of the

beam to x_1 is w, which of course is the function of x_1 and time t. The center of the tip mass M_p in (x_2, y_2) frame is (a_c, b_c). The result of applying the three coordinates is,

$$M_p = \iint_s \rho ds, \qquad I_p = \iint_s \rho({x_2}^2 + {y_2}^2) ds,$$
$$a_c = \frac{1}{\mu} \iint_s \rho x_2 ds, \qquad b_c = \frac{1}{\mu} \iint_s \rho y_2 ds \tag{3.1}$$

where ρ and s are the mass density and domain occupied by the tip load respectively.

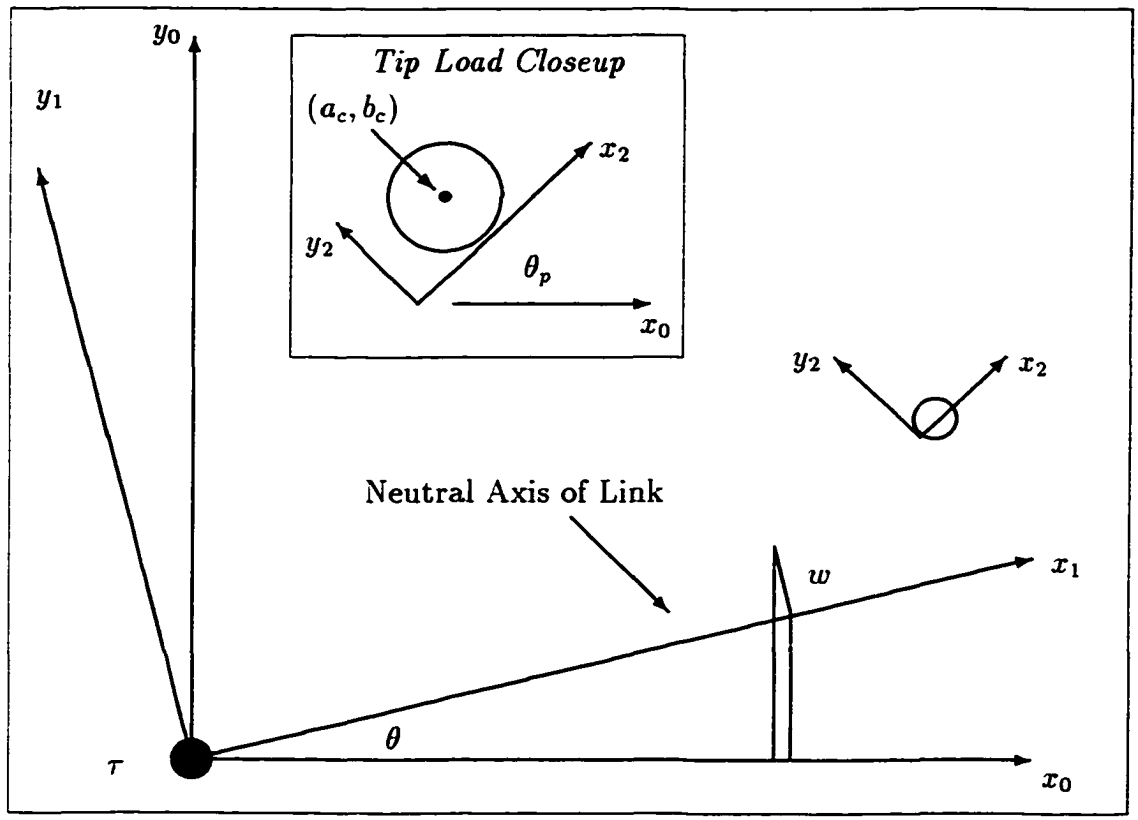

Figure 3.1: Flexible Manipulator Mode.

The Euler-Bernoulli beam theory [93] is employed to model the system. All normal assumptions are implied. These include the entire transverse section of the

beam remaining planar, the joint being assumed to be a symmetric object in xy plane, on the gravitational field being in the z direction. The rotatory inertia is considered in order to improve the modeling accuracy. This requires that the difference of the velocity of every point on a cross section of the beam is taken into account.

From all these assumptions, we have,

$$V(x_1, t) = x_1\theta + w(x_1, t), \tag{3.2}$$

where $V(x_1, t)$ is the total displacement along the beam spatial coordinate. Also we have,

$$x_0 = x_1 \cos\theta - w\sin\theta, \qquad y_0 = x_1 \sin\theta + w\cos\theta, \tag{3.3}$$

and the tip load coordinates are,

$$x_0 = L\cos\theta - w(L,t)\sin\theta + x_2\cos\theta_L - y_2\sin\theta_L, \tag{3.4}$$

$$y_0 = L\sin\theta + w(L,t)\cos\theta + x_2\sin\theta_L + y_2\cos\theta_L, \tag{3.5}$$

where $\theta_L = \theta + \alpha(L)$, and $\alpha(L) = \frac{dw(L,t)}{dx_1}$ for a small deformation. The velocity of the beam with respect to the base frame is,

$$v^2(x_1, t) = (x_1\dot{\theta} + \dot{w})^2 + (w\dot{\theta})^2, \tag{3.6}$$

where $\dot{()} = \partial()/\partial t$.

3.2 Calculation of Energies

Energy balance of a flexible manipulator requires,

$$T + W - P = 0, \tag{3.7}$$

where T is the system total kinetic energy, W is the work done by external force, and P is the system total potential energy.

The kinetic energy of the system is represented as follows,

$$T = T_h + T_b + T_p. \tag{3.8}$$

where T_h is the hub kinetic energy, T_b is the link kinetic energy, T_p is the tip load kinetic energy. T_h is specified as,

$$T_h = \frac{1}{2} I_h \dot{\theta}^2. \tag{3.9}$$

If we consider the beam kinetics due to two contributions, (i) link velocity and (ii) the effect of the rotatory inertia, then,

$$T_b = \frac{1}{2} \int_0^L [v^2(x_1, t) + S(\dot{w}'(x_1, t) + \dot{\theta})^2] \rho dx \tag{3.10}$$

where $v(x_1, t)$ is the velocity of a point at the neutral axis, $S = \frac{I}{A}$ is the parameter characterizing the effect of rotatory inertia, A is the area of beam cross section, and ρ is the mass density per unit length of the link, $()' = \partial()/\partial x$.

After substituting Eq. (3.6) for Eq. (3.10) and dropping off high order term $(w\dot{\theta})^2$, we have,

$$T_b = \frac{1}{2} \int_0^L [(x_1 \dot{\theta} + \dot{w})^2 + S(\dot{w}' + \dot{\theta})^2] \rho dx_1. \tag{3.11}$$

The kinetics of the tip load is,

$$T_p = \frac{1}{2} \iint_s \rho_L {v_L}^2 ds, \tag{3.12}$$

where ρ_L is the tip load mass density per unit area and v_θ is the velocity of a point on the cross section of tip load to the base frame.

Using Eq. (3.5) and ${v_L}^2 = \dot{x}_0^2 + \dot{y}_0^2|_L$, after omitting higher order terms,

$$T_p = \frac{1}{2}M_p(\dot{\theta}L + \dot{w}|_L)^2 + \frac{1}{2}J_p(\dot{\theta} + \dot{w}'|_L)^2 + M_p a_c(\dot{\theta} + \dot{w}'|_L)(L\dot{\theta} + \dot{w}|_L). \quad (3.13)$$

The strain energy of the link,

$$P = \frac{1}{2}\int_0^L EIw''(x_1,t)^2 dx_1, \quad (3.14)$$

where E is the Young's Modulus of Elasticity and I is the transverse moment of inertia and EI is known as bending rigidity of the link.

Work done by external force applied to the system by an actuator is,

$$W = \tau\theta. \quad (3.15)$$

3.3 Derivations Based on Variational Methods

In the derivative of dynamics of the flexible link, the Hamiltonian Principle is applied. First, the variational method is applied to Eq. (3.9), Eq. (3.11), Eq. (3.13) - Eq. (3.15). After dropping off high order terms, they become,

$$\delta T_h = I_h\dot{\theta}\delta\dot{\theta}, \quad (3.16)$$

$$\delta T_b = \int_0^L a_1\delta\dot{\theta}dx + \int_0^L a_2\delta\dot{w}dx + a_3\delta\dot{w}|_L - a_3\delta\dot{w}|_0, \quad (3.17)$$

$$\delta T_p = b_1\delta\dot{\theta} + b_2\delta\dot{w}|_L + b_3\delta\dot{w}'|_L, \quad (3.18)$$

$$\delta P = C_1\delta w'|_0^L - C_1'\delta w|_0^L + \int_0^L C''_1\delta w dx, \quad (3.19)$$

$$\delta W = \tau\delta\theta. \quad (3.20)$$

where,

$a_1 = [x_1(x_1\dot{\theta} + \dot{w}) + S(\dot{w}' + \dot{\theta})]\rho,$

$a_2 = [(x_1\dot{\theta} + \dot{w}) - S(\dot{w}' + \dot{\theta})']\rho,$

$a_3 = S(\dot{w}' + \dot{\theta})\rho,$

$b_1 = M_pL(\dot{\theta}L + \dot{w}) + J_p(\dot{\theta} + \dot{w}') + M_pLa_c(\dot{\theta} + \dot{w}') + M_pa_c(L\dot{\theta} + \dot{w})|_L,$

$b_2 = M_pa_c(\dot{\theta} + \dot{w}') + M_p(L\dot{\theta} + \dot{w})|_L,$

$b_3 = J_p(\dot{\theta} + \dot{w}') + M_pa_c(\dot{\theta}L + \dot{w})|_L,$

$C_1 = EIw''(x,t),$

In order to employ the Hamiltonian Extended Principle [40], the variational calculus for above Eq. (3.16) is calculated as,

$$\int_{t_0}^{t_f} \delta T_h dt = I_h\dot{\theta}\delta\theta|_{t_0}^{t_f} - \int_{t_0}^{t_f} I_h\bar{\theta}\delta\theta dt = -\int_{t_0}^{t_f} I_h\bar{\theta}\delta\theta dt. \tag{3.21}$$

In the same way, Eq. (3.17) - Eq. (3.20) are,

$$\int_{t_0}^{t_f} \delta T_b dt = -\int_{t_0}^{t_f} a_1\delta\theta dt - \int_{t_0}^{t_f}\int_0^L a_2\delta w dx dt + - \int_{t_0}^{t_f} a_3\delta w(L,t)dt + \int_{t_0}^{t_f} a_3\delta w(0,t)dt, \tag{3.22}$$

$$\int_{t_0}^{t_f} \delta T_p dt = -\int_{t_0}^{t_f} b_1\delta\theta dt - \int_{t_0}^{t_f} b_2\delta w(L,t)dt - \int_{t_0}^{t_f} b_3\delta w'(L,t)dt, \tag{3.23}$$

$$\int_{t_0}^{t_f} \delta P dt = \int_{t_0}^{t_f} (C_1|_0^L\delta w' - C_1'|_0^L\delta w + \int_{t_0}^{t_f}\int_0^L C_1''\delta w dx)dt(L), \tag{3.24}$$

$$\int_{t_0}^{t_f} \delta W dt = \int_{t_0}^{t_f} \tau\delta\theta dt. \tag{3.25}$$

The Hamiltonian Extended Principle is,

$$\delta\int_{t_0}^{t_f}(T + W - P)dt = 0, \tag{3.26}$$

or

$$\int_{t_0}^{t_f}(\delta T + \delta W - \delta P)dt = 0. \tag{3.27}$$

Substituting Eq. (3.21) - Eq. (3.25) into Eq. (3.26), we have,

$$\begin{aligned}\int_{t_0}^{t_f}\{&[-I_h\ddot{\theta} - \dot{a}_1 - \dot{b}_1 + \tau]\delta\theta + [\dot{a}_3 - C_1'(0)]\delta w(0,t)\\ &+[\dot{a}_3 - C_1'(L,t) + \dot{b}_2]\delta w(L,t) - [\dot{b}_3 + C_1(L,t)]\delta w'(L,t)\\ &+\int_{t_0}^{t_f} C_1(0)\delta w'(0)dt + [\int_0^L(-\dot{a}_2 - C_1'')dx]\delta w(x,t)\}dt = 0.\end{aligned} \tag{3.28}$$

Since $\delta w(0,t) = 0$, and $\delta\theta, \delta w(L,t), \delta w(x,t)$ are arbitrary, each coefficient in these brackets must be equal to zero. They individually result in,

$$\int_0^L(-\dot{a}_2 - C_1'')dx = 0, \tag{3.29}$$

$$-I_h\ddot{\theta} - \dot{a}_1(0,t) - \dot{b}_1(0,t) + \tau = 0, \tag{3.30}$$

$$\dot{a}_3(L,t) - C_1'(L,t) + \dot{b}_2(L,t) = 0, \tag{3.31}$$

$$-\dot{b}_3(L,t) - C_1(L,t) = 0. \tag{3.32}$$

From beam theory, Eq. (3.29) is the same as,

$$\dot{a}_2 + c_1'' = 0, \tag{3.33}$$

that is,

$$\frac{d}{dt}\{\rho(x\dot{\theta} + \dot{w}) - [S(\dot{w}' + \dot{\theta})]'\} + (EIw'')'' = 0, \tag{3.34}$$

which is the beam governing equation.

From Eq. (3.30), after a long substitution process and dropping off less significant terms, it is approximately in the form of,

$$\tau = I_h\ddot{\theta} - EIw''(0,t), \tag{3.35}$$

which is the torque balance of the beam at the hub side.

From Eq. (3.31), we have,

$$\frac{d}{dt}[M_p(\dot{\theta}L + \dot{w}) + M_p a_c(\dot{\theta} + \dot{w}')] + \frac{d}{dt}[\rho S(\dot{w}' + \dot{\theta})] - [EIw'']'|_L = 0. \tag{3.36}$$

This is the bending moment balance equation at the intersection between the beam tip and the tip load.

And Eq. (3.32) becomes,

$$\frac{d}{dt}[M_p a_c(\dot{\theta}L + \dot{w}) + J_p(\dot{\theta} + \dot{w}')] + EIw''|_L = 0, \tag{3.37}$$

which is the shearing force requirement applied to the intersection.

We notice

$$w(0,t) = 0, \tag{3.38}$$

$$w'(0,t) = 0. \tag{3.39}$$

From the above derivation, the results of the dynamic equations and boundary conditions, in terms of displacement w, are,

$$[EIw''(x_1,t)]'' + \rho(x_1)\{x_1\ddot{\theta} + \ddot{w} - [S(\ddot{w}' + \ddot{\theta})]'\} = 0, \tag{3.40}$$

$$\tau = I_h\ddot{\theta} - EI(0)w''(0,t), \tag{3.41}$$

$$w(0,t) = 0, \quad w'(0,t) = 0, \tag{3.42}$$

$$\frac{d}{dt}[M_p(\dot{\theta}L + \dot{w}) + M_p a_c(\dot{\theta} + \dot{w}')] + \frac{d}{dt}[\rho S(\dot{w}' + \dot{\theta})] - [EIw'']'|_L = 0, \tag{3.43}$$

$$EI(L)w''(L,t) + J_p(\ddot{w}' + \ddot{\theta}) + M_p a_c[L\ddot{\theta} + \ddot{w}(L,t)] = 0. \tag{3.44}$$

The above governing equations can be rewritten as functions of total displacement V,

$$[EIV''(x_1,t)]'' + \rho(x_1)\ddot{V}(x_1,t) - \rho(x_1[S\ddot{V}(x_1,t)']' = 0, \tag{3.45}$$

$$\tau = I_h\ddot{\theta} - EI(0)V''(0,t), \tag{3.46}$$

$$V(0,t) = 0, \quad V'(0,t) = \theta, \tag{3.47}$$

$$-M_p[\ddot{V}(L,t) + a_c\ddot{V}'(L,t)] - \rho S\ddot{V}'(L,t) + [EI(L)V''(L,t)]' = 0, \tag{3.48}$$

$$EI(L)V''(L,t) + J_p\ddot{V}'(L,t) + M_p a_c\ddot{V}(L,t) = 0. \tag{3.49}$$

Eq. (3.48) and Eq. (3.49) are the shearing force balance and the bending moment balance at the cross section of the tip load and the link, respectively.

3.4 System Equations

In order to obtain the system equations in the frequency domain and to prepare for information comprising the next chapters, the harmonic vibration equations and the normalized system equations are obtained. From last section, supposing the link undergoes (x, y) harmonic vibration, the total displacement can be separable and the angular displacement of the link is,

$$V(x_1,t) = V(x_1)\sin(\omega t), \quad \theta = \theta_0 \sin(\omega t), \tag{3.50}$$

where ω is the vibration frequency. Applying above equations to Eq. (3.47), we now get $V'(0) = \theta_0$. It will be applied to the following torque equations. Eq. (3.45) Eq. (3.46) can be written as,

$$[D(x_1)V''(x_1)]'' - \rho(x_1)\omega^2 V(x_1) + \omega^2[\rho(x_1)S\bar{V}(x_1)']' = 0, \tag{3.51}$$

$$\tau = I_h\omega^2 V(0) + D(0)V''(0), \tag{3.52}$$

with the boundary conditions,

$$V(0) = 0, \qquad V'(0) = \theta, \tag{3.53}$$

$$M_p\omega^2[V(L) + a_c V'(L)] + \rho S\omega^2 V'(L) + [D(L)V''(L)]' = 0, \tag{3.54}$$

$$-D(L)V''(L) + I_p\omega^2 V'(L) + M_p a_c\omega^2 V(L) = 0.$$

where $D = EI$.

If we normalize the link axis coordinate and let variable $\xi = x_1/L$, then,

$\frac{\partial()}{\partial x_1} = \frac{1}{L}\frac{\partial()}{\partial \xi}$, $\qquad \frac{\partial^2()}{\partial x_1^2} = \frac{1}{L^2}\frac{\partial^2()}{\partial \xi^2}$, $\qquad 0 \le \xi \le 1$,

the vibration equations are,

$$[D(\xi)V''(\xi)]'' - \rho L^4\omega^2 V(\xi) + L^2[\rho S V(\xi)']' = 0 \tag{3.55}$$

$$I_h L\omega^2 V'(0) + D(0)V(0)'' = \tau \tag{3.56}$$

with boundary conditions,

$$V(0) = 0, \qquad V'(0) = \theta, \tag{3.57}$$

$$D(1)V''(1) - I_p L\omega^2 V'(1) - M_p a_c L^2\omega^2 V(1) = 0, \tag{3.58}$$

$$[D(1)V''(1)]' + M_p L^3\omega^2 V(1) + M_p a_c L^2\omega^2 V'(1) - L^2\rho S V(\xi)' = 0 \tag{3.59}$$

For the sake of numerical computation in the finite difference method [117], we now proceed to nondimensionalize the governing differential equations (Eq. (3.45)-Eq. (3.46)) of the flexible link and the boundary conditions (Eq. (3.47)-Eq. (3.49)), by further introducing the whole set of reference quantities for the variables and parameters as follows,

$$\xi = \frac{x}{L}, \quad t_{new} = \frac{t_{old}}{c}, \quad c^2 = \frac{M_0 L^3}{D_0}, \qquad z(\xi) = \frac{v}{L}, \tag{3.60}$$

$$\alpha(\xi) = \frac{\rho(L\xi)L}{M_0}, \qquad \beta(\xi) = \frac{D(L\xi)}{D_0}, \qquad \delta(\xi) = \frac{S(L\xi)}{L^2}, \tag{3.61}$$

$$\mu = \frac{M_p}{M_0}, \quad \eta = \frac{I_h}{M_0 L^2}, \quad \kappa = \frac{J_p}{M_0 L^2}, \quad \zeta = \frac{a_c}{L}. \tag{3.62}$$

where M_0 and D_0 are nominal values of beam mass and bending rigidity respectively.

In terms of these new functions, variables, and parameters, the dynamic equations can be rewritten as follows,

$$(\beta z'')'' - (\alpha\delta\ddot{z}')' + \alpha\ddot{z} = 0, \tag{3.63}$$

$$\eta\ddot{\theta} - \beta(0)z(0)'' = \frac{\tau L}{D_0}; \tag{3.64}$$

with boundary conditions being,

$$z(0) = 0, \qquad z' = \theta; \tag{3.65}$$

$$\beta(1)z''(1) + \kappa\ddot{z}'(1) + \zeta\mu\ddot{z}(1) = 0, \tag{3.66}$$

$$(\beta z'')'(1) - \alpha\delta\ddot{z}'(1) = \mu[\ddot{z}(1) + \zeta\ddot{z}'(1)]. \tag{3.67}$$

A prime now indicates the differentiation with respect to coordinate ξ, and a dot now indicates the differentiation with respect to time t_{new}.

In next chapter, system natural frequencies and associated modal shapes will be obtained based on these dynamic equations. These modal shapes will be used to calculate the system state space equations for the mechatronic design.

CHAPTER 4

NATURAL FREQUENCIES AND MODAL SHAPES

In this chapter, we focus on determining the natural frequencies and their associated modal shapes to achieve the state space equation which will be addressed in next chapter. Since modal shapes provide the basis for a state space calculating system, these frequencies and their modal shapes will be extracted from a uniform beam.

Classical analytic techniques can be employed to derive the resonant frequencies and the modal shapes. The most useful technique is the separability of the modal shape, which is a function of only a spatial variable, from the time-varying amplitude of the modal shape, which is a function of time. The admissible modal functions will then satisfy the governing equation Eq. (3.45). After taking the assumed form of the solution and substituting them for the beam boundary conditions Eq. (3.46) - Eq. (3.49) listed in Chapter 3, four simultaneous equations are the obvious results and are applicable to the natural frequencies and their modal shapes.

4.1 Modal Determinant

For uniform flexible manipulators, the governing equation of Eq. (3.45) is,

$$EI\tilde{V}'''' - \rho S\tilde{V}'' + \rho\tilde{V} = 0. \tag{4.1}$$

Assuming that the beam undergoes harmonic vibrations, that is, $V(x,t) = \psi(x)q(t)$, where $\psi(x)$ is called the modal shape or eigenfunction and $q(t)$ is the time-varying amplitude of the mode shape, the admissible function is,

$$q(t) = C_1 \sin(\omega t) + C_2 \cos(\omega t), \tag{4.2}$$

where ω is the resonant frequency of the system.

Applying Eq. (4.2) to Eq. (4.1), we have,

$$EI\psi'''' + \rho S\omega^2\psi'' - \rho\omega^2\psi = 0. \tag{4.3}$$

It is obvious that the eigenvalues of this equation are,

$$\lambda_{1,2} = \pm\alpha, \qquad \lambda_{3,4} = \pm i\beta, \tag{4.4}$$

where $\alpha = \sqrt{\frac{\gamma - \rho S\omega^2}{2EI}}$, $\beta = \sqrt{\frac{\gamma + \rho S\omega^2}{2EI}}$, $\gamma = \sqrt{(\rho S\omega^2)^2 + 4EI\rho\omega^2}$.

The complementary solution for the Eq. (4.3) is,

$$\psi(x) = A\cosh\alpha x + B\sinh\alpha x + C\cos\beta x + D\sin\beta x, \tag{4.5}$$

which is the modal shape or eigenfunction. This assumed solution must meet the constraints Eq. (3.46) - Eq. (3.49), which are, in terms of above coefficients,

$$A + C = 0, \tag{4.6}$$

$$EI\alpha^2 A + I_h\omega^2\alpha B - EI\beta^2 C + I_h\omega^2\alpha_1 D = 0, \tag{4.7}$$

$$\alpha_1 A + \alpha_2 B + \alpha_3 C + \alpha_4 D = 0, \tag{4.8}$$

$$\beta_1 A + \beta_2 B + \beta_3 C + \beta_4 D = 0, \tag{4.9}$$

where

$$\alpha_1 = M_p\omega^2 \cosh \alpha L + (\rho S\omega^2 + a_c M_p\omega^2)\alpha \sinh \alpha L + EI\alpha^3 \sinh \alpha l,$$

$$\alpha_2 = M_p\omega^2 \sinh \alpha L + (\rho S\omega^2 + a_c M_p\omega^2)\alpha \cosh \alpha L + EI\alpha^3 \cosh \beta l,$$

$$\alpha_3 = M_p\omega^2 \cos \beta L - (\rho S\omega^2 + a_c M_p\omega^2)\beta \cos \beta L + EI\beta^3 \sin \beta l,$$

$$\alpha_4 = M_p\omega^2 \sin \beta L + (\rho S\omega^2 + a_c M_p\omega^2)\beta \cosh \beta L - EI\beta^3 \cos \beta l,$$

$$\beta_1 = EI\alpha^2 \cosh \alpha L - J_p\omega^2\alpha \sinh \alpha L - M_p a_c\omega^2 \cosh \alpha L,$$

$$\beta_2 = EI\alpha^2 \sinh \alpha L - J_p\omega^2\alpha \cosh \alpha L - M_p a_c\omega^2 \sinh \alpha l,$$

$$\beta_3 = -EI\beta^2 \cos \beta L + J_p\omega^2\beta \sin \beta L - M_p a_c\omega^2 \cos \beta l,$$

$$\beta_4 = -EI\beta^2 \sin \beta L - J_p\omega^2\beta \cos \beta L - M_p a_c\omega^2 \sin \beta l.$$

The matrix form of Eq. (4.6) - Eq. (4.9) is,

$$\begin{bmatrix} 1 & 0 & 1 & 0 \\ EI\alpha^2 & I_h\omega^2\alpha & -EI\beta^2 & I_h\omega^2\beta \\ \alpha_1 & \alpha_2 & \alpha_3 & \alpha_4 \\ \beta_1 & \beta_2 & \beta_3 & \beta_4 \end{bmatrix} \begin{bmatrix} A \\ B \\ C \\ D \end{bmatrix} = 0 \qquad (4.10)$$

The natural frequencies are obtained by solving the determinant equal to zero.

4.2 Modal Frequencies and Modal Shapes

For a given material and parameters of a beam as in Table 4.1,

Table 4.1: Parameters of Uniform Beam.

E	I	L	ρ	M	M_p	J_p	a_c	I_h
1.0	10.0	1.0	1.0	10.0	1.0	0.5	0.1	5.0

if we set $A = 1$, then $C = -1$. Eq. (4.10) is redundant, and for each frequencies, it becomes,

$$\begin{bmatrix} \alpha_2 & \alpha_4 \\ \beta_2 & \beta_4 \end{bmatrix} \begin{bmatrix} B \\ D \end{bmatrix} = \begin{bmatrix} \alpha_3 - \alpha_1 \\ \beta_3 - \beta_1 \end{bmatrix}. \tag{4.11}$$

By solving this, B, D are obtained. After normalized the eigenfunction to meet

$$\int_0^L \psi(x)^2 dx = 1, \tag{4.12}$$

the coefficients are obtained with their frequencies as shown in Table 4.2.

Actually, the number of modal shapes is infinite, because of the distributed parameter beam system. Only the first ten modal shapes and their frequencies are listed for calculating state-space equation in next chapter. Generally speaking, the more modal shapes involved in the system, the more complicated the system model will be. According to Hasting (1987) [36] and Hughes [37], the first two modes have a greater influence on the model accuracy than the higher order modes. For typical applications, the higher order must be truncated to meet the computation time. Also, many factors impact the modal shape, including hub position. Geniele *et al* [29] showed that this affects the actual modal shape since Coulomb friction coefficients are related to hub position. The first ten modal shapes are plotted as in Fig. (4.1) - Fig. (4.10). Conventionally, the horizontal axis is the spatial coordinator, while the vertical is the amplitude meter. From them, it is obvious that if the high order modal shapes are not taken into account, the high frequency terms in the system dynamics

are dropped off. In later chapters, these terms are treated as model uncertainties in the controller design.

Table 4.2: Modal Frequencies and Coefficients of Modal Shapes.

Mode	Frequency	A	B	C	D
1	2.1925	1.2550	-0.9898	-1.2550	0.1652
2	11.7525	1.1383	-1.1977	-1.1383	0.6655
3	52.3515	0.7134	-0.3563	-0.7134	-0.0022
4	114.7315	1.3788	-1.9441	-1.3788	0.3466
5	218.4795	0.6135	-0.2488	-0.6135	-0.0045
6	336.5055	1.2830	-1.9606	-1.2830	0.1882
7	497.3505	0.5965	-0.2294	-0.5965	-0.0031
8	671.0485	1.2464	-1.9514	-1.2464	0.1290
9	888.0655	0.5906	-0.2226	-0.5906	-0.0023
10	1117.5115	1.2301	-1.9457	-1.2301	0.0985

In theory, the fundamental frequency for a rigid manipulator is infinitely large, therefore it can move fast without vibration. Because of beam flexibility, the resonant frequency is dramaticly reduced (the first one is 2.1925 rad/sec here). This means that it has to move slowly to experience small vibrations under normal operation. In later chapters, we will design and control the flexible beam to achieve better results. But first let's get a state-space model by using these modal shapes.

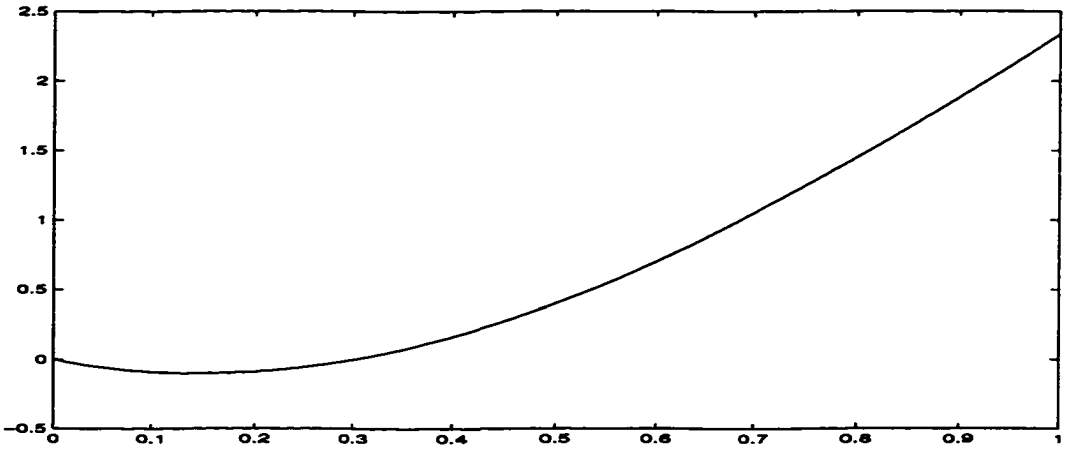

Figure 4.1: The First Modal Shape

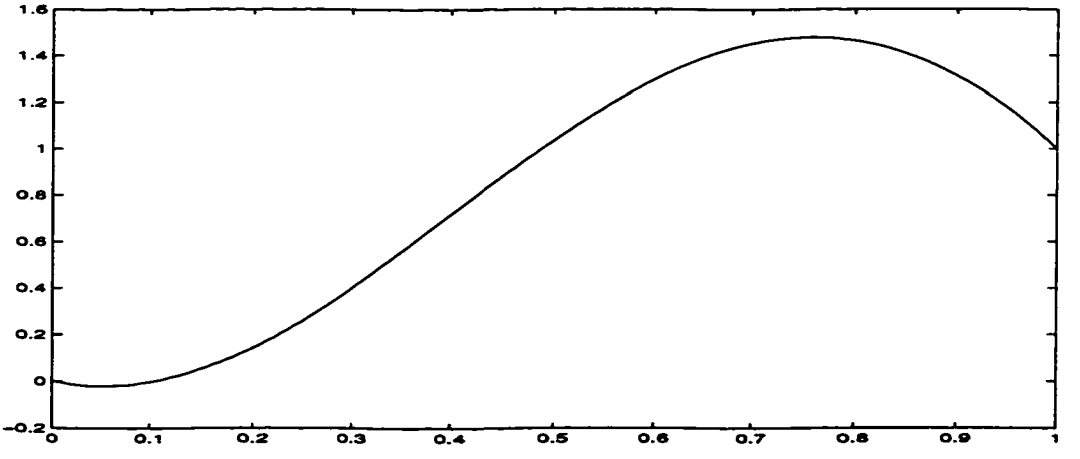

Figure 4.2: The Second Modal Shape

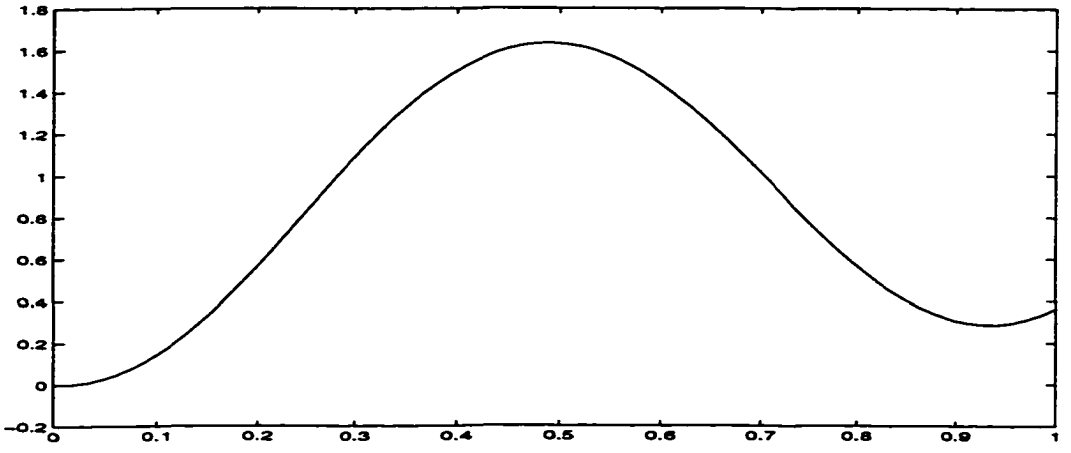

Figure 4.3: The Third Modal Shape

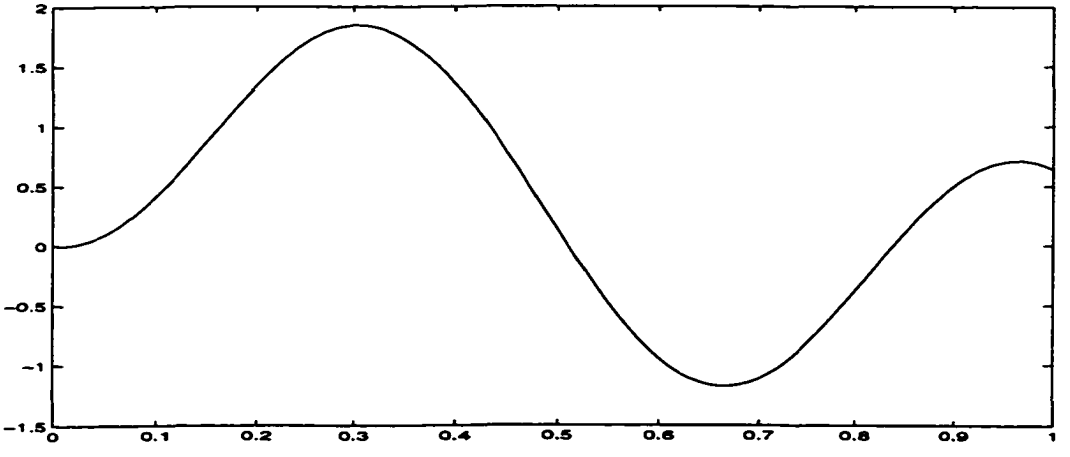

Figure 4.4: The Fourth Modal Shape

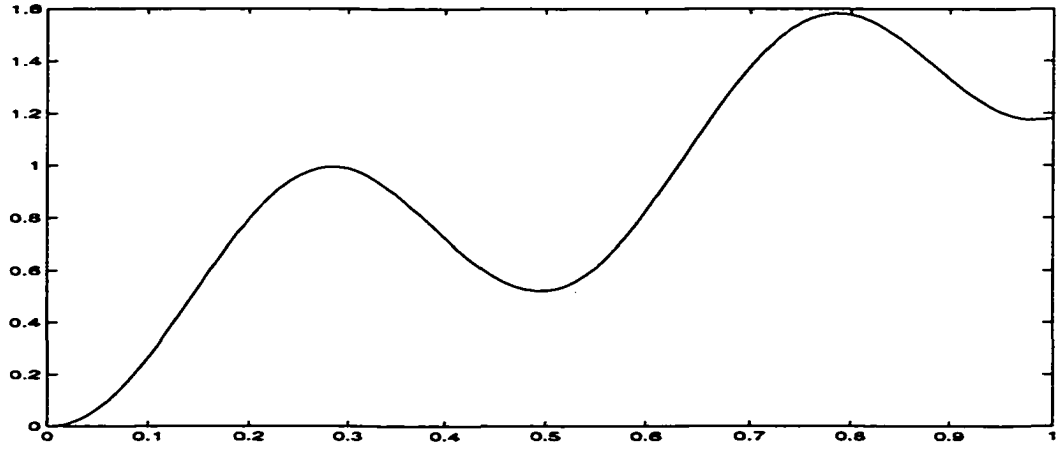

Figure 4.5: The Fifth Modal Shape

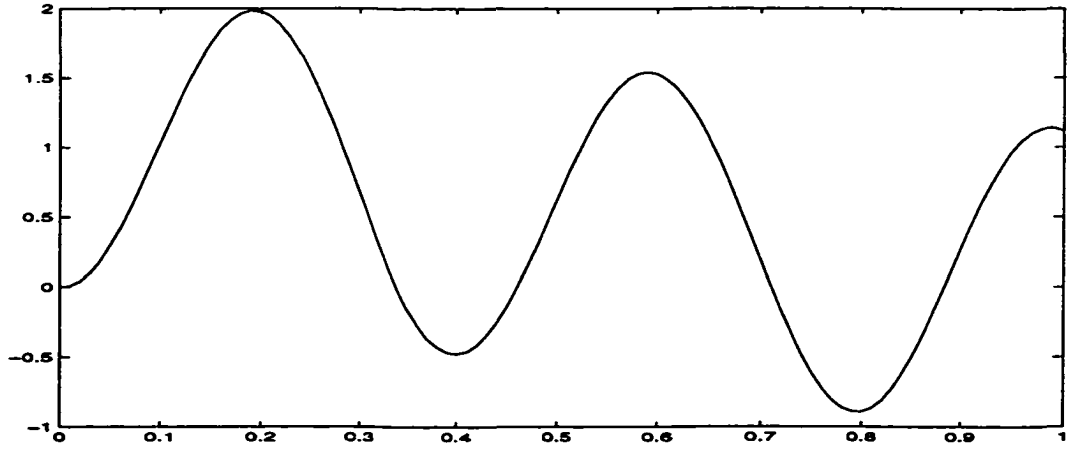

Figure 4.6: The Sixth Modal Shape

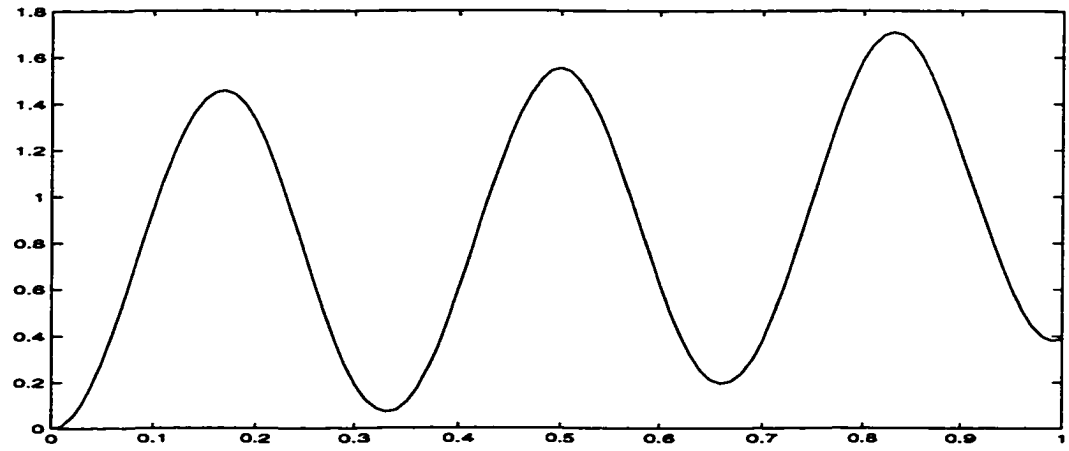

Figure 4.7: The Seventh Modal Shape

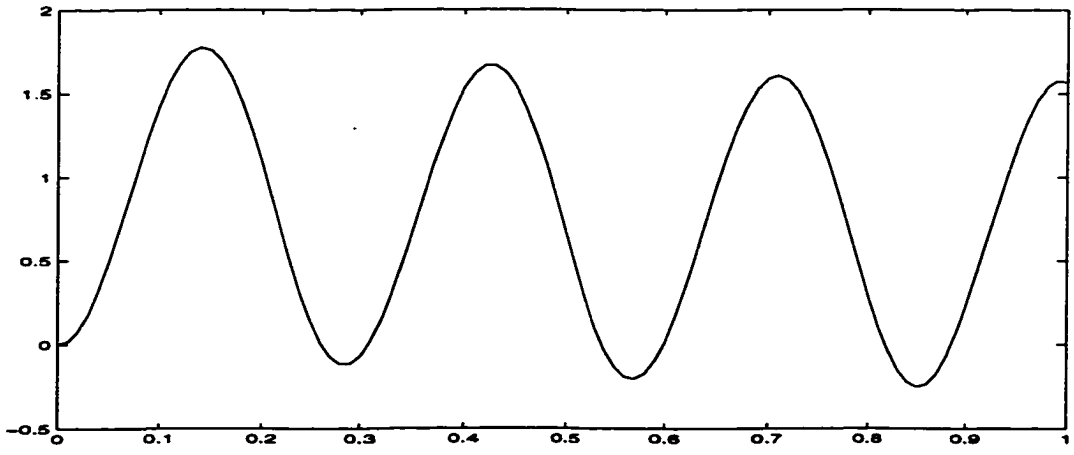

Figure 4.8: The Eighth Modal Shape

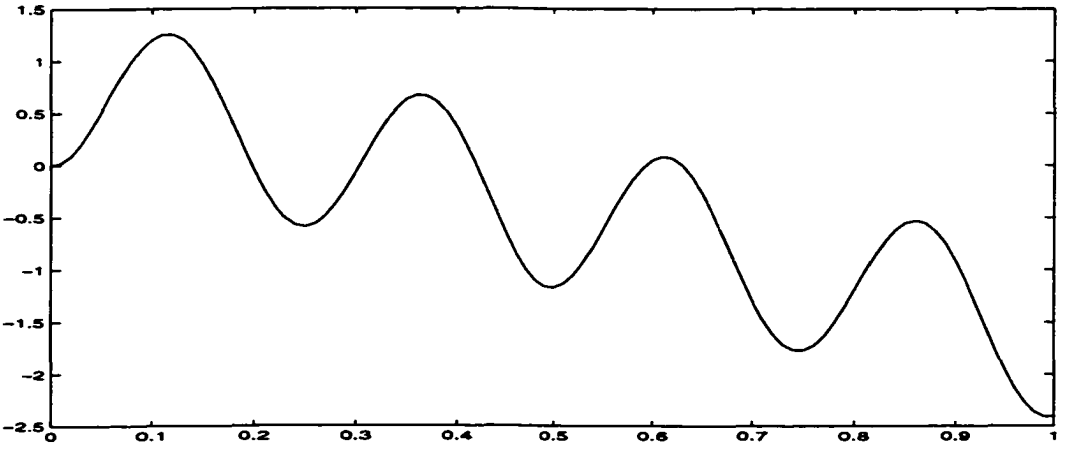

Figure 4.9: The Ninth Modal Shape

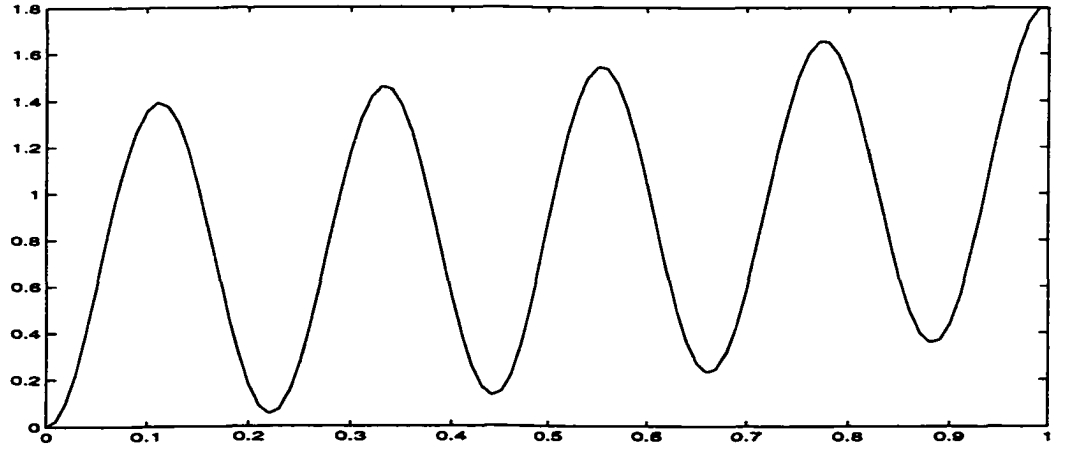

Figure 4.10: The Tenth Modal Shape

CHAPTER 5

A FINITE DIMENSIONAL MODEL OF FLEXIBLE MANIPULATORS

The dynamics of a flexible manipulator system are described by an infinite-dimensional mathematical model, since the model consists of partial differential equations. From Chapter 4, we know that the number of modal shapes and frequencies of a flexible manipulator is infinite. But to design a finite-dimensional controller, a finite-dimensional system model is needed. To achieve this goal, a finite dimensional approximation needs to be used to model a flexible manipulator, that is, to retain a finite number of modes, and to drop off the other, less significant modes based on the requirements of the controller. Generally speaking, the proper selection of modes and the number of modes required are unknown. Fortunately, many previous studies such as [37] have shown that those modes associated with lower natural frequencies are the most significant modes. In this chapter, this track will be followed in order to build a $2(N+1)$-dimensional state-space representation from an N-mode for a flexible manipulator. Furthermore, the overall system equations will be addressed by integrating the beam dynamics with the actuator dynamics. The output specifications for feedback controller are also discussed at the end of this chapter.

The N-mode expansion for the displacement $w(x,t)$ can be given by,

$$w(x,t) = \sum_{i=1}^{N} \psi_i(x) q_i(t). \tag{5.1}$$

The separability in this case refers to describing the displacement as a series of terms which are products of two separate functions, each of that is a function of a single variable, a spatial variable x, and time t, respectively. ψ_i is the ith modal shape, or eigenfunction. q_i is the corresponded generalized modal coordinate describing the flexible deformation.

There are two ways to develop the $2(N+1)$-dimensional state space. The first one is to substitute Eq. (5.1) for Eq. (3.40), Eq. (3.41), then multiply the resulted equations by $\psi_j(x)$ and integrate over the spatial domain $[0, L]$ followed by applying the orthogonality property of the modal shapes to get second order ordinary differential equations with $N+1$ dimensions. The state variables are $\theta, q_i (1 \leq i \leq N)$ and their first order differentials. The accuracy of this approach is bounded by the accuracy of the given partial differential model, since linearization and truncation methods are already applied to get a concrete, operable model. Thus the state space model would inherit all these model's errors.

The other scheme in developing a mathematical model is to use the Lagrangian method or Hamiltonian's Principle to the total kinetic energy, total potential energy and virtual work done by the torque actuated to the joint. This method will not introduce extra errors into system. This is the procedure which will be used to obtain the state-space model for a flexible manipulator suggested in this dissertation.

5.1 State-Space Equations of Flexible Manipulators

In this model, the hub kinetics is rewritten as,

$$T_h = \frac{1}{2} I_h [\dot{\theta}^2 + \dot{\omega}^2(0,t)']. \tag{5.2}$$

After applying Eq. (5.1) into Eq. (5.2),

$$T_h = \frac{1}{2} I_h \dot{\theta}^2 + \frac{1}{2} I_h \sum_{i=1}^{N} \sum_{j=1}^{N} \dot{q}_i \dot{q}_j \psi_i'(0) \psi_j'(0), \tag{5.3}$$

In the same way, the kinetics of the tip load is,

$$T_p = \frac{1}{2} M_p (\dot{\theta} L + \dot{\omega}(L,t))^2 + \frac{1}{2} J_p (\dot{\theta} + \dot{\omega}(L,t)')^2 + a_c M_p (\dot{\theta} + \dot{\omega}(L,t)')(\dot{\theta} L + \dot{\omega}(L,t)) \tag{5.4}$$

which is the same as,

$$T_p = \frac{1}{2} \Gamma_1 \dot{\theta}^2 + \dot{\theta} \sum_{i=1}^{N} \dot{q} \Gamma_2(i) + \frac{1}{2} \sum_{i=1}^{N} \sum_{j=1}^{N} \dot{q}_i \dot{q}_j \Gamma_3(i,j), \tag{5.5}$$

where,

$\Gamma_1 = (M_p L^2 + J_p + 2 M_p L a_c)$,

$\Gamma_2(i) = (J_p + M_p L a_c) \psi_i'(L) + (L + a_c) M_p \psi_i(L)$.

$\Gamma_3(i,j) = J_p \psi_i'(L) \psi_j'(L) + M_p \psi_i(L) \psi_j(L) + 2 a_c M_p \psi_i'(L) \psi_j(L)$.

The kinetic energy of the link,

$$T_L = \frac{1}{2} \int_0^L [(x\dot{\theta} + \dot{\omega})^2 + S(\dot{\omega}' + \dot{\theta})^2] \rho dx \tag{5.6}$$

is equal to,

$$T_L = \frac{1}{2} \Lambda_1 \dot{\theta}^2 + \dot{\theta} \sum_{i=1}^{N} \dot{q}_i \Lambda_2(i) + \frac{1}{2} \sum_{i=1}^{N} \sum_{j=1}^{N} \dot{q}_i \dot{q}_j \Lambda_3(i,j), \tag{5.7}$$

where

$\Lambda_1 = \int_0^L (x^2 + S)\rho dx,$

$\Lambda_2(i) = \int_0^L [x\psi_i(x) + S\psi_i'(x)]\rho dx,$

$\Lambda_3(i,j) = \int_0^L [\psi_i(x)\psi_j(x) + S\psi_i'(x)\psi_j'(x)]\rho dx.$

S is the function of cross section area of the link. The total potential energy is

$$P = \frac{1}{2}\int_0^L EI(x)w^2(x)''dx = \frac{1}{2}\sum_{i=1}^{N}\sum_{j=1}^{N} q_i q_j k(i,j), \tag{5.8}$$

where $k(i,j) = \int_0^L EI(x)\psi_i''(x)\psi_j''(x)dx.$

The generalized virtual work is derived as,

$$W = \tau v'(0,t) = \tau\theta + \tau\omega'(0,t) = \tau\theta + \tau\sum_{i=1}^{N}\psi_i'(0)q_i(t). \tag{5.9}$$

In order to apply the Hamiltonian Principle, let us substitute Eq. (5.3, 5.5, 5.7, 5.8, 5.9) for the following formula and group it in terms of θ, δq_i, and their derivatives,

$$\Xi = T_L + T_h + T_p - P + W = \frac{1}{2}\Omega_1\dot{\theta}^2 + \dot{\theta}\sum_{i=1}^{N}\dot{q}_i\Omega_2(i)$$
$$+\frac{1}{2}\sum_{i=1}^{N}\sum_{j=1}^{N}\dot{q}_i\dot{q}_j\Omega_3(i,j) + \tau\theta + \tau\sum_{i=1}^{N}\psi_i'(0)q_i - \frac{1}{2}\sum_{i=1}^{N}\sum_{j=1}^{N}q_i q_j k(i,j), \tag{5.10}$$

where

$\Omega_1 = I_h + \Gamma_1 + \Lambda_1,$

$\Omega_2 = \Gamma_2(i) + \Lambda_2(i),$

$\Omega_3(i,j) = I_h\psi_i'(0)\psi_j'(0) + \Gamma_3(i,j) + \Lambda_3(i,j),$

After applying the Hamiltonian method, we obtain,

$$\delta\Xi = \Omega_1\dot{\theta}\delta\dot{\theta} + \sum_{i=1}^{N}\Omega_2(i)\dot{q}_i\delta\dot{\theta} + \dot{\theta}\sum_{i=1}^{N}\Omega_2(i)\delta\dot{q}_i$$
$$+\sum_{i=1}^{N}\sum_{j=1}^{N}\dot{q}_j\Omega_3(i,j)\delta\dot{q}_i + \tau\delta\theta + \tau\sum_{i=1}^{N}\psi_i'(0)\delta q_i - \sum_{i=1}^{N}\sum_{j=1}^{N}q_j k(i,j)\delta q_i. \qquad (5.11)$$

since,

$\int_{t_0}^{t_f}\dot{\theta}\delta\dot{\theta}dt = \dot{\theta}\delta\theta|_{t_0}^{t_f} - \int_{t_0}^{t_f}\ddot{\theta}\delta\theta dt = -\int_{t_0}^{t_f}\ddot{\theta}\delta\theta dt.$

In the same way, we have,

$\int_{t_0}^{t_f}\dot{q}_i\delta\dot{\theta}dt = -\int_{t_0}^{t_f}\ddot{q}_i\delta\theta dt, \qquad \int_{t_0}^{t_f}\dot{\theta}\delta\dot{q}_i dt = -\int_{t_0}^{t_f}\ddot{\theta}\delta q_i dt$

$\int_{t_0}^{t_f}\dot{q}_i\delta\dot{q}_j dt = -\int_{t_0}^{t_f}\ddot{q}_i\delta q_i dt.$

The Hamilton Extended Principle results in,

$$\int_{t_0}^{t_f}\delta\Xi dt = \int_{t_0}^{t_f}\{[-\Omega_1\ddot{\theta} - \sum_{i=1}^{N}\ddot{q}_i\Omega_2(i) + \tau]\delta\theta$$
$$-[\ddot{\theta}\sum_{i=1}^{N}\Omega_2(i) + \sum_{i=1}^{N}\sum_{j=1}^{N}\ddot{q}_j\Omega_3(i,j) + \sum_{i=1}^{N}\sum_{j=1}^{N}q_j k(i,j) - \tau\sum_{i=1}^{N}\psi_i'(0)]\delta q_i\}dt = 0. \qquad (5.12)$$

These coefficients of $\delta\theta, \delta q_i, 1 \le i \le N$ must be zero, that is,

$$\Omega_1\ddot{\theta} + \sum_{i=1}^{N}\ddot{q}_i\Omega_2(i) - \tau = 0, \qquad (5.13)$$

$$-\ddot{\theta}\Omega_2(i) - \sum_{j=1}^{N}\ddot{q}_j\Omega_3(i,j) - \sum_{j=1}^{N}q_j k(i,j) + \tau\psi_i'(0) = 0, \qquad 0 \le i \le N \qquad (5.14)$$

or in matrix form, they are,

$$M\ddot{x} + Kx = b\tau, \qquad (5.15)$$

where,

$x = [\theta, q_1, q_2, q_3, \ldots, q_N]^T_{(N+1,1)}, \qquad b = [1, \psi_1'(0), \psi_2'(0), \ldots, \psi_N'(0)]^T_{(N+1,1)},$

$$M = \begin{bmatrix} \Omega_1 & \Omega_2(1) & \Omega_2(2) & . & \Omega_2(N) \\ \Omega_2(1) & \Omega_3(1,1) & \Omega_3(1,2) & . & \Omega_3(1,N) \\ . & . & . & . & . \\ \Omega_2(N) & \Omega_3(N,1) & \Omega_3(N,2) & . & \Omega_3(N,N) \end{bmatrix},$$

$$K = \begin{bmatrix} 0 & 0 & 0 & . & 0 \\ 0 & k(1,1) & k(1,2) & . & k(1,N) \\ . & . & . & . & . \\ 0 & k(N,1) & k(N,2) & . & k(N,N) \end{bmatrix}.$$

As has been shown, $\Omega_3(i,j) = \Omega_3(j,i)$, $k(i,j) = k(j,i)$, thus the matrices M, K are symmetric and named mass and rigidity matrices respectively.

Next, the actuator dynamics need to be incorporated into the link system. It is assumed that the arm is driven by a permanent magnet DC-motor. Therefore, the actuator dynamics can be described as,

$$-J_m\ddot{\theta} - (B_m + \frac{K_b K_m}{R})\dot{\theta} + \frac{K_m}{R}v_c = \tau, \tag{5.16}$$

where J_m is the actuator inertia, B_m the friction coefficient, K_m the torque constant, K_b the back emf constant, R the armature resistance, and θ, v_c the hub rotation and armature voltage, respectively. In general, all motor circuit parameters can be

considered as design variables. The overall state variable is defined as,

$$q = \begin{bmatrix} x \\ \dot{x} \end{bmatrix} \tag{5.17}$$

Combining Eq. (5.15) with Eq. (5.16), we present the overall system state space equations as,

$$\dot{q} = Aq + Bu, \quad u = v_c, \tag{5.18}$$

where

$$A = \begin{bmatrix} 0 & I \\ -\overline{M}^{-1}K & -\overline{M}^{-1}\overline{B} \end{bmatrix}, \qquad B = \begin{bmatrix} 0 \\ \overline{M}^{-1}\overline{D} \end{bmatrix}$$

and

$$\overline{M} = (M + J_m b\underline{e}_1)^{-1}, \quad \overline{B} = (B_m + \frac{K_b K_m}{R})b\underline{e}_1, \quad \overline{D} = b\frac{K_m}{R}, \quad \underline{e}_1 = \begin{bmatrix} 1 & 0 & \dots & 0 \end{bmatrix}_{1\times n}.$$

A is the function of beam construction, thus any changes in beam mechanical shape will result in a different A, which provides the basis for simultaneously optimal construction and control based on the mechatronic formulation discussed early.

5.2 Output Specifications

As can be seen from the system state-space equations, the state vector consists of θ, the generalized modal coordinates q_i, and their first order derivatives. So all controllers based on the state feedback are indirect, which means that the states need to be predicted. This will trade off with computation time and bring one more

inaccuracy into a closed-loop, cutoff closed-loop bandwidth. This presents hindrances to real-time processing and high motion speed. Output feedback takes precedence over state space feedback as far as the mechatronic approach and objectives of this dissertation are concerned.

Tip deflection output, which is,

$$y = w(L,t) = \sum_{i=1}^{N} \psi_i(L) q_i = \begin{bmatrix} 0 & \psi_1(L) & \psi_2(L) & \dots & \psi_N(L) & \bar{0} \end{bmatrix} q, \quad (5.19)$$

where ψ_i is the ith eigenfunction, $\bar{0}_{1\times(n+1)}$ is zero vector. A CCD camera clipped on the hub can be used to measure the output such as [94].

The tip position output is,

$$y = v(L,t) = L\theta + \sum_{i=1}^{N} \psi_i(L) q_i = \begin{bmatrix} L & \psi_1(L) & \psi_2(L) & \dots & \psi_N(L) & \bar{0} \end{bmatrix} q, \quad (5.20)$$

These two strategies are noncollocated control.

The hub tangent angle output is,

$$y = \Theta = \theta + \sum_{i=1}^{N} \psi_i'(0) q_i = \begin{bmatrix} 1 & \psi_1'(0) & \psi_2'(0) & \dots & \psi_N'(0) & \bar{0} \end{bmatrix} q, \quad (5.21)$$

A potentiometer may be used for measuring Θ. this is collocated control.

Combining Eq. (5.21) with Eq. (5.22) or/and Eq. (5.23) results in hybrid control.

In this mechatronic design, output feedback may be one of above three outputs, or the mixture, such as,

$$y = Cq = \begin{bmatrix} w(L,t) \\ v'(L,t) \end{bmatrix} q, \quad (5.22)$$

where

$$C = \begin{bmatrix} 0 & \psi_1(L) & \psi_2(L) & \dots & \psi_N(L) & \bar{0} \\ 1 & \psi_1'(0) & \psi_2'(0) & \dots & \psi_N'(0) & \bar{0} \end{bmatrix}.$$

The corresponding state-variable equations are,

$$\dot{q} = Aq + bu, \qquad y = Cq. \tag{5.23}$$

These output feedbacks will be used in control design in the later chapters to show the improvement of the suggested mechatronic approach and to make comparison between them.

5.3 Numerical Example: State-Space Model for a Uniform Beam

For a uniform beam, if the first four modal shapes are chosen for system model development, these matrices in Eq. (5.15) are,

$$M = \begin{bmatrix} 25.9488 & 7.6017 & 25.2215 & 10.6770 & 5.7002 \\ 7.6017 & 14.9599 & 2.0715 & -23.2634 & -7.4223 \\ 25.2215 & 2.0715 & 55.8251 & 55.3095 & -60.8994 \\ 10.6770 & -23.2634 & 55.3095 & 261.5816 & -46.5147 \\ 5.7002 & -7.4223 & -60.8994 & -46.5147 & 644.4792 \end{bmatrix},$$

$$K = \begin{bmatrix} 0 & 0 & 0 & 0 & 0 \\ 0 & 91.40 & 47.82 & 43.47 & 0.74 \\ 0 & 47.82 & 787.52 & 680.23 & -413.40 \\ 0 & 43.47 & 680.23 & 10723.27 & -2107.19 \\ 0 & 0.74 & -413.40 & -2107.19 & 53297.74 \end{bmatrix},$$

$$b = \begin{bmatrix} 1.0000 & -0.9951 & 0.1654 & -0.7646 & 0.1567 \end{bmatrix}^T.$$

The eigenvalues of the Eq. (5.15) are

$$\begin{bmatrix} 0 & 0 & \pm 11.2297i & \pm 7.9028i & \pm 5.2421i & \pm 2.4698i \end{bmatrix}.$$

After combining the beam dynamics Eq. (5.15) with the motor equation Eq. (5.16), the matrices in state-space model Eq. (5.18) with feedback Eq. (5.21) and Eq. (5.19) are,

$$A = \begin{bmatrix} 0 & 0 & 0 & 0 & 0 & 1.0 & 0 & 0 & 0 & 0 \\ 0 & 0 & 0 & 0 & 0 & 0 & 1.0 & 0 & 0 & 0 \\ 0 & 0 & 0 & 0 & 0 & 0 & 0 & 1.0 & 0 & 0 \\ 0 & 0 & 0 & 0 & 0 & 0 & 0 & 0 & 1.0 & 0 \\ 0 & 0 & 0 & 0 & 0 & 0 & 0 & 0 & 0 & 1.0 \\ 0 & 0.48 & 2.97 & 0.22 & 23.60 & -0.042 & 0 & 0 & 0 & 0 \\ 0 & -3.0200 & 27.3021 & -103.013 & 212.363 & 0.047 & 0 & 0 & 0 & 0 \\ 0 & -0.9238 & -22.060 & 55.465 & -158.593 & 0.015 & 0 & 0 & 0 & 0 \\ 0 & -0.1241 & 5.2126 & -61.303 & 50.981 & 0.004 & 0 & 0 & 0 & 0 \\ 0 & -0.1439 & -0.8249 & 2.8944 & -92.135 & 0.003 & 0 & 0 & 0 & 0 \end{bmatrix},$$

$$B = \begin{bmatrix} 0 & 0 & 0 & 0 & 0 & 0.0014 & -0.0016 & -0.00051 & -0.00013 & -0.00087 \end{bmatrix}^T,$$

$$C = \begin{bmatrix} 1.0000 & -0.9951 & 0.1654 & -0.7646 & 0.1567 & 0 & 0 & 0 & 0 & 0 \\ 0 & -0.6803 & -0.6590 & 1.4726 & -1.2781 & 0 & 0 & 0 & 0 & 0 \end{bmatrix}.$$

The eigenvalues of the Eq. (5.18) are

$$\begin{bmatrix} 0 & -0.0003 \pm 10.0377i & \pm 7.8098i & -0.0013 \pm 3.8801i & -0.0013 \pm 2.1348i & -0.0340 \end{bmatrix}.$$

Notice some eigenvalues now are located on the left half plane. This is because of the contribution of the motor dynamics.

CHAPTER 6

MECHATRONIC DESIGN OF FLEXIBLE MANIPULATORS-BASED ON LQR FORMULA WITH IHR PROGRAMMING

As stated in Chapter 1, mechatronic design is a global optimization of the overall system. For a flexible manipulator, the overall system is the integration of link dynamics, DC motor equation, measuring sensors, and the selected controller. The optimization process will result in an optimal link geometric distribution, suitable DC motor parameters and an optimal controller structure subject to one of the performance index referred to in Chapter 1. To demonstrate this approach and also due to the computation complexity, the following restrictions are applied here. A rectangular beam is considered and divided into N segments equally along with the beam spatial coordinate. Each segment is uniform. In each segment, the width is the only variable to be optimized for the link geometrics . Motor dynamics are also given in order to simplify the design process.

It was pointed out in the last chapter that output feedback instead of state space feedback is a feasible choice. It is also predictable that the system optimum performance index may not matter in the selection of the controller to a large degree,

since the resulting index is the result of the overall system optimization. Due to this factor, the linear quadratic regulator (LQR) is admissible as the selected controller.

In this chapter, we will discuss the mechatronic design based on the LQR formula. The LQR feedback is outlined in [48] as an inner loop followed by an Adaptive Iterative algorithm (IHR) as an outer loop searching for the beam width distribution. The mechatronic design procedure is addressed through detailing the integration of the inner loop with the outer loop.

6.1 LQR Formula and Its Optimization

For the flexible manipulator system given by Eq. (5.23), the LQR controller will be a linear output feedback in the form of

$$u = -\Re y \tag{6.1}$$

where $\Re$ is an $1 \times p$ (p is the dimension of output) vector of constant feedback coefficients to be determined according to the following quadratic performance index (PI):

$$J(u) = \frac{1}{2}\int_{t_0}^{\infty}(q^T(t)Qq(t) + u^T(t)Ru(t))dt, \tag{6.2}$$

where the Q, R are symmetric positive semidefinite weighting matrices.

By substituting the output feedback control Eq. (6.1) for Eq. (5.23), the closed loop equation is found to be

$$\dot{q} = (A - B\Re C)q = A_c q. \tag{6.3}$$

Therefore, PI is found to be

$$J = \frac{1}{2}\int_{t_0}^{\infty} q^T(t)(Q + C^T\Re^T R\Re C)q(t)dt, \tag{6.4}$$

Now, the LQR design problem is to choose gain $\Re$ such that J reaches its minimum value subject to the condition of stablizing the closed-loop system given by Eq. (6.3).

Since $Q + C^T\Re^T R\Re C$ is a symmetric, positive-semidefinite matrix, a symmetric, positive-semidefinite matrix P can be found [27] so that,

$$\frac{d}{dt}(q^T P q) = -q^T(Q + C^T\Re^T R\Re C)q. \tag{6.5}$$

Using P, then J can be rewritten as

$$J = \frac{1}{2}q^T(0)Pq(0) - \frac{1}{2}\lim_{t\to\infty} q^T(t)Pq(t). \tag{6.6}$$

Assuming that the system is asymptotically stable, so the $q(t)$ vanishes with time,

$$\lim_{t\to\infty} q^T(t)Pq(t) = 0. \tag{6.7}$$

This leads to,

$$J = \frac{1}{2}q^T(0)Pq(0) = \frac{1}{2}tr(PX), \tag{6.8}$$

where the $n \times n$ symmetric matrix X is defined by $q(0)q^T(0)$.

Furthermore, from Eq. (6.3) and Eq. (6.5), we find that

$$A_c^T P + PA_c + C^T\Re^T R\Re C + Q = 0. \tag{6.9}$$

This is the Lyapunov equation for solving P given $\Re$ and Q.

It is now clear that the problem of selecting $\Re$ to minimize J subject to the dynamical constraint of Eq. (6.2) on the states is equivalent to the algebraic problem of selecting $\Re$ to minimize Eq. (6.8) subject to the constraint of Eq. (6.9) on the auxiliary matrix P. To solve this modified problem, we use the Lagrange multiplier method. Following the procedure described in [48], two additional equations which can be used to solve the LQR problem are derived,

$$A_c S + S A_c^T + X = 0, \tag{6.10}$$

$$\Re = R^{-1} B^T P S C^T (C S C^T)^{-1}, \tag{6.11}$$

where S is a symmetric $n \times n$ matrix of Lagrange multipliers.

The equations for P, S, and $\Re$ are coupled among these nonlinear matrix equations, therefore, some trial-and-error iterative design methods have to be used to find the $\Re$. The process to find the feedback matrix $\Re$ is described as following for a given set of A, B, C.

LQR – Feedback Optimization:

1. Initialize:

   i =0, select an initial $\Re_0$ so thatA_c is asymptotically stable;

   Set system initial state values $X = q(0)q(0)^T$, the Stop criteria ϱ.

2. i-th iteration:

   Set $A_i = A - B\Re_i C$.

Using **lyap.m** in the Control Toolbox of Matlab to solve the equations

$A_i^T P + P A_i + C1 = 0$, where $C1 = C^T \Re_i^T R \Re_i C + Q$ and $A_i S + S A_i^T + X = 0$ for P_i and S_i.

Set $J = \frac{1}{2} tr(P_i X)$.

3. Updating:

   Gain updating direction: $\Delta \Re = R^{-1} B^T P_i S_i C^T (C S_i C^T)^{-1} - \Re_i$.

   Update gain: $\Re_{i+1} = \Re_i + \alpha \Delta \Re$,

   where α is chosen so that $A - B \Re_{i+1} C$ is asymptotically stable.

   Check the eigenvalues of new A, if unstable, go to Step 5.

4. Criteria:

   $J_{i+1} = \frac{1}{2} tr(P_{i+1} X) \leq J_i$.

   If $(J_{i+1} - J_i) \leq \varphi$, the given criteria, go to 5. Otherwise set $i = i + 1$ and go to 2.

5. Stop:

   Set $\Re = \Re_{i+1}, J = J_{i+1}$.

   If index =0, go to step 2.

This process will be referred to in this paper as the inner loop and will converge to J, the minimum performance index for the set of A, B, C by searching proper feedback matrix $\Re$. In the next section, the outer loop searching the optimal beam shape will be discussed.

6.2 IHR and Its Algorithm

In Chapter 5, it was established that the components in the matrices of the state equations are related to a given link shape, that is, the matrices A, B, C are the functions of beam geometric distribution. Here a procedure to find out the link geometrics based on the Adaptive Iterative Hit and Run (IHR) algorithm [80] [114] is conducted. Some restrictions shall be made clear from the perspective of the mechatronic design. First the beam weight holds constant, which, in terms of beam volume, means that the whole volume is constant. The only variable for the beam geometric is the width of the cross section for each segment, however, the sum of these width variables must remain a constant in order to keep the total volume constant based on N segment solution. Another consideration, realistically speaking, is that minimum stress on the beam is required, which in term of beam width, is its minimum width. These restrictions are applied to modify the IHR algorithm. This iterative procedure of the modified IHR can be specified as:

IHR – Hit - Run Optimization:

1. Set uniform area A_0, minimum and maximum area constraints, A_{min} and A_{max} according to the beam strength requirement. Set $j = 1$. Set beam material parameters.

2. Calculate the uniform beam PI as the starting value.

3. Initialize loop vectors, loop factors, direction vector D and stop criteria.

4. Select changing positions: randomly select $N/2$ of the N segments and mark them with 1's in vector D_j of length N. Mark the remaining $N/2$ segments with -1's. If N is odd, one randomly selected area will remain constant and will be marked by a 0.

5. Set direction vector: get $N/2$ samples from a $N(0,1)$ normal distribution and place them in each position of D_j where there is a 1. Place the negatives of this same sample in each position of D_j where there is a -1. This arrangement will ensure a constant volume during optimization. Here, D_j is called the direction vector.

6. Implement direction: generate a step size, S, uniformly from L_j, the set of feasible step sizes in the direction D_j, where,

   $L_j = \{S \in \Re : A_{min} < A_j + SD_j < A_{max}\}$

   If $L_j = \emptyset$, go to Step 4.

7. Set $S = S$ * MUL, while $0 <$ MUL ≤ 1.

8. Update the area vector, A_j,

   $A_{j+1} = A_j + SD_j$.

6.3 Integrated Optimization

Traditionally, the LQR algorithm is used to find the optimal output feedback gain $\Re$ for a system given by (A, B, C) , at which point the design process stops as in Fig. (6.1), where U^* is the controller output and J is the performance index. In

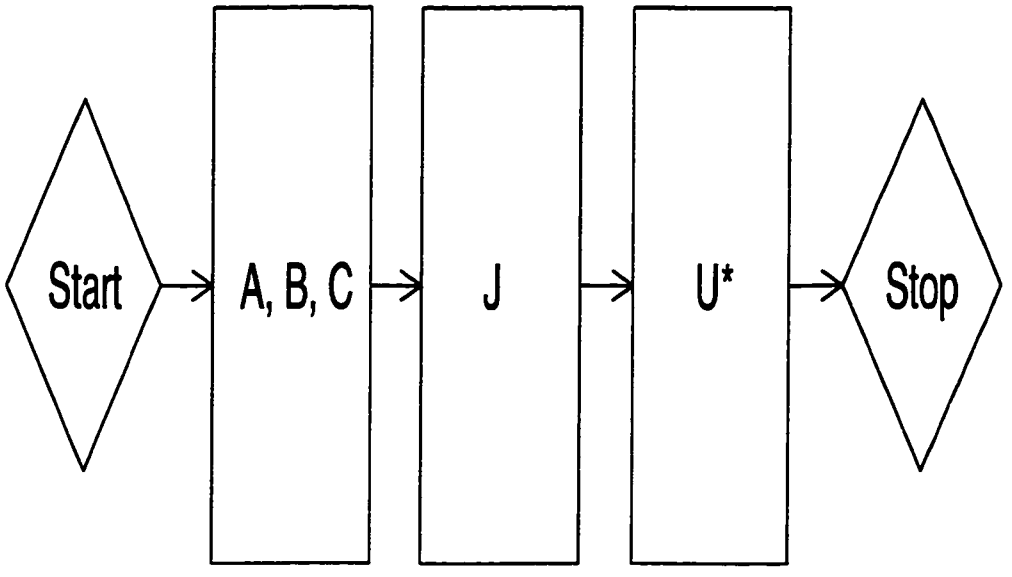

Figure 6.1: Traditional Design Algorithm

other words, someone constructs the plant first, which is A, B, C in terms of parameters and gives it to a control engineer, who then has to select an optimal control U^* according to the performance index (PI) J based on the given plant A, B, C. Clearly, this is a fixed-step design process. The plant will effect the optimal control and, consequently, the optimal performance index. However, for our applications, the plant, i.e., the flexible beam, can be constructed differently. Therefore, one must evaluate different plant designs to improve the performance. While the mechatronic

design is that it chooses the best plant and finds out the associated controller for the performance requirement. It is an overall optimization process, as in Fig. (6.2).

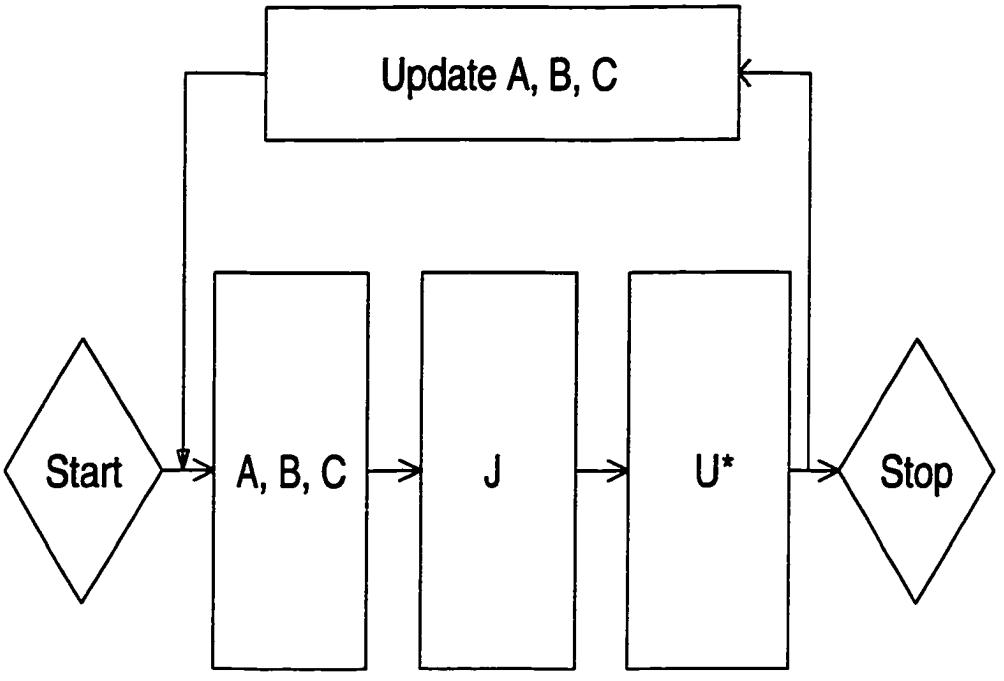

Figure 6.2: Mechatronic Design Algorithm

To explain this clearly, let's assume that Ω is the space of all feasible manipulator designs. Then the objective is to minimize the performance index with respect to link construction, and control design, i.e.,

$$J^* = \inf_{(A,B,C)\in\Omega, u\in\Lambda} J(u; A, B, C) \tag{6.12}$$

Obviously, the mechatronic approach considers the mechanical, electronical, and control components of a robotic flexible manipulator as a whole and carries their developments out simultaneously. Clearly, this concurrent design approach should lead to

a global optimal performance because now the coupling effects and the interrelations between these different parts of the manipulator system are taken into account in the very beginning of the design process. This is the so-called mechatronic design approach.

Since,

$$J^* = \inf_{(A,B,C)\in\Omega, u\in\Lambda} J(u; A, B, C) = \inf_{(A,B,C)\in\Omega} [\inf_{u\in\Lambda} J(u; A, B, C)], \tag{6.13}$$

the global optimization can be carried in two steps. The first step (the inner-loop optimization) is to find an optimal control and its associated optimal value of the performance index based on a given plant (A, B, C), which is the traditional optimal control design problem, as discussed in Section 6.1. The second step (the outer loop optimization) is to find a feasible plant that will minimize the performance index obtained by the optimal controller, as in Section 6.2. With the iterative process of these two steps, the global optimum solution is finally reached. When the LQR formulation is used, this will lead to,

$$\begin{aligned} J^* = \inf_{(A,B,C)\in\Omega, u\in\Lambda} J(u; A, B, C) &= \inf_{(A,B,C)\in\Omega} [\inf_{u\in\Lambda} J(u; A, B, C)] \\ &= \inf_{(A,B,C)\in\Omega} tr[P(A, B, C)X] \end{aligned} \tag{6.14}$$

where P is found by solving the equations given in the previous section.

Based on the open-loop optimal design [80], conventional optimization methods, such as gradient-based methods, are not effective in solving the outer-loop optimization problem since so many variables are involved in the optimization procedure.

Therefore, an Improved Hit and Run (IHR) [114] adaptive random search algorithm is used for the outer-loop optimization. However, some modifications must be made to ensure a constant volume during the optimization process and the minimum stress requirement as discussed early.

For the sake of simplicity, only one situation is considered where the area of cross sections determines both the mass and stiffness distributions of the flexible beam (such as circular cross sections or rectangular cross sections with fixed width/height or fixed ratio of width and height). In this case, we only need find out the width distribution with a constant beam weight. The IHR algorithm can search all the space of feasible beam heights, and the LQR algorithm will calculate the best PI for a given height distribution by choosing an optimal feedback. This algorithm can be easily applied to other situations with minor modifications such as in circular beam. Now the combined iterative procedure of the modified IHR and the LQR with output feedback can be specified as:

IP–Intergrated Optimization

1. Set design vector $\Xi = [I_H, M_p, a_c, J_p, L, B, E]$, and number of segments, N. Set step multiplier MUL to 1 and FACTOR to an appropriate constant.
2. Set weighting matrices Q and R.
3. Load precalculated coefficients for Modal Shapes.

4. Calculate A_0 (uniform shape radius or width) from Chapter 5, set initial $index = 0$, call **LQR** to get the corresponding J_0.

5. Update the area vector, A_j,

   1). call **IHR**, to find the A_j

   2). based on Mode Shape coefficients and current link geometric, calculate mass matrix M, potential matrix K, vector B, C, and state equations after integrated with motor dynamics.

   3). call **LQR** to find J. If the J is improving:

   Set $J_{j+1} = J(A_{j+1})$.

   If J is improved, store it in an array and save this A_j. Update all loop variables and factors.

6. If all the differences between two J's in the array is smaller than stopping criteria, stop. Otherwise, go to Step 5.

7. Stop: Output optimal feedback matrix $\Re^*$, optimal performance index J^*, and optimal flexible link structure A^*.

6.4 Results and Discussion

In order to verify the mechatronic method presented in this chapter, a rectangular aluminum flexible link is used for simulation. The mechatronic algorithm is intended to find the beam geometric shape, or the width distribution so that the PI reaches the minimum.

To meet the minimum stress requirement pointed out earlier, the maximum width H_{max} and the minimum width H_{min} are set at twice and a quarter of the uniform width separately. For the IHR algorithm, all criteria values were set to 0.000001.

To fully test this mechatronic design algorithm, the different output feedback, combined with various state weighting matrix Q, and the number of segments N, but $R = I$ (identity) were tried. Three sets of feedback were considered. They were the hub tangent angle $\{\Theta(0,t)\}$ feedback (Eq. (5.21)), the hub tangent angle with the tip deflection $\{\Theta(0,t), w(L,t)\}$ (Eq. (5.19), Eq. (5.21)), and the hub tangent angle with the tip position $\{\Theta(0,t), v(L,t)\}$ (Eq. (5.20), Eq. (5.21)). These sets of feedback have very clear physical meanings and are detectable. The initial state set is $q_1(0) = [\sqrt{10}, 0, ...0]^T$. The senario ($\{$*feedback list*$\}$, *number of segments*, Q) was used, meaning that the feedback strategy is as $\{$*feedback list*$\}$, that the beam is divided into *number of segments*, and that the value Q in LQR is Q. These notations are applied in the following figures and tables.

Note that it was necessary to show the PI's with different number of segments. To do that, a performance index was set with $q(0) = q_1(0)$, $Q = 100 * I$, and with various $n = 4, 6, 12$, and one of these three sets of feedback. For uniform and associated optimal shape, performance indexes were obtained with different feedback and different number of segments as Table 6.1. Column one is the type of feedback, while the column 2, column 3 and column 4 are for the different number of segments

respectively. The performance indexes of the optimal shape are improved over that of the associated uniform shape. For example, when $n = 4$ and $\{\Theta(0,t), w\}$ feedback is applied, the PI for uniform shape is 3789.143, while the result of mechatronic design is smaller, which is 3591.341. But the number of segments has less impacts on the performance index than the type of the feedback. The associated feedback constants are listed in Table 6.2.

Table 6.1: Performance Index with $Q = 100 * I$.

Feedbacks List	$n = 4$	$n = 6$	$n = 12$
$\{\Theta(0,t)\}$ feedback -uniform shape	4665.504	4665.504	4665.504
$\{\Theta(0,t)\}$ feedback -optimal shape	4647.230	4646.571	4643.038
$\{\Theta(0,t), w\}$ feedback -uniform shape	3789.143	3789.143	3789.143
$\{\Theta(0,t), w\}$ feedback -optimal shape	3591.341	3585.945	3580.064
$\{\Theta(0,t), v\}$ feedback -uniform shape	4342.569	4342.569	4342.569
$\{\Theta(0,t), v\}$ feedback -optimal shape	4180.548	4178.569	4176.437

Table 6.2: Optimal Feedback Constants with $Q = 100 * I$.

Feedback List	$n = 4$	$n = 6$	$n = 12$
$\{\Theta(0,t)\}$ -uniform	3.674	3.674	3.674
$\{\Theta(0,t)\}$ -optimal	3.686	3.677	3.675
$\{\Theta(0,t), w\}$ -uniform	(2.7599 -422.398)	(2.7599 -422.398)	(2.7599 -422.398)
$\{\Theta(0,t), w\}$ -optimal	(2.498 -337.071)	(2.539 -380.396)	(2.423 -378.554)
$\{\Theta(0,t), v\}$ -uniform	(2502.705 -2499.521)	(2502.707 -2499.521)	(2502.705 -2499.521)
$\{\Theta(0,t), v\}$ -optimal	(1768.423 -1765.672)	(1732.346 -1747.358)	(1746.276 -1764.428)

The related optimal shapes are illustrated as following. In all figures, the solid outline is the optimal shape, and the dot one is for the unif orm shape. The horizontal axis is the link spatial coordinate, the vertical one is the beam width. Fig. (6.3 - 5) are for $\Theta(0,t)$ feedback (hub tangent angle) with $Q = 100 * I$ and $n = 4, 6, 12$

separately. All three optimal shapes have one common feature with a large size at the hub end, a small size at the tip end.

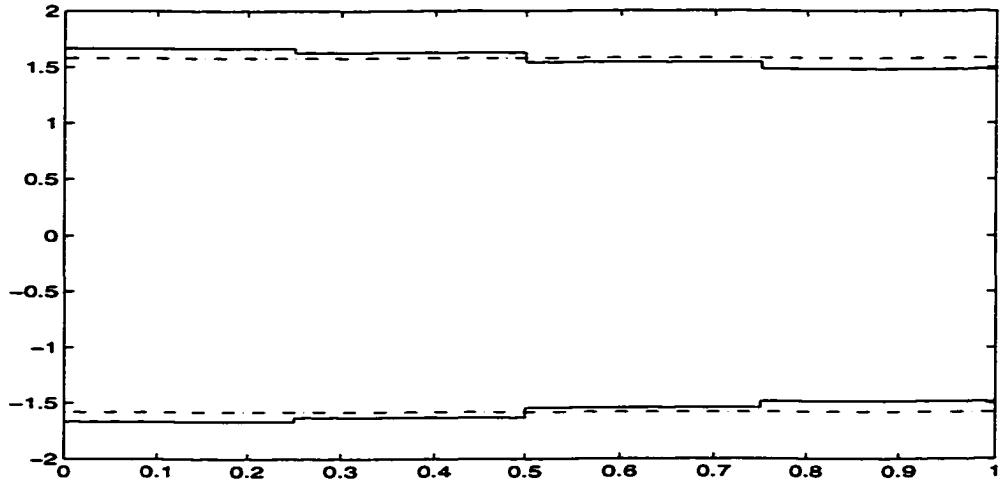

Figure 6.3: Optimal Shape for ($\{\Theta(0,t)\}$, 4, 100)

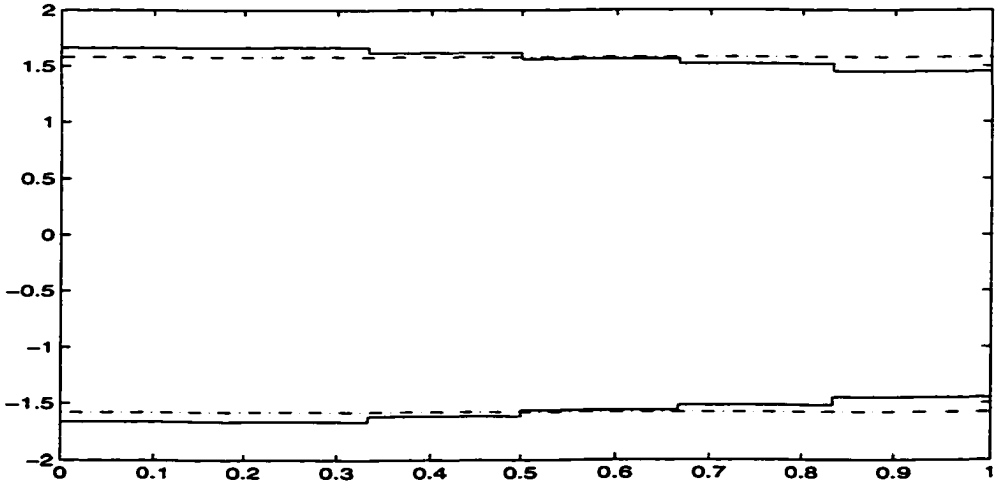

Figure 6.4: Optimal Shape for ($\{\Theta(0,t)\}$, 6, 100)

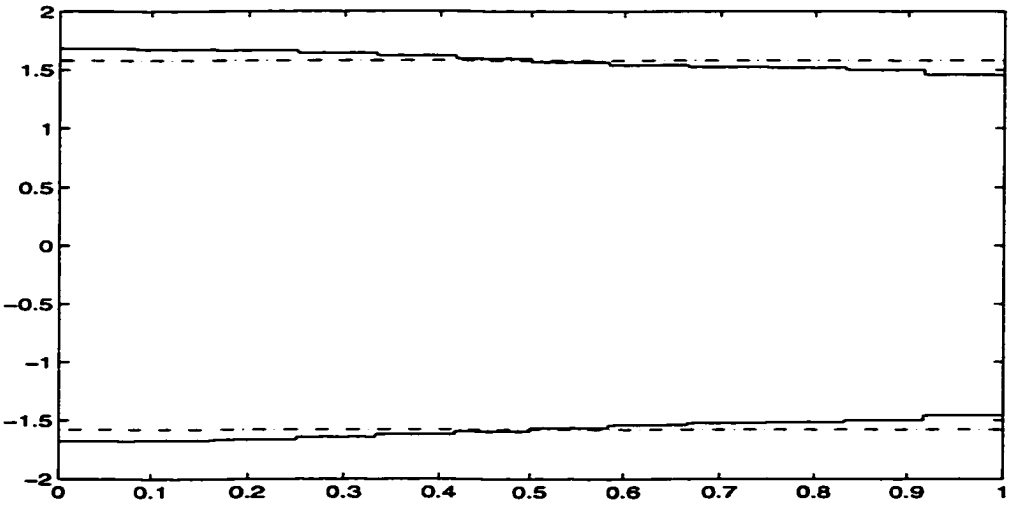

Figure 6.5: Optimal Shape for ($\{\Theta(0,t)\}$, 12, 100)

Fig. (6.6 - 8) are for $(\Theta(0,t), w(L,t))$ feedback (hub tangent angle, tip deflection) with $Q = 100 \star I$ and $n = 4, 6, 12$ separately. In the same behavior, the best performance indexes are almost the same for different number of segments. A common feature for these three optimal shapes is a large beam size in the middle, and a relatively small size at both ends.

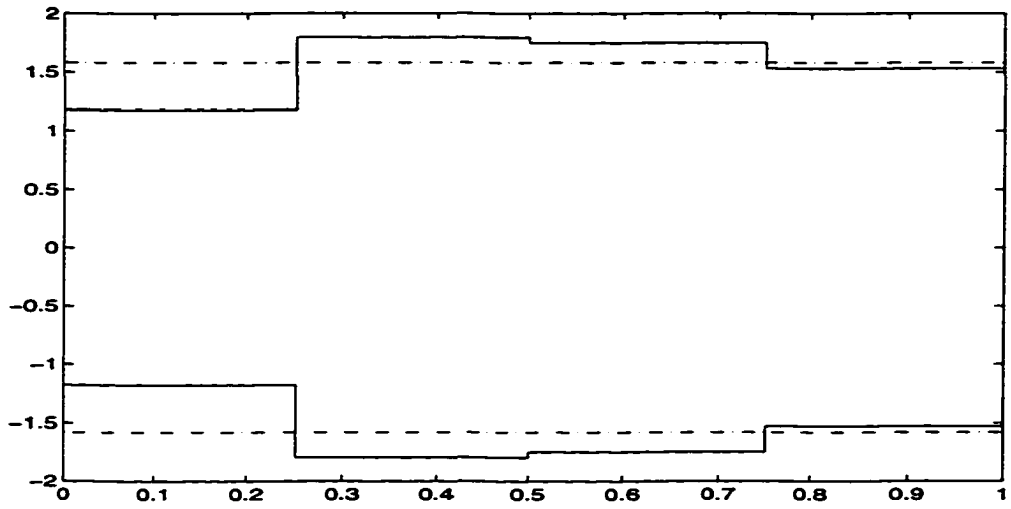

Figure 6.6: Optimal Shape for ($\{\Theta(0,t), w\}$, 4, 100)

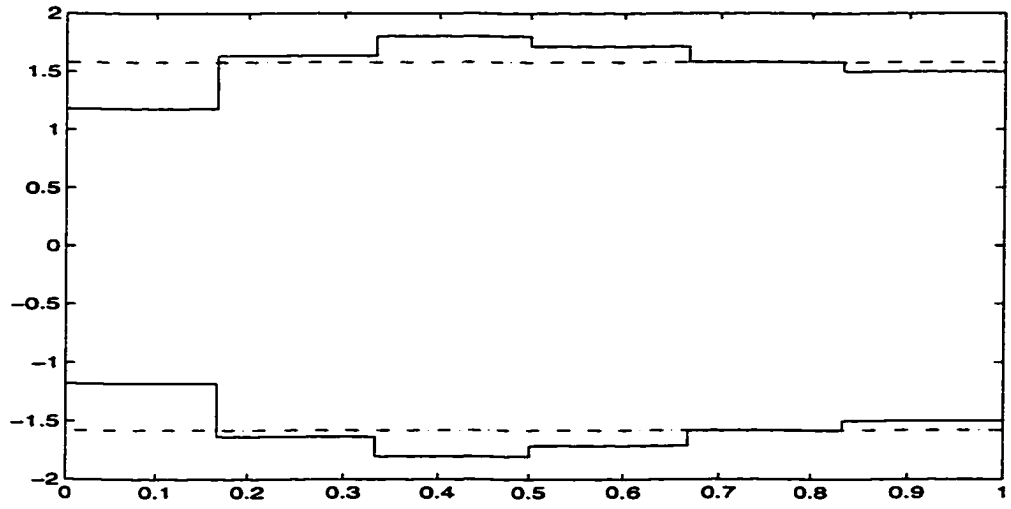

Figure 6.7: Optimal Shape for ($\{\Theta(0,t), w\}$, 6, 100)

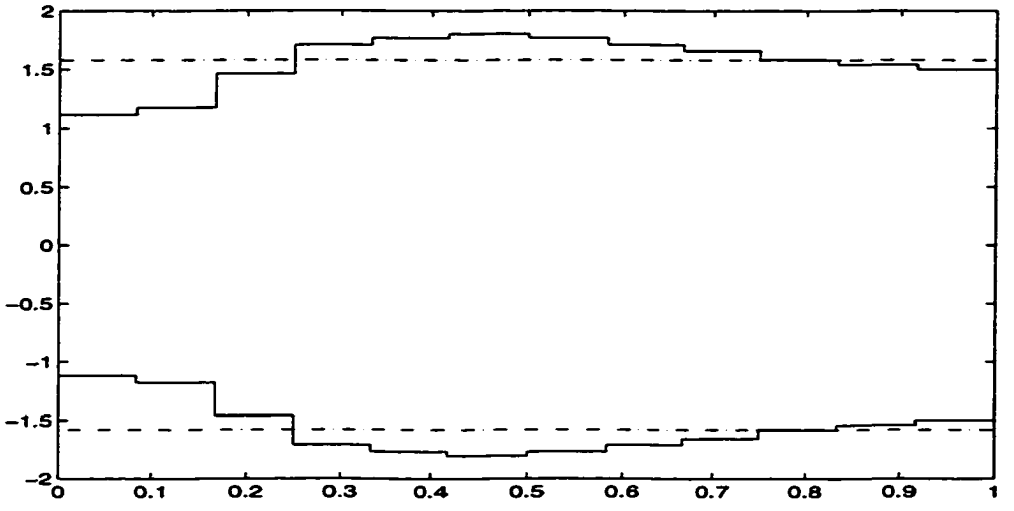

Figure 6.8: Optimal Shape for ($\{\Theta(0,t), w\}$, 12, 100)

Fig. (6.9 - 11) are for $(\Theta(0,t), v(L,t))$ feedback (hub tangent angle, tip position) with $Q = 100 \star I$ and $n = 4, 6, 12$ respectively. As usual, the best performance indexes are almost the same for different numbers of segments. A common feature for these three optimal shapes is a relatively small beam dimension in the middle, and a large dimension at the ends.

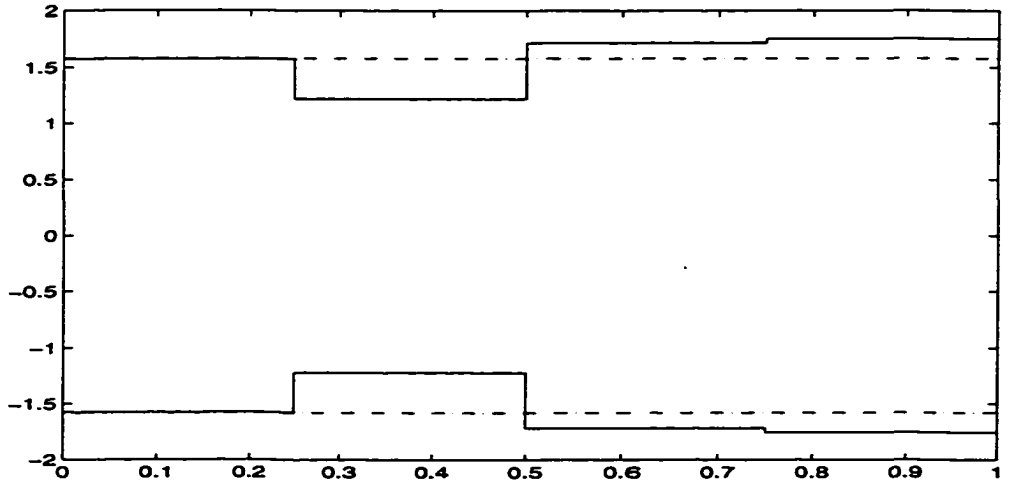

Figure 6.9: Optimal Shape for $(\{\Theta(0,t),v\}, 4, 100)$

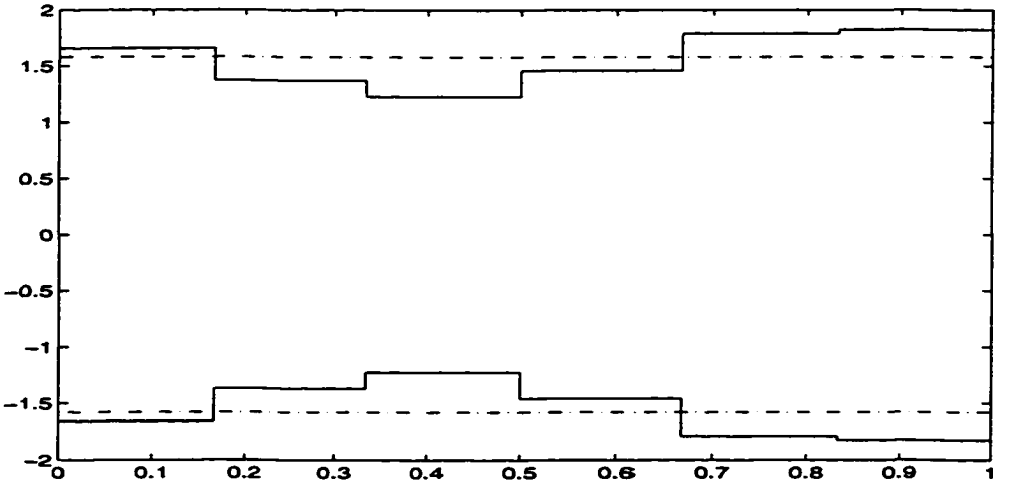

Figure 6.10: Optimal Shape for $(\{\Theta(0,t),v\}, 6, 100)$

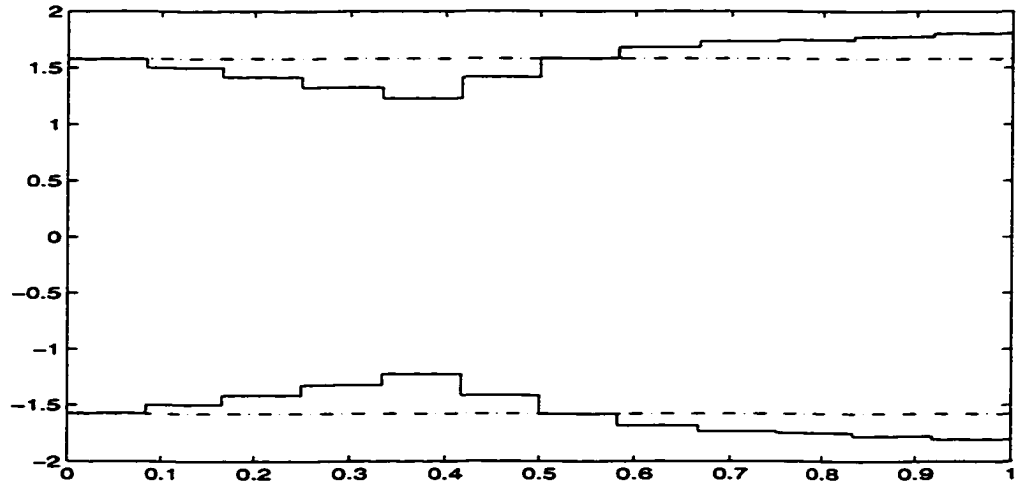

Figure 6.11: Optimal Shape for ($\{\Theta(0,t), v\}$, 12, 100)

As shown in these figures, the geometric shapes of these optimal shape are pretty much relied on the type of the feedback, not much relied on the number of segments. Next, this mechatronic approach was applied to different weighting matrix Q with these types of feedback. But the number of segments fixed as 4 since the number of segments plays a less important role here. Q are $50 * I$ and $10 * I$ separately. The performance indexes are listed in Table 6.3, where the column is for

different type of feedback, and the row is for the value of Q. The associated feedback constants are listed in Table 6.4.

Table 6.3: Performance Index with Different $Q = 100 * I, 50 * I, 10 * I$.

Beam Shape	$\{\Theta(0,t)\}$	$\{\Theta(0,t), w\}$	$\{\Theta(0,t), v\}$
$Q = 100 * I$ -uniform shape	4665.504	3781.547	4342.763
$Q = 100 * I$ -optimal shape	4647.230	3591.538	4180.546
$Q = 50 * I$ -uniform shape	2611.373	2174.499	2421.595
$Q = 50 * I$ -optimal shape	2540.470	2098.374	2388.850
$Q = 10 * I$ -uniform shape	679.856	630.266	670.482
$Q = 10 * I$ -optimal shape	663.834	621.442	638.356

Table 6.4: Optimal Feedback Constants with Different $Q = 100 * I, 50 * I, 10 * I$.

Beam Shape	$\{\Theta(0,t)\}$	$\{\Theta(0,t), w\}$	$\{\Theta(0,t), v\}$
$Q = 100 * I$ -uniform shape	3.674	(2.7599 -422.398)	(2502.705 -2499.521)
$Q = 100 * I$ -optimal shape	3.686	(2.498 -337.071)	(1768.423 -1765.672)
$Q = 50 * I$ -uniform shape	(2.7599 -422.398)	(2.279 -395.458)	(2.7599 -422.398)
$Q = 50 * I$ -optimal shape	(2.759 -422.398)	(2.096 -335.370)	(2.423 -378.554)
$Q = 10 * I$ -uniform shape	1.659	(1.604 -167.576)	(1138.098 -1194.508)
$Q = 10 * I$ -optimal shape	1.653	(1.386 -166.142)	(1045.568 -1065.754)

Fig. (6.12 - 13) are for $\Theta(0,t)$ feedback (hub tangent angle) with different weighting matrix Q. As usual, the optimal shapes have relatively large dimensions at the hub side.

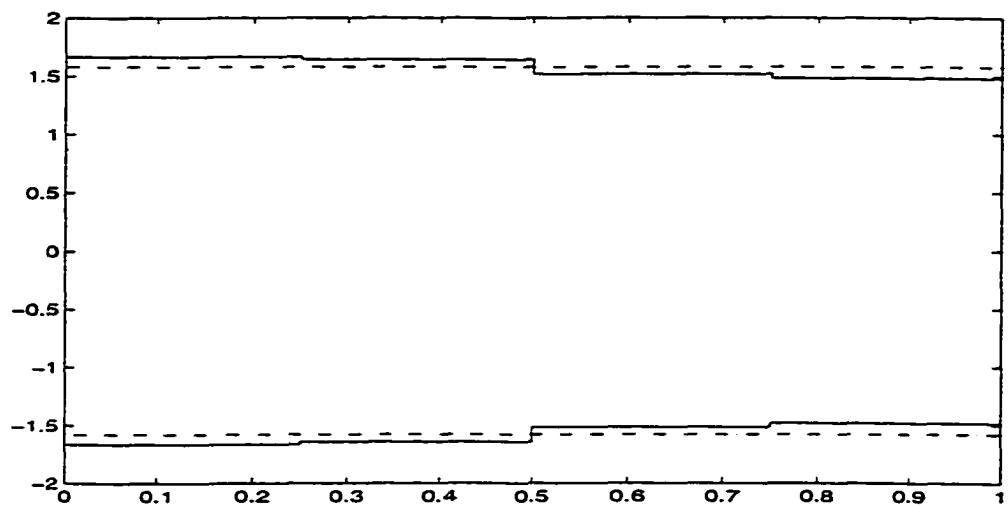

Figure 6.12: Optimal Shape for ($\{\Theta(0,t)\}$, 4, 50)

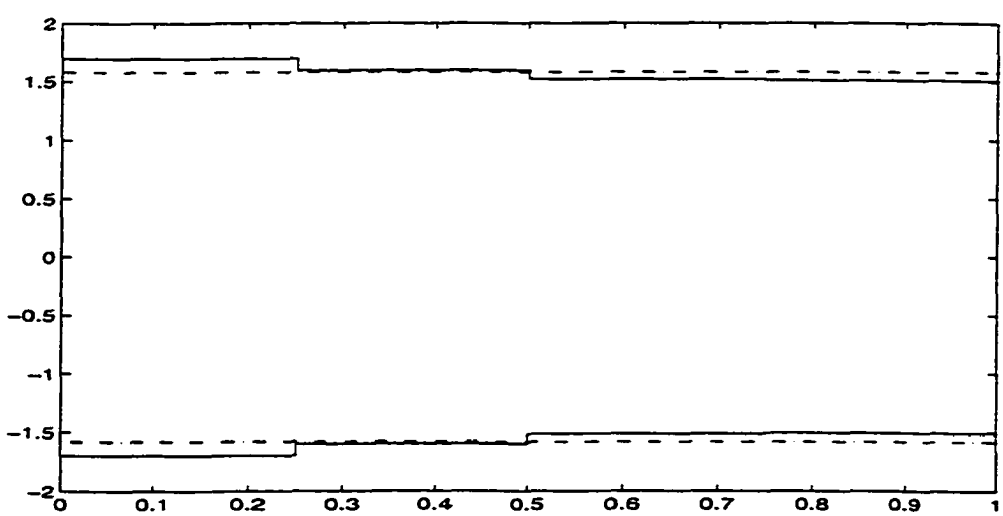

Figure 6.13: Optimal Shape for ($\{\Theta(0,t)\}$, 4, 10)

Fig. (6.14 - 15) are for $(\Theta(0,t), w(L,t))$ feedback (hub tangent angle, tip deflection) with a different weighting matrix Q. The optimal shapes have a relatively large dimension at the middle.

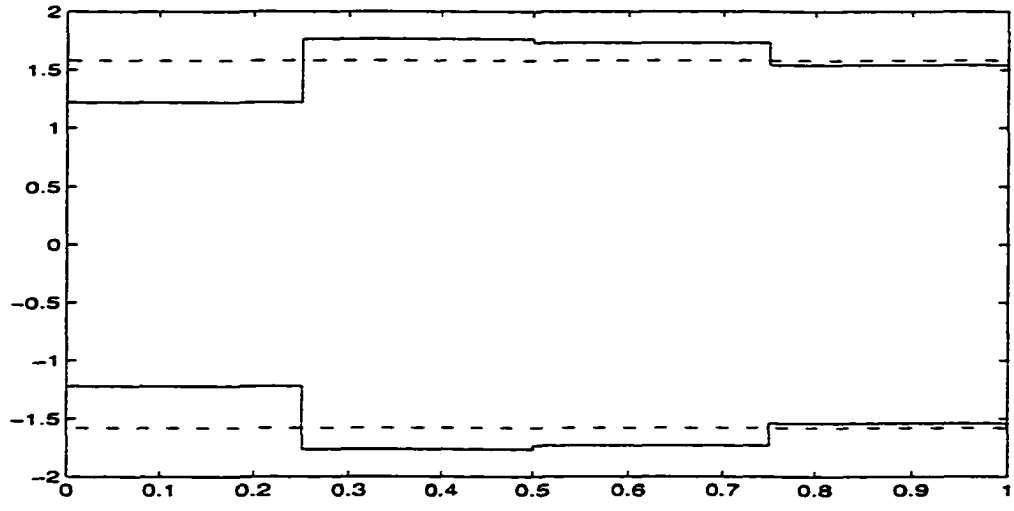

Figure 6.14: Optimal Shape for $(\{\Theta(0,t), w\}, 4, 50)$

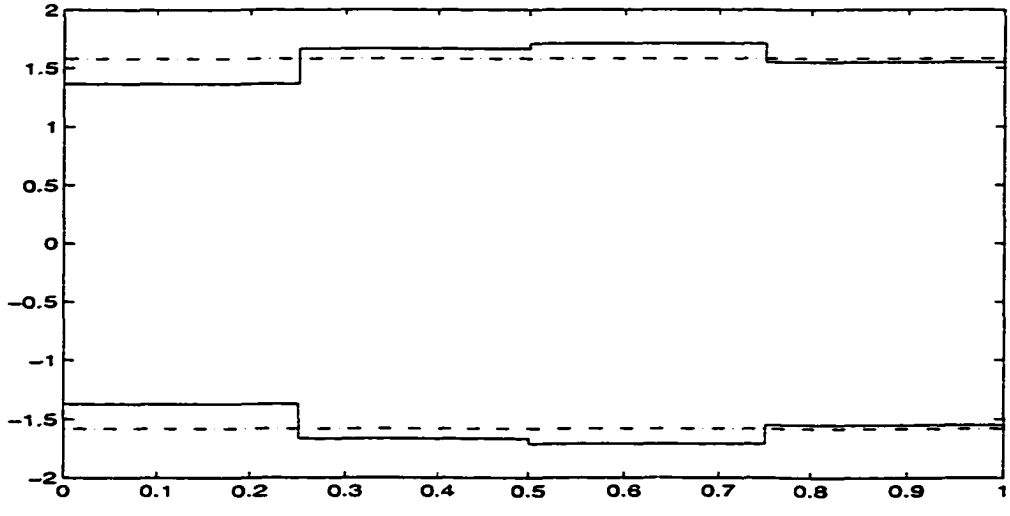

Figure 6.15: Optimal Shape for $(\{\Theta(0,t), w\}, 4, 10)$

Fig. (6.16 - 17) are for $(\Theta(0,t), v(L,t))$ feedback (hub tangent angle, tip position) with different weighting matrix Q. The optimal shapes have relatively small dimensions in the middle.

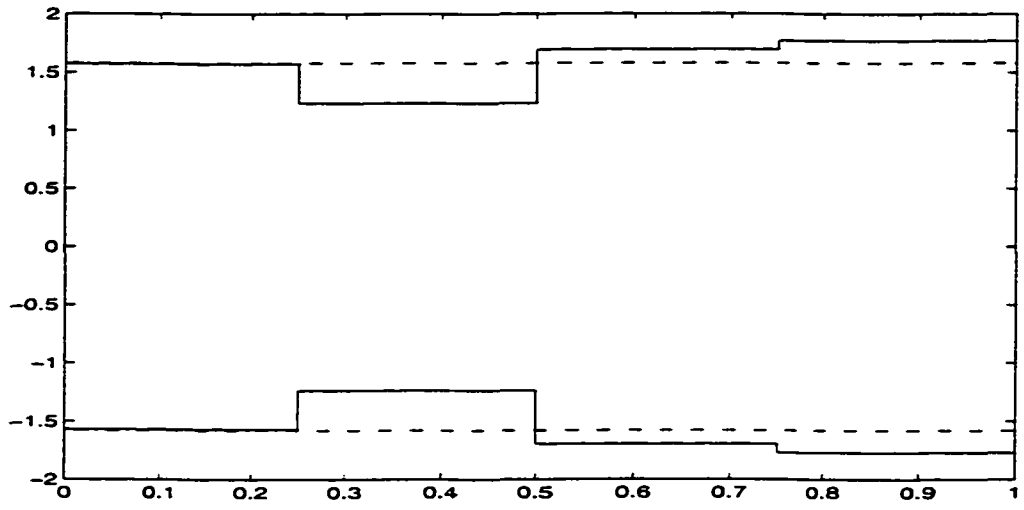

Figure 6.16: Optimal Shape for $(\{\Theta(0.t), v\}, 4.50)$

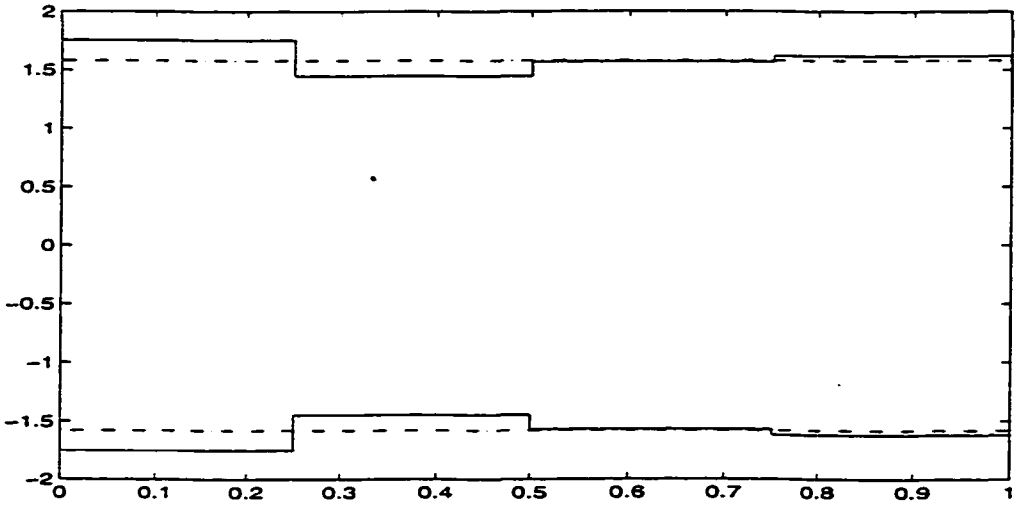

Figure 6.17: Optimal Shape for $(\{\Theta(0.t), v\}, 4.10)$

Fig. (6.18 - 19) are the hub tangent angle responses to initial state $q_1(0)$ for $\Theta(0,t)$ (hub tangent angle) and $(\Theta(0,t), w(L,t))$ (hub tangent angle, tip deflection) feedback separately.

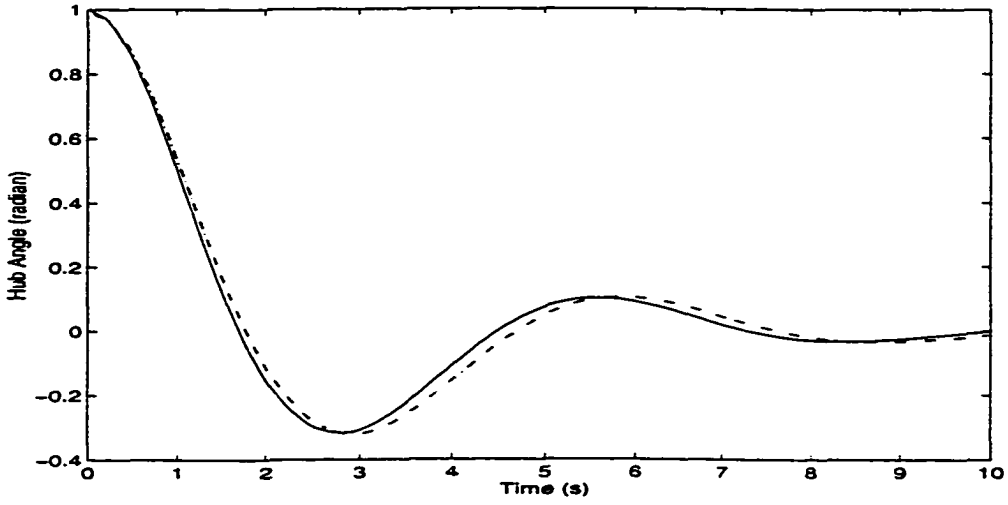

Figure 6.18: Hub Tangent Angle Initial Response for $(\{\Theta(0,t)\}, 4, 100)$

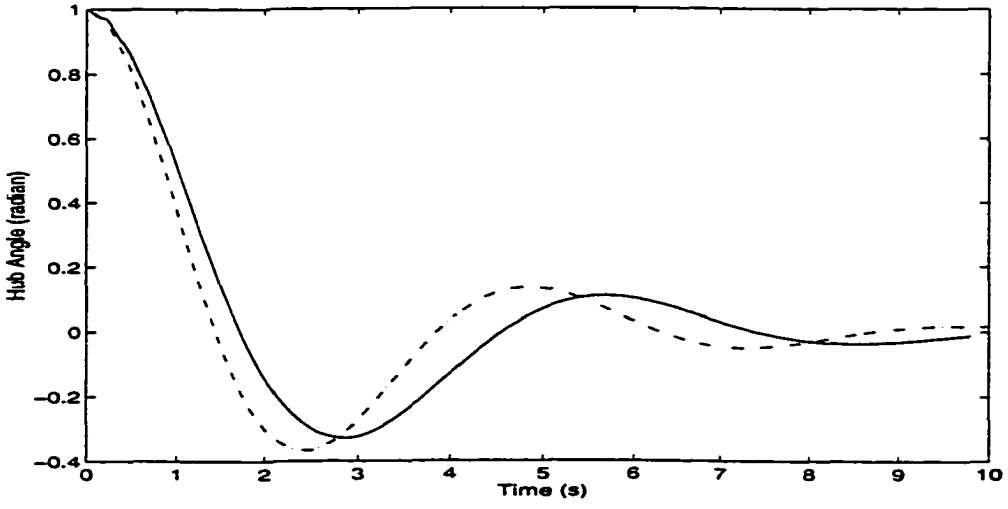

Figure 6.19: Hub Tangent Angle Initial Response for $(\{\Theta(0,t), w(L,t)\}, 4, 100)$

Fig. (6.20 - 21) are the hub tangent angle responses to step input for $\Theta(0,t)$ (hub tangent angle) and $(\Theta(0,t), w(L,t))$ (hub tangent angle, tip deflection) feedback separately.

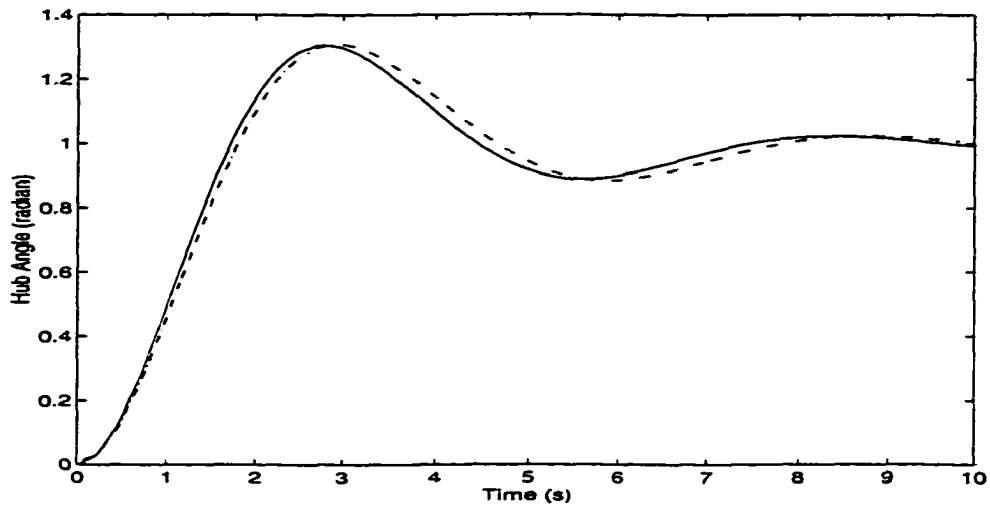

Figure 6.20: Hub Tangent Angle Step Input Response for $(\{\Theta(0.t)\}, 4, 100)$

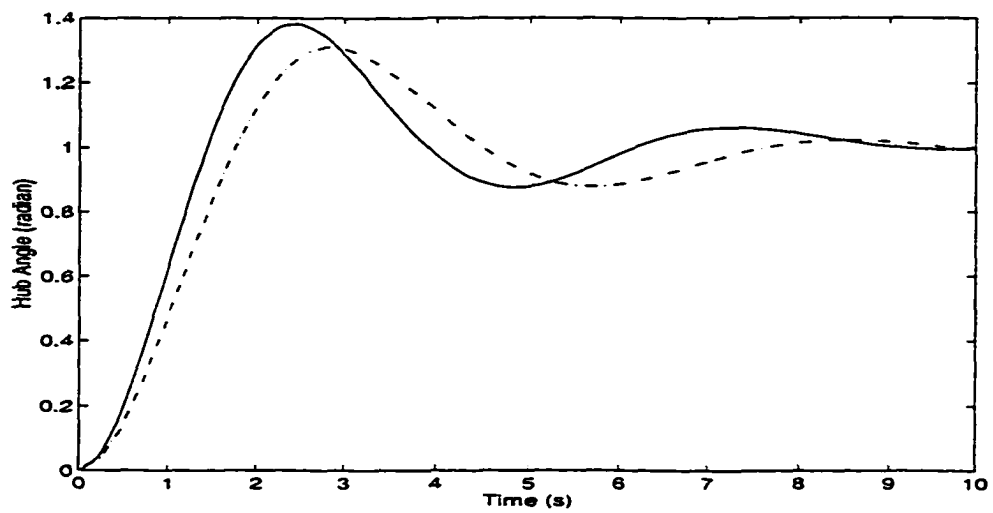

Figure 6.21: Hub Tangent Angle Step Input Response for $(\{\Theta(0.t), w(L.t)\}, 4, 100)$

Fig. (6.22 - 23) are the tip deflection responses to initial $q_1(0)$ for $\Theta(0,t)$ (hub tangent angle) and $(\Theta(0,t), w(L,t))$ (hub tangent angle, tip deflection) feedback separately.

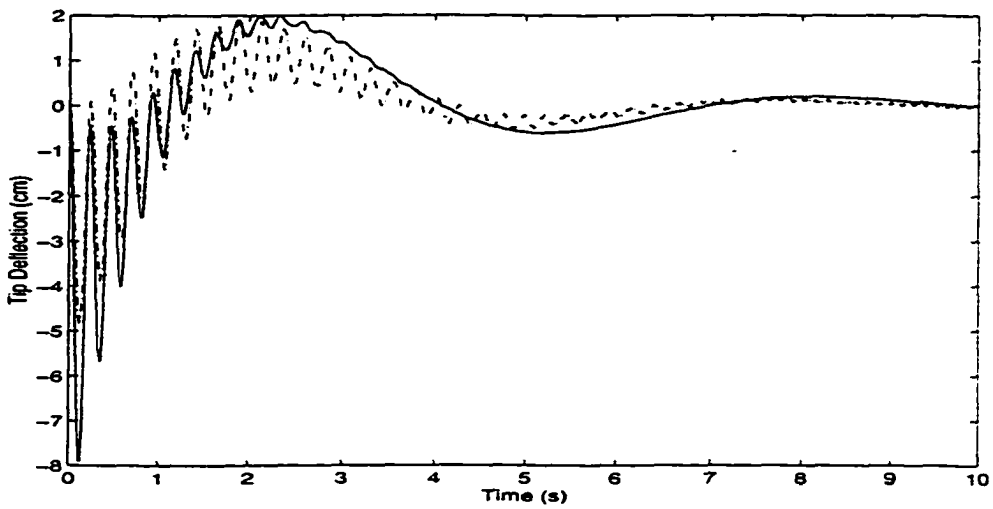

Figure 6.22: Tip Deflection Initial Response for $(\{\Theta(0,t)\}, 4, 100)$

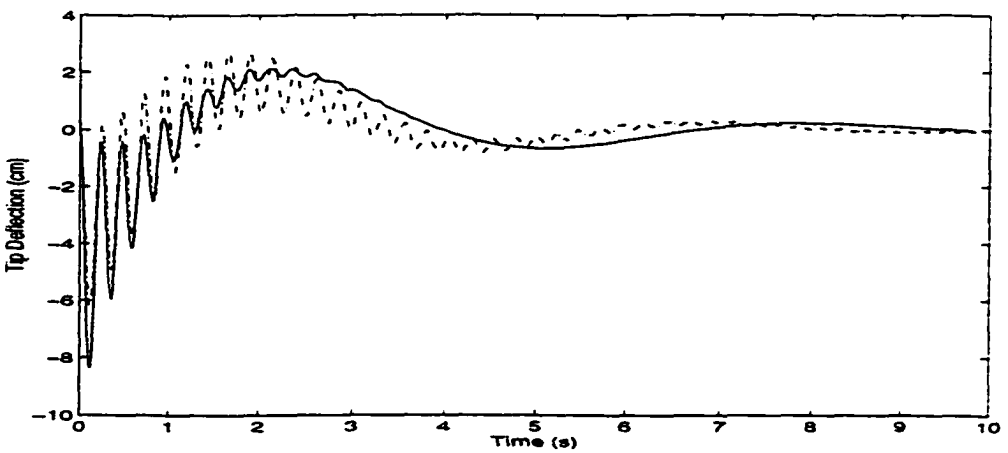

Figure 6.23: Tip Deflection Initial Response for $(\{\Theta(0,t), w(L,t)\}, 4, 100)$

Fig. (6.24-25) are the tip deflection step input responses for $\Theta(0,t)$ (hub tangent angle) and $(\Theta(0,t), w(L,t))$ (hub tangent angle, tip deflection) feedback separately.

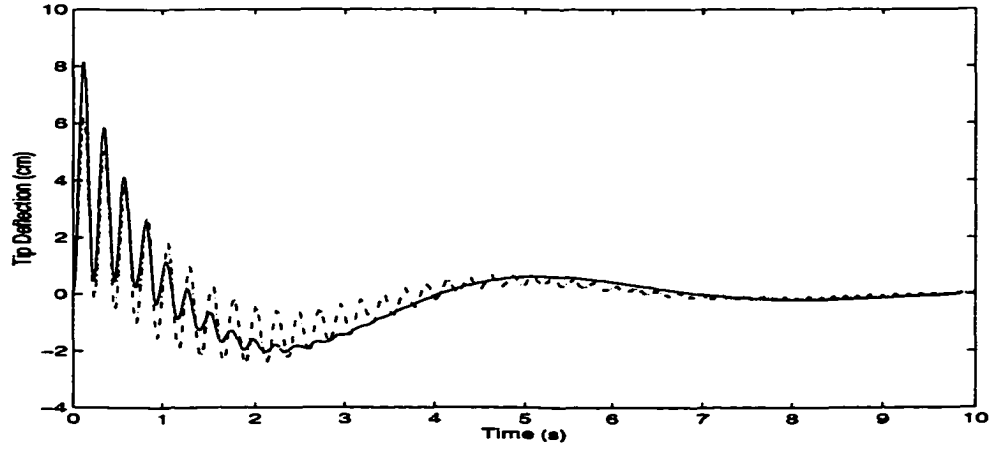

Figure 6.24: Tip Deflection Step Input Response for ($\{\Theta(0,t)\}$, 4, 100)

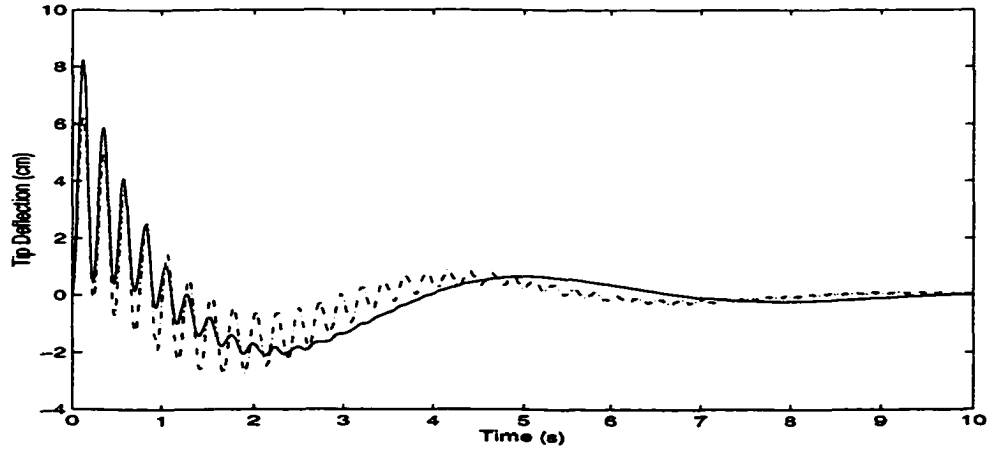

Figure 6.25: Tip Deflection Step Input Response for ($\{\Theta(0,t), w(L,t)\}$, 4, 100)

These results show that the performance index does not depend much on the number of segments, because according to this mechatronic algorithm, the final shape converges to its optimal shape. A system with two output feedbacks has a relatively lower performance index than one with only one output feedback, since the former has a higher degree of freedom to work with. The optimal shape for $\Theta(0,t)$ feedback is always a larger at the hub side, and smaller at the tip end. The optimal shape to $\{\Theta(0,t), w(L,t)\}$ has smaller dimensions at the ends, while the optimal shape to $\{\Theta(0,t), v(L,t)\}$ is smaller in the middle. For optimal shapes, the initial responses have less vibration and fast convergence. The step input response of hub tangent angle for the optimal shape has a smaller rising time and the tip deflection converges much faster than those of uniform shapes.

CHAPTER 7

MECHATRONIC DESIGN BASED ON H_∞ CONTROLLER WITH IHR ALGORITHM

Since the work of Zames [115] in feedback controller to minimize the H_∞ norm for the closed-loop transfer function, H_∞ design has raised a lot interest in robust control for complex systems such as parameter distributed systems. A four-block, a two-block and a one-block formula were developed for H_∞ control by Foias [23] and references therein. In its applications to flexible manipulator control, most early concerns were with frequency domain. μ-synthesis [5] was pursued as an extended H_∞ approach. Sideris and Rotstein [87] developed a combination technique of frequency-domain with time-domain constraints. Tchernychev *et al* [91] presented experimental comparisons for these controllers. Recently, Glover and Doyle [21] [32] gave the state-space solutions of H_∞-norm for a generalized plant with frequency weighting transfer functions, internally stabilizing the closed-loop system while minimizing the norm of error transfer functions. Fujita and co-authors [25] applied this method to a flexible beam magnetic suspension system.

The main issue in the application of an H_∞ control technique is the use of an appropriate model and a quantitative description of model uncertainty. In this pursuit, state-space model uncertainties arise. Furthermore, a generalized plant with

two frequency weighting functions results. The IHR algorithm is also applied to search the best beam shape as in Chapter 6. A number of results are presented to demonstrate the robustness of the designed H_∞ controller.

7.1 State-Space Formulae for H_∞ Control Problem

A basic block diagram used in state-space H_∞ controller [21] [32] is

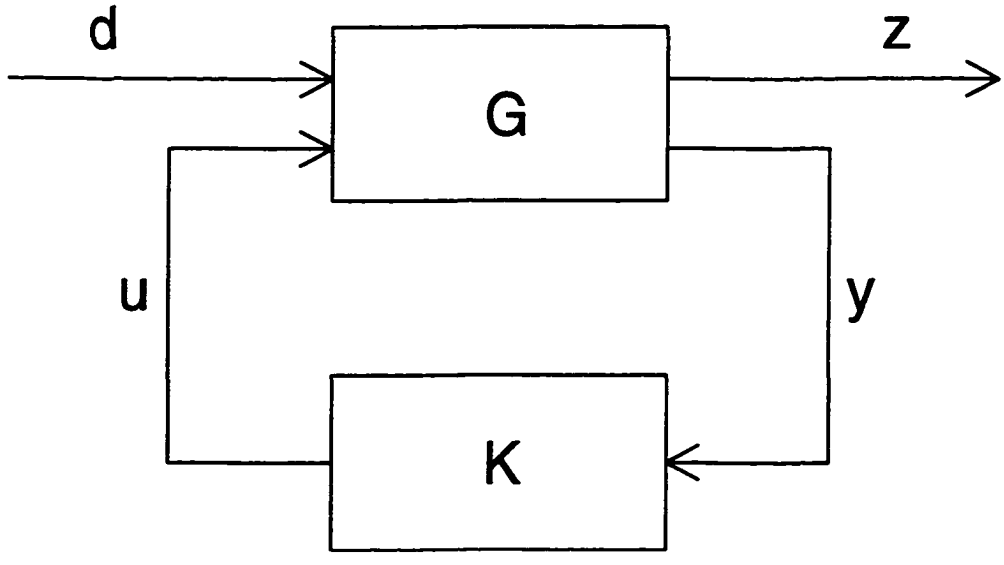

Figure 7.1: H_∞ Control Problem Configuration

where $G(s)$ is a generalized plant which includes what is usually called plant and all weighting functions, and K is the controller. They are all real-rational and proper. All external inputs such as disturbances, measurement noise, model uncertainties, and unmodeled high order vibrational dynamics are characterized as d. Signal z is the error output, u is the control input and y is the measured variable.

If state-space equations in [32] is referred, the linear system

$$\dot{x}(t) = Ax(t) + B_1 d(t) + B_2 u(t), \tag{7.1}$$

$$z(t) = C_1 x(t) + D_{11} d(t) + D_{12} u(t), \tag{7.2}$$

$$y(t) = C_2 x(t) + D_{21} d(t) + D_{22} u(t) \tag{7.3}$$

is obtained. Then the transfer function $G(s)$ is denoted as

$$G(s) = \begin{bmatrix} G_{11}(s) & G_{12}(s) \\ G_{21}(s) & G_{22}(s) \end{bmatrix} =$$

$$\begin{bmatrix} C_1 \\ C_2 \end{bmatrix} (sI - A)^{-1} \begin{bmatrix} B_1 & B_2 \end{bmatrix} + \begin{bmatrix} D_{11} & D_{12} \\ D_{21} & D_{22} \end{bmatrix} := \begin{bmatrix} A & B_1 & B_2 \\ C_1 & D_{11} & D_{12} \\ C_2 & D_{21} & D_{22} \end{bmatrix} = \begin{bmatrix} A & B \\ C & D \end{bmatrix} \tag{7.4}$$

The transfer function from d to z is

$$T_{dz}(G, k) = G_{11} + G_{12} K (I - G_{22})^{-1} G_{21} \tag{7.5}$$

Then the H_∞ control problem is to design the controller $K(s)$, so that

1. the system is internally stable, that is, the states of $G(s)$and $K(s)$ go to zero from all initial values when $d = 0$,

2. $\min ||T_{dz}||_\infty = \min \sup_\omega \overline{\Delta}(T_{dz}(j\omega))$, where $\overline{\Delta}()$ denotes the maximum singular value.

If A, R, Q are $n \times n$ matrix and with symmetric R, Q, the Hamiltonian matrix is defined as

$$H := \begin{bmatrix} A & R \\ -Q & -A' \end{bmatrix}.$$

Then there exists a symmetric $x := Ric(H)$ which satisfies the Riccati equation

$A\dot{x} + xA' + xRx + Q = 0.$

Two Hamiltonian matrices are involved in the H_∞ control problem,

$$H_\infty := \begin{bmatrix} A & r^{-2}B_1B_1' - B_2B_2' \\ -C_1'C_1 & -A' \end{bmatrix}, \tag{7.6}$$

$$J_\infty := \begin{bmatrix} A' & r^{-2}C_1'C_1 - C_2'C_2 \\ -B_1B_1' & -A \end{bmatrix}. \tag{7.7}$$

For $||T_{dz}||_\infty \leq r$, a performance index for noise attentuation from input d to output z, an admissible H_∞ controller [21] exists iff

1. $X_\infty := Ric(H_\infty) \geq 0$,

2. $Y_\infty := Ric(J_\infty) \geq 0$,

3. and $\rho(X_\infty Y_\infty) \leq r^2$, where $\rho(.)$ is the maximum singular value.

One such controller is

$$K(s) := \begin{bmatrix} A_\infty & -Z_\infty L_\infty \\ F_\infty & 0 \end{bmatrix}, \tag{7.8}$$

where

$A_\infty = A + r^{-2}B_1B_1'X_\infty + B_2F_\infty + Z_\infty L_\infty C_2,$

$F_\infty = -B_2' X_\infty$,

$L_\infty = -Y_\infty C_2'$,

$Z_\infty = (I - r^{-2} Y_\infty X_\infty)^{-1}$.

As seen from the above formulae, $K(s)$ is coupled with r. In this case, the attempt is made to find a minimum r to which the above three conditions still hold and $K(s)$ exits, so that the attenuation from error inputs d to error output z reaches the maximum degree.

In the next sections, the flexible beam system is modeled referring to Eq. (7.1) -Eq. (7.3), and an iterative algorithm is implemented to search the possible minimum r.

7.2 Generalized Plant of a Flexible Beam System

In Eq. (5.4), the omitted high order terms in the kinetics of the tip load are considered to be

$\frac{1}{2} M_p \dot{\theta}^2 w(L,t)^2 + M_p(\dot{\theta} + \dot{w}(L,t)) w(L,t) \dot{\theta} b_c$, then Eq. (5.5) is,

$$T_{pnew} = T_p + \frac{1}{2} M_p \dot{\theta}^2 \sum_{i=1}^{N} \sum_{j=1}^{N} q_i q_j \psi_i(L) \psi_j(L)$$
$$+ M_p b_c \dot{\theta}^2 \sum_{i=1}^{N} q_i \psi_i(L) + M_p b_c \dot{\theta} \sum_{i=1}^{N} \sum_{j=1}^{N} q_i \dot{q}_j \psi_i(L) \psi_j(L). \tag{7.9}$$

In the same way, if the term $\frac{1}{2} \int_0^L (w\dot{\theta})^2 \rho dx$ in Eq. (5.6) is considered, then the link kinetics is,

$$T_{bnew} = T_b + \frac{1}{2} \dot{\theta}^2 \sum_{i=1}^{N} \sum_{j=1}^{N} q_i q_j \int_0^L \psi_i \psi_j \rho dx. \tag{7.10}$$

After going through all derivative processes,

$$M\ddot{x} + Kx = b_{new}, \tag{7.11}$$

is obtained, where

$b_{new} = b\tau + b_0$,

$$b_0 = \begin{bmatrix} -\sum_{i=1}^{N}\sum_{j=1}^{N}(\dot{\theta}q_i\dot{q}_j)\Omega_4(i,j) - 2\sum_{i=1}^{N}(\dot{\theta}\dot{q}_i)\Omega_5(i) - \sum_{i=1}^{N}\sum_{i=1}^{N}(q_i\dot{q}_j)\Omega_6(i,j) \\ \dot{\theta}^2\Omega_5(1) + \dot{\theta}^2\sum_{i=1}^{N}q_i\Omega_4(1,i) + \Omega_6(1,i) \\ \cdot \\ \dot{\theta}^2\Omega_5(j) + \dot{\theta}^2\sum_{i=1}^{N}q_i\Omega_4(j,i) + \Omega_6(j,i) \\ \cdot \\ \dot{\theta}^2\Omega_5(N) + \dot{\theta}^2\sum_{i=1}^{N}q_i\Omega_4(N,i) + \Omega_6(N,i) \end{bmatrix},$$

$\Omega_4(i,j) = M_p\psi_i(L)\psi_j(L) + \int_0^L \psi_i\psi_j\rho dx$,

$\Omega_5(i) = M_p b_c\psi_i(L)$,

$\Omega_6(i,j) = M_p b_c\psi_i(L)\psi_j(L)$.

Then Eq. (5.18) will be,

$$\dot{q} = Aq + Bu + v_0, \tag{7.12}$$

where

$$v_0 = \begin{bmatrix} 0 \\ \overline{M}^{-1}b_0 \end{bmatrix}$$

The system model is now as in Fig. (7.2).

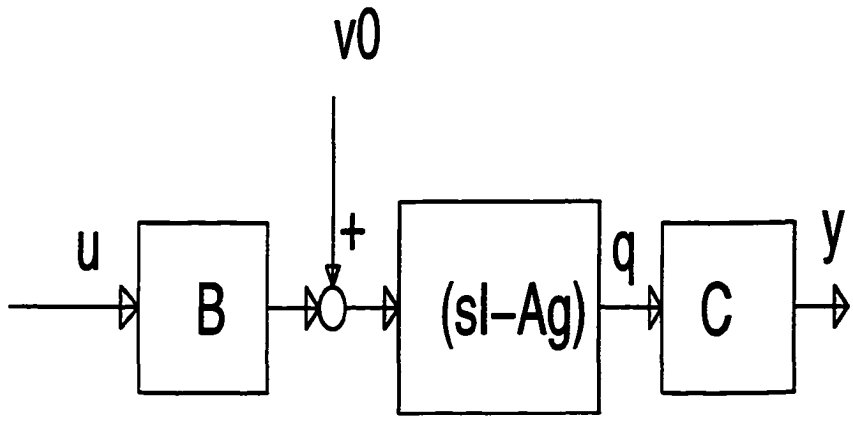

Figure 7.2: System Model Uncertainties

In this model, v_0 is a time-varying term, acting like a system disturbance but originating from model uncertainties. To describe these uncertainties, a frequency weighting function in practice in form of

$$v_0(s) = W_1(s)v(s), \tag{7.13}$$

is introduced, where

$W_1(s) = C_{w1}(sI - A_{w1})^{-1}B_{w1} + D_{w1}$.

$W_1(s)$ will be specified later.

If the fact that measured output y is affected by measuring noise and higher frequency model uncertainties is considered, then the system state-space model in Eq. (5.23) turns into,

$$\dot{q} = A_g q + Bu + D_g v_0, \tag{7.14}$$

$$y = Cq + w_0 \tag{7.15}$$

Where $q = [\theta\ q_1\ q_2\ \ldots\ \dot{q}_1\ \dot{q}_2\ \ldots]'_{n\times n}$, D_g is an identy matrix with the same dimension of q.

Following the same pattern, to describe w_0,

$$w_0(s) = W_2(s)w(s) \tag{7.16}$$

is introduced, where

$W_2(s) = C_{w_2}(sI - A_{w_2})^{-1}B_{w_2} + D_{w_2}$. These coefficients will be specified in next section.

Naturally beam system stability is the main concern, therefore, the regulated variables are chosen as,

$$z_g = q = H_g x \tag{7.17}$$

where H_g is an identity matrix. The 'error vector' is

$$z = \begin{bmatrix} z_1 \\ \\ z_2 \end{bmatrix} = \begin{bmatrix} \Theta z_g \\ \\ \Upsilon u \end{bmatrix} \tag{7.18}$$

where $\Theta = diag(\Theta_1\Theta_2 \ldots \Theta n)$ is the weighting matrix on variable z_g, and Υ is the scalar factor. All states and the control variables are in the 'error vector', and the states are expected to die out to stabilize the closed-loop under the regulation of K, while the control variable will also become zero thus saving energy consumption. The generalized plant of this control problem is in Fig. (7.3).

Let the state variable vector be as

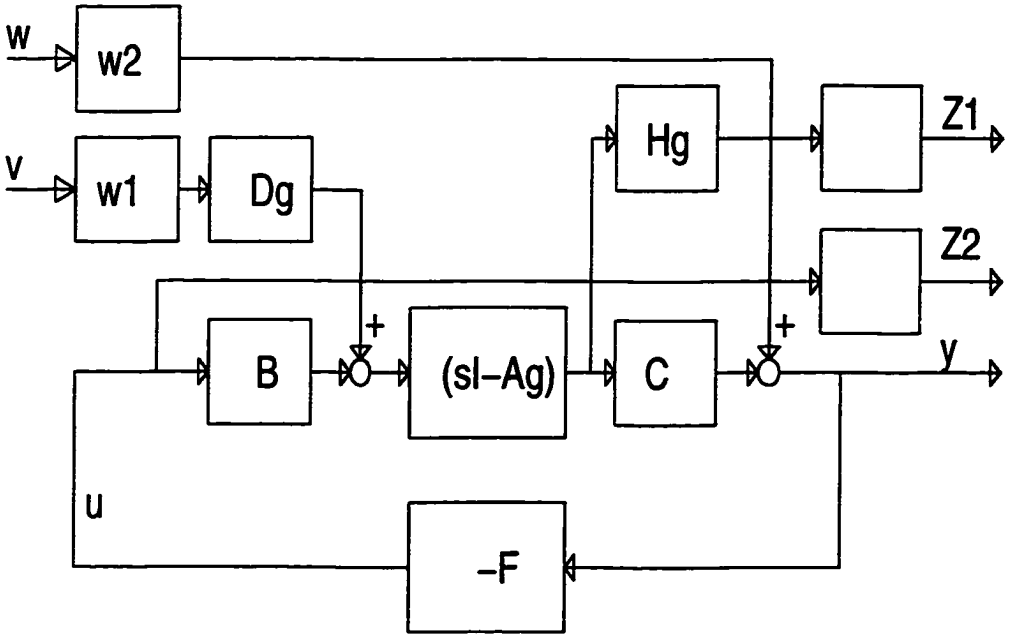

Figure 7.3: Generalized Plant Setup of H_∞

$$x = \begin{bmatrix} q \\ x_{w_1} \\ x_{w_2} \end{bmatrix}, \quad d = \begin{bmatrix} v \\ w \end{bmatrix}$$

where x_{w_1} and x_{w_2} are the the states of the frequency weighting function $w_1(s)$ and $w_2(s)$ respectively.

After some manipulations, the state-space representation [25] referred to in Eq. (7.1) - Eq. (7.3) is

$$A = \begin{bmatrix} A_g & D_g C_{W_1} & 0 \\ 0 & A_{w_1} & 0 \\ 0 & 0 & A_{w_2} \end{bmatrix}, \quad B_1 = \begin{bmatrix} D_g D_{w_1} & 0 \\ B_{w_1} & 0 \\ 0 & B_{w_2} \end{bmatrix}, \quad B_2 = \begin{bmatrix} B \\ 0 \\ 0 \end{bmatrix} \tag{7.19}$$

$$C_1 = \begin{bmatrix} \Theta H_g & 0 & 0 \\ 0 & 0 & 0 \end{bmatrix}, \qquad D_{11} = \begin{bmatrix} 0 & 0 \\ 0 & 0 \end{bmatrix}, \qquad D_{12} = \begin{bmatrix} 0 \\ \Upsilon I \end{bmatrix} \tag{7.20}$$

$$C_2 = \begin{bmatrix} C & 0 & C_{w_2} \end{bmatrix}, \qquad D_{21} = \begin{bmatrix} 0 & D_{w_2} \end{bmatrix}, \qquad D_{22} = \begin{bmatrix} 0 \end{bmatrix} \tag{7.21}$$

After substituting $u(s) = -F(s)y(s)$, the transfer functions

$$T_{z_1 v} = \Theta H_g \phi (I + BFC\phi)^{-1} D_g W_1, \tag{7.22}$$

$$T_{z_2 v} = -\Upsilon FC\phi (I + BFC\phi)^{-1} D_g W_1, \tag{7.23}$$

$$T_{z_1 w} = -\Theta H_g \phi BF (I + G_g F)^{-1} W_2, \tag{7.24}$$

$$T_{z_2 w} = -\Upsilon F (I + G_g F)^{-1} W_2 \tag{7.25}$$

are obtained, where

$\phi = (sI - A_g)^{-1}, \quad G_g = C(sI - A_g)^{-1}B.$

From above equations, the H_∞ control problem now is to design $F(s)$ to internally stabilize, the system but satisfy

$$\left\| \begin{matrix} T_{z_1 v} & T_{z_1 w} \\ T_{z_2 v} & T_{z_2 w} \end{matrix} \right\|_\infty \leq r. \tag{7.26}$$

The purpose of the H_∞ controller here is to find out the minimum r thus attenuating z to maximum degree while still holding the necessary and sufficient stable conditions discussed in Section 7.1. The implementation algorithm is presented in the following sections.

7.3 H_∞ Controller Design

To design the H_∞ controller discussed in the last section, we must specify those weighting functions and factors. Because v_0 is in relatively low frequency range for low frequency model uncertainties, $W_1(s)$ with the 'cutting frequency' around $250Hz$ is chosen. So $W_1(s)$ is as,

$$W_1(s) = \frac{9.79 \times 10^3}{(1 + s/(1.72\pi))(1 + s/(2.0\pi))}. \tag{7.27}$$

Its bode plot is illustrated in Fig. (7.4). $W_2(s)$ assures robustness for high frequency noise. It is in Fig. (7.5).

$$W_2(s) = \frac{5.21 \times 10^{-7}(1 + s/(0.02\pi))(1 + s/(0.1\pi))(1 + s/(200.0\pi))}{(1 + s/(6.0\pi))(1 + s/(20.0\pi))(1 + s/(160.0\pi))} \tag{7.28}$$

The parameters Θ, and Υ are adjusted by the cost,

$$J_(u,(v,w)) = \int_{-\infty}^{\infty} [(z_g^T Q z_g + u^T R u - (v^T v + w^T w)]dt. \tag{7.29}$$

where $Q = \Theta^T\Theta$ and $R = \Upsilon^2$. The H_∞ can be interpreted to reduce this cost. Based on the observations in [25], and our simulations, the weighting matrix Θ for our beam system with ten states is

$\Theta = diag(60.0 \quad 80.36 \quad 15.91 \quad 10.7 \quad 5.1 \quad 15.1 \quad 2.1 \quad 6.2 \quad 5.2 \quad 5.1)$,

and the scalar factor $\Upsilon = 5 \times 10^{-5}$. The output feedback used here is as in Eq. (5.21).

In order to search the minimum value r, and since it is not known in which region such an index r constitutes a controller, an adequate number of random r's (usually $r \leq 1$) are tested. All the r's to which such a controller exists are saved,

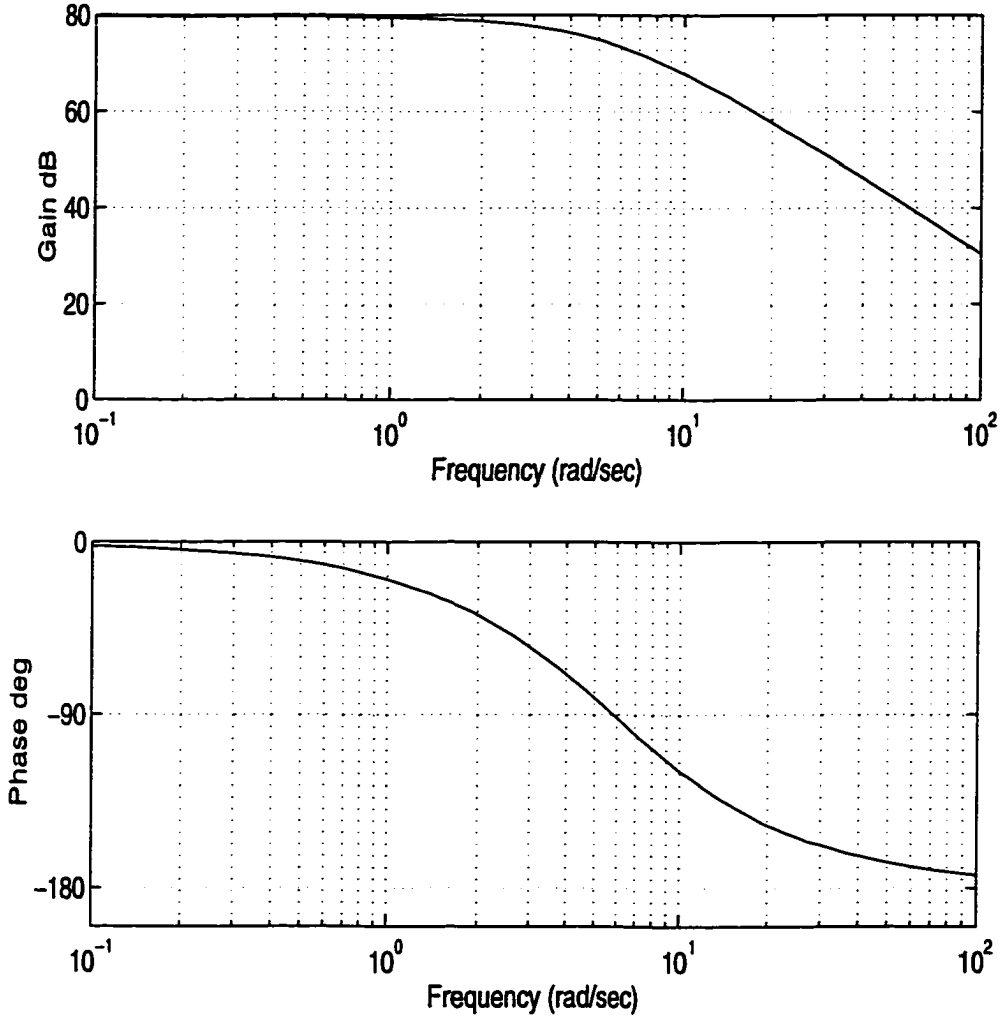

Figure 7.4: Model Uncertainty Frequency Weighting Function W_1

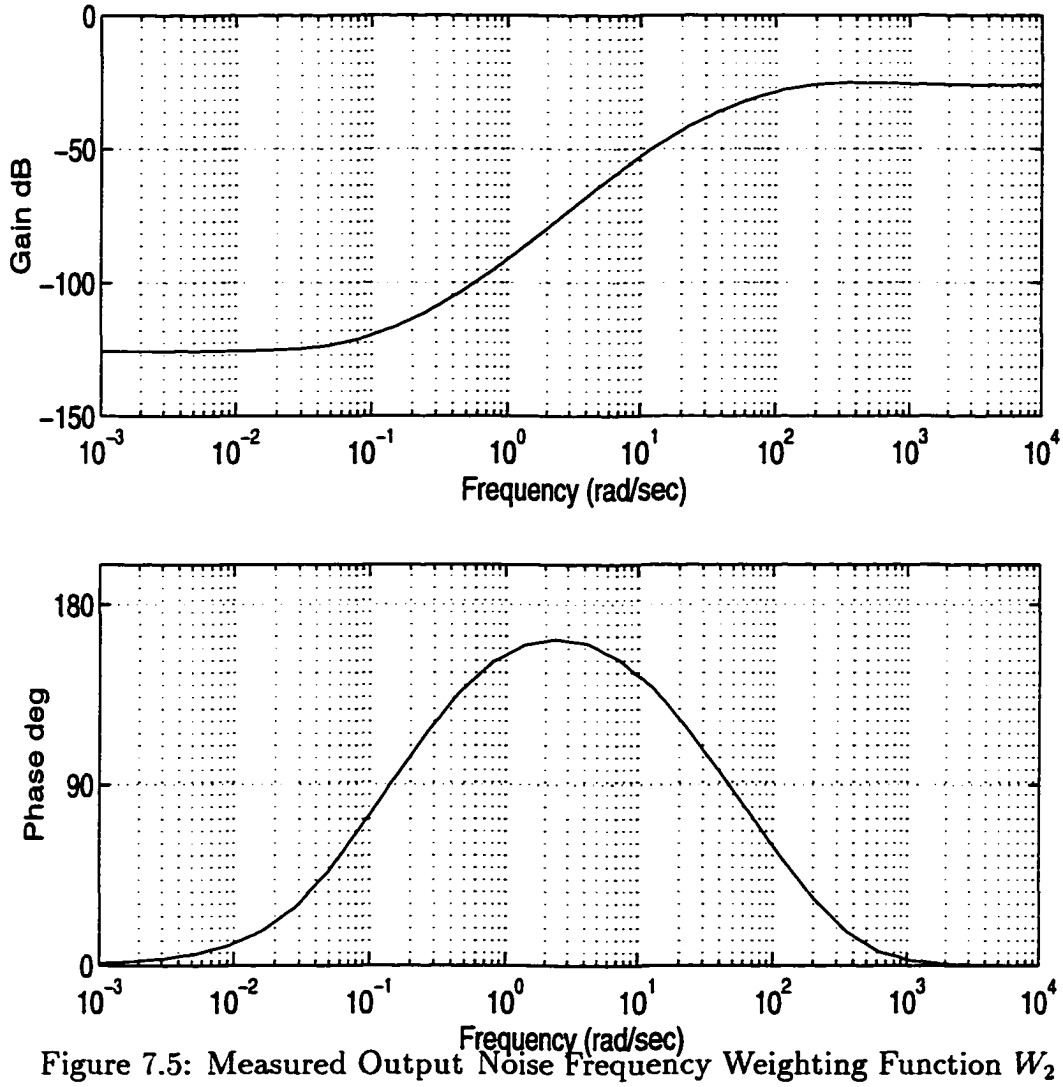

Figure 7.5: Measured Output Noise Frequency Weighting Function W_2

and the minimum r represents the cost function for its beam shape. The loop in the H_∞ controller is,

H_∞ loop

1. For a given beam construction distribution, calculate beam system dynamics A_g, B, C.
2. Calculate generalized plant matrices,

   Get the state-space matrices for frequency weighting functions

   $A_{w_1}, B_{w_1}, C_{w_1}, D_{w_1}$;

   $A_{w_2}, B_{w_2}, C_{w_2}, D_{w_2}$;

   Get weighting factor Θ and scalar factor Υ;

   Generate $A, B_1, B_2, C_1, C_2, D_{11}, D_{12}, D_{21}, D_{22}$.
3. Search for minimum index r loop for a beam shape distribution,

   A) randomly pick a r;

   B) check X_∞, Y_∞, ρ conditions;

   C) decide to save this r in a vector or discard it;

   D) choose next r which is smaller than the last valid r, go to B);

   E) after a certain number of iterations, single out the minimum r from the vector to represent this shape. Save this r and its shape.
4. Check stop criteria. If the differences between the three smallest r's in this r vector meet the criteria, stop here. Otherwise, go back to Step 3 for another routine;

5. Calculate F_∞, L_∞, Z_∞, A_∞ to get the controller $K(s)$ based on the minimum r and A_g, B, C.

7.4 Simulation Results

There are two blocks in the searching loop, the H_∞ controller block and IHR algorithm block. The former is used to find the best controller which has a minimum index r based on the input of beam geometric shape as specified in last chapter. The latter is used to generate a feasible beam shape distribution. This loop stops until the index vector meets criteria as described in the last chapter.

For a given beam shape, one such admissible H_∞ controller associated with an index r is shown as Eq. (7.8), which conforms to all the required conditions. The beam consists of 4 segments, and the number of degrees of its mechanic dynamics is set to 10 (the first four modal shapes are used here).

For Θ feedback controller as Eq. (5.21), Fig. (7.6) is one of the best shapes, having a minimum index of $r = 0.832$.

The admissible H_∞ controller associated with the shape and this r is

$$-F(s) = 2.158 \times 10^3 \frac{(s+50.2655)(s+31.4159)(s+6.1133+18.8706i)(s+6.1133-18.8706i)}{(s+50.2577)(s+31.4219)(s+5.7432+18.5868i)(s+5.7432-18.5868i)}$$

$$\frac{(s+18.8496)(s+17.4371)(s+13.1358+11.0675i)(s+13.1358-11.0675i)}{(s+13.2079+11.0351i)(s+13.2079-11.0351i)(s+17.1713)(s+0.4437+9.9505i)(s+0.4437-9.9505i)}$$

$$\frac{(s+0.2660+9.2176i)(s+0.2660-9.2176i)(s+0.4664+3.9841i)(s+0.4664-3.9841i)(s+0.1299)(s+3.9720)}{(s+3.9752)(s+0.0376+5.0332i)(s+0.0376-5.0332i)(s+0.0658+2.4910i)(s+0.0658-2.4910i)(s+18.8489)}.$$

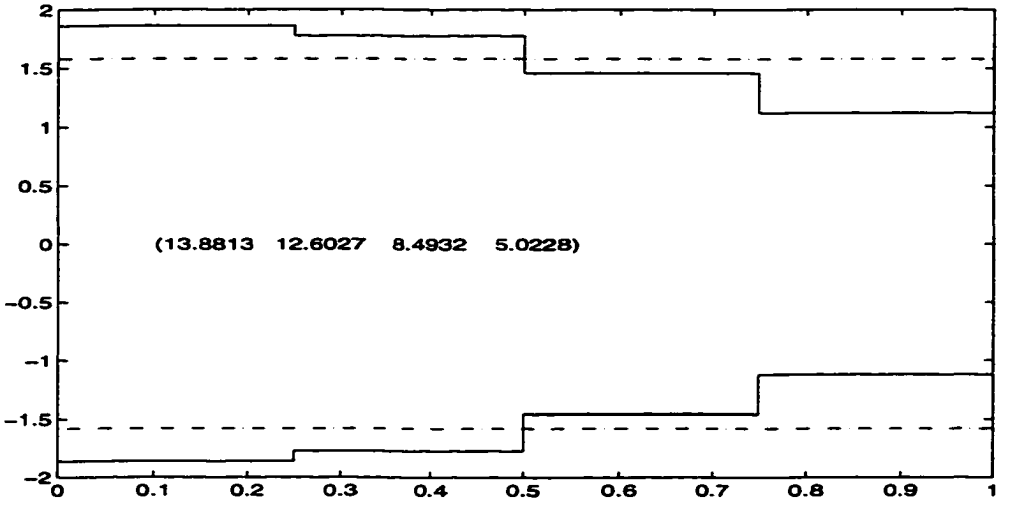

Figure 7.6: Optimal Shapes for H_∞

This controller is 15 degrees, ten of them having been contributed by the beam dynamics, two from the frequency weighting function $w_1(s)$, the rest originating from frequency weighting function $w_2(s)$.

This controller is tested with the same initial state as in Chapter 6, $q(0) = [\sqrt{10}, 0, \ldots, 0]^T$. As usual, the dash curve is for uniform beam, the solid one is the response of the optimal beam shape. For Θ feedback, the initial responses of the hub tangent angle is in Fig. (7.7). It has a small overshoot, but nevertheless steadily converges to the equilibrium point with several pulses. The optimal shape has faster convergency than the uniform. Fig. (7.8) is the associated initial responses of the tip deflection. It has a significant first deflective pulse and larger than that of uniform beam, but this deceases promptly, almost at the same speed as that of the hub tangent angle.

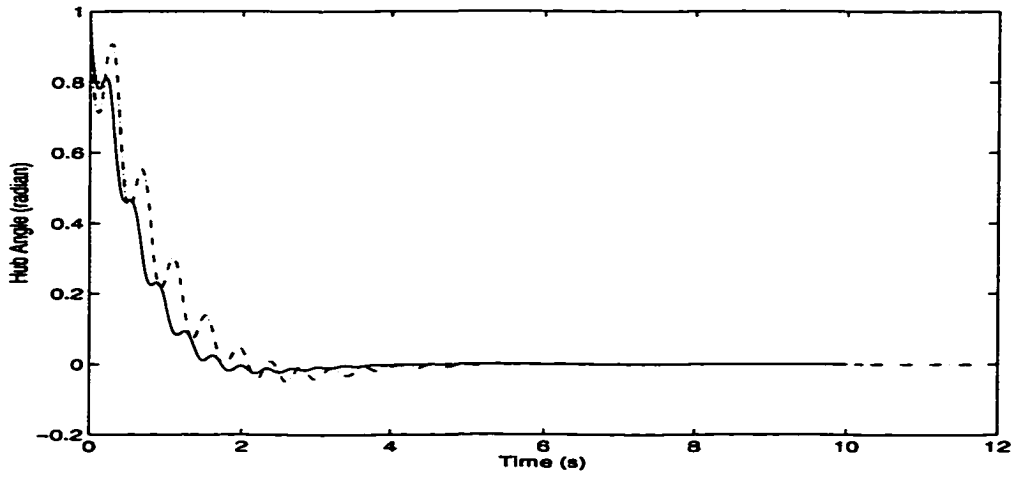

Figure 7.7: Hub Tangent Angle Initial Response of Θ (H_∞) Feedback

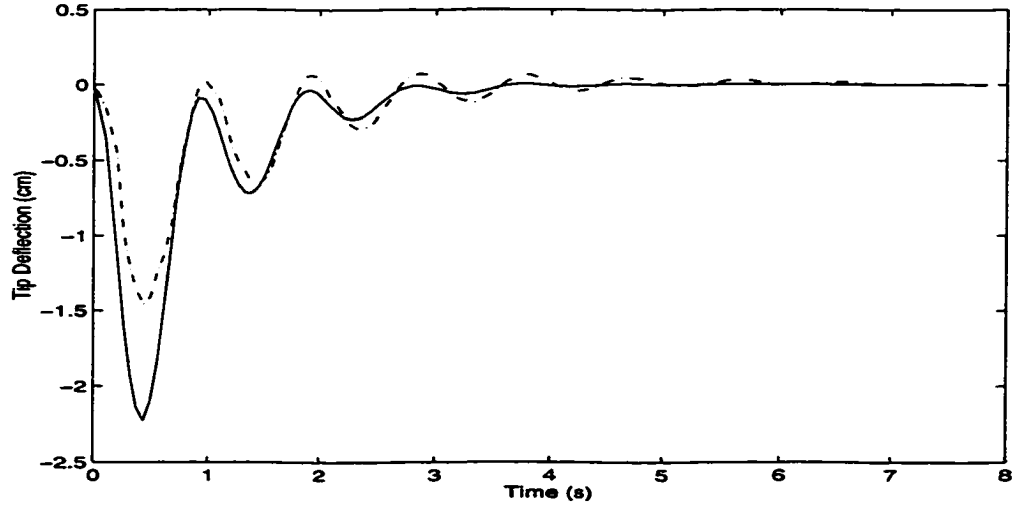

Figure 7.8: Tip Deflection Initial Response of Θ (H_∞) Feedback

Fig. (7.9) is the step responses of the hub tangent angle for uniform and associated optimal beam respectively. They both have an overshoot after crossing the given input reference, but this fades away gradually. Fig. (7.10) is the step responses of tip deflection. Both two responses progress through several cyclic oscillations, and each transition lasts slightly longer than that of the hub tangent angle. The deflection of the optimal beam is smaller, and converges faster. The step-type disturbance is added as disturbance v for the stable test, as derived early, v is assumed to describe the system uncertainties. The results are as in Fig. (7.11) and Fig. (7.12). They have a notable deflective pulse, but recover to the equilibrium point promptly.

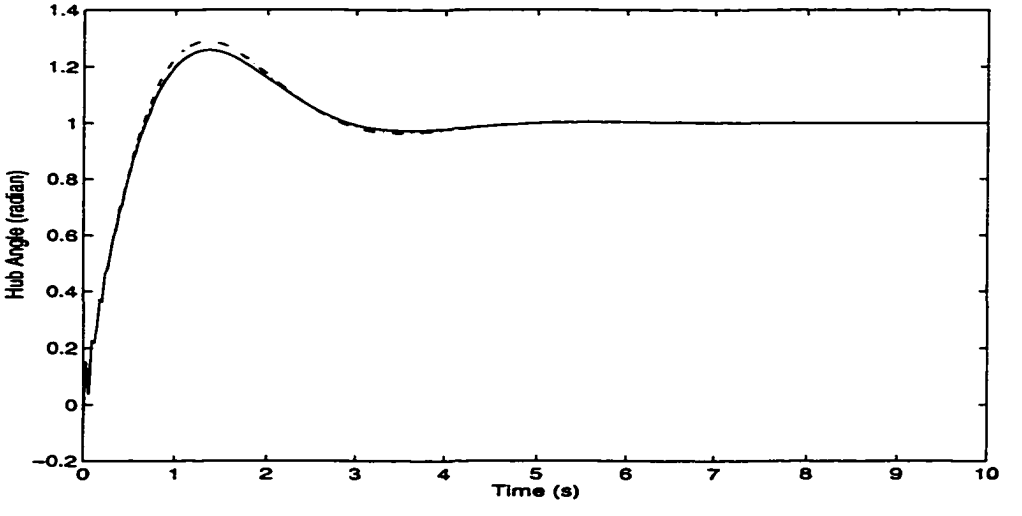

Figure 7.9: Step Response of Hub Angle for Θ (H_∞) Feedback

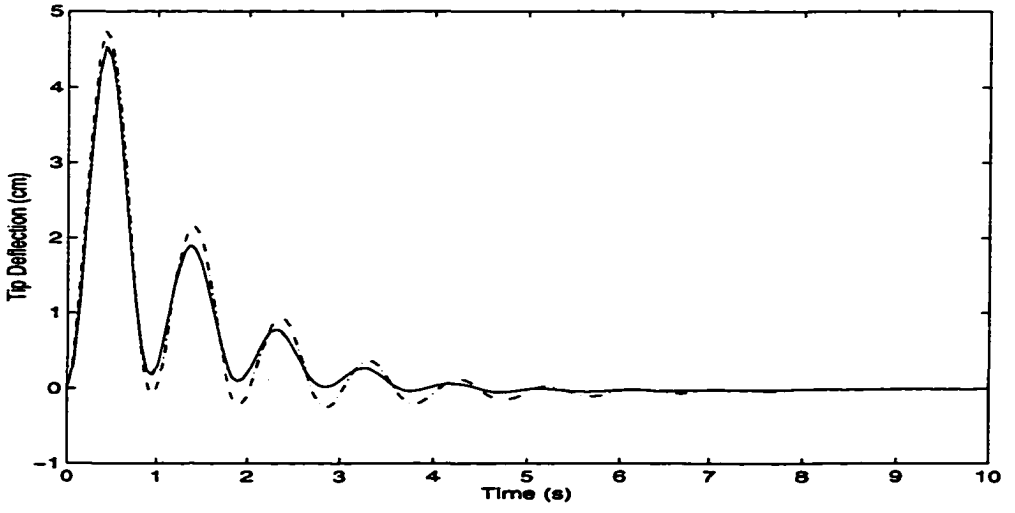

Figure 7.10: Step Response of Tip Deflection for Θ (H_∞) Feedback

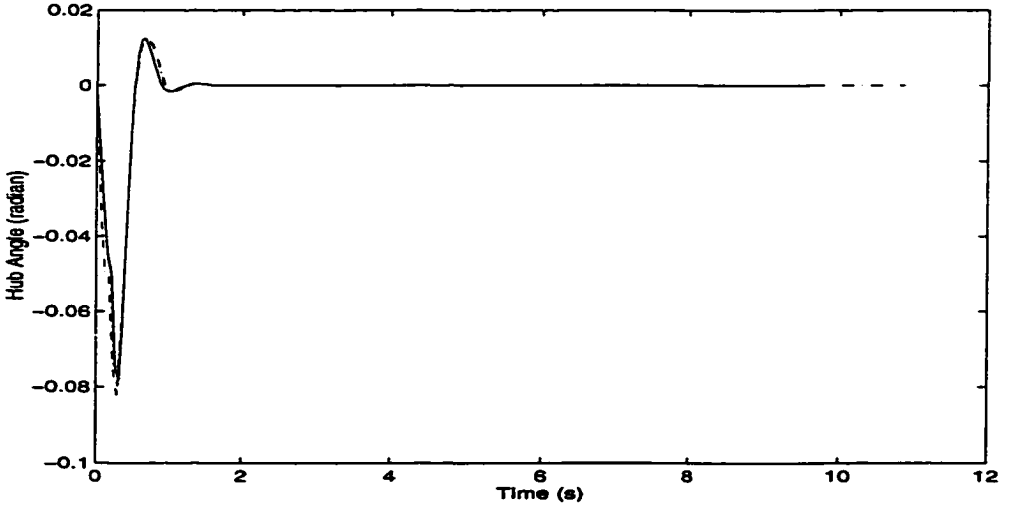

Figure 7.11: Step-Type Disturbance Response of Hub Angle for Θ (H_∞) Feedback

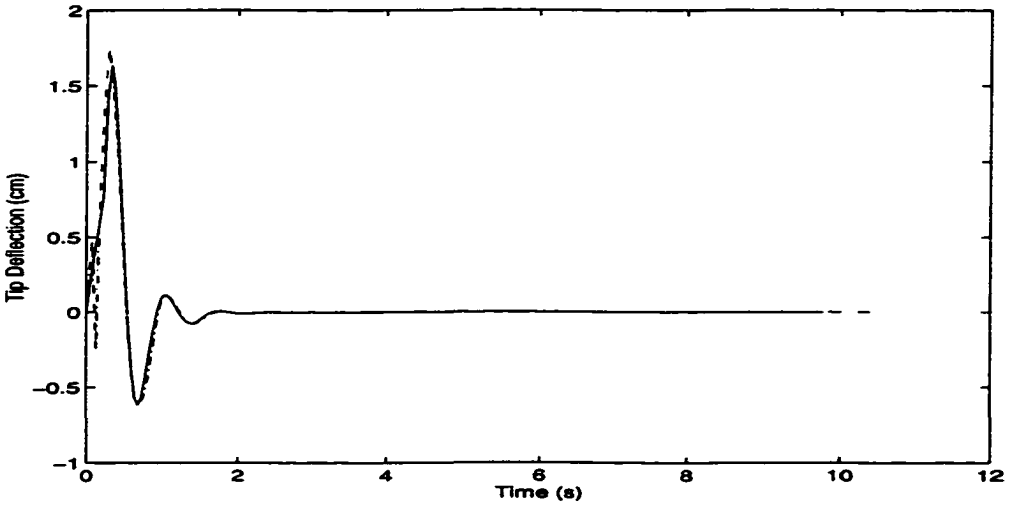

Figure 7.12: Step-Type Disturbance Response of Tip Deflection for Θ (H_∞) Feedback

For tip deflection w feedback as Eq. (5.19), the optimal shape is as Fig. (7.13) with $r = 0.952$. The initial responses of the hub tangent angle is in Fig. (7.14). The response of the optimal beam has smaller vibration then the uniform beam, but both have higher frequency vibration then the responses of Θ feedback. Fig. (7.15) is the associated initial responses of the tip deflection. The optimal shape has a bigger first pulse, but decays faster for the whole transient.

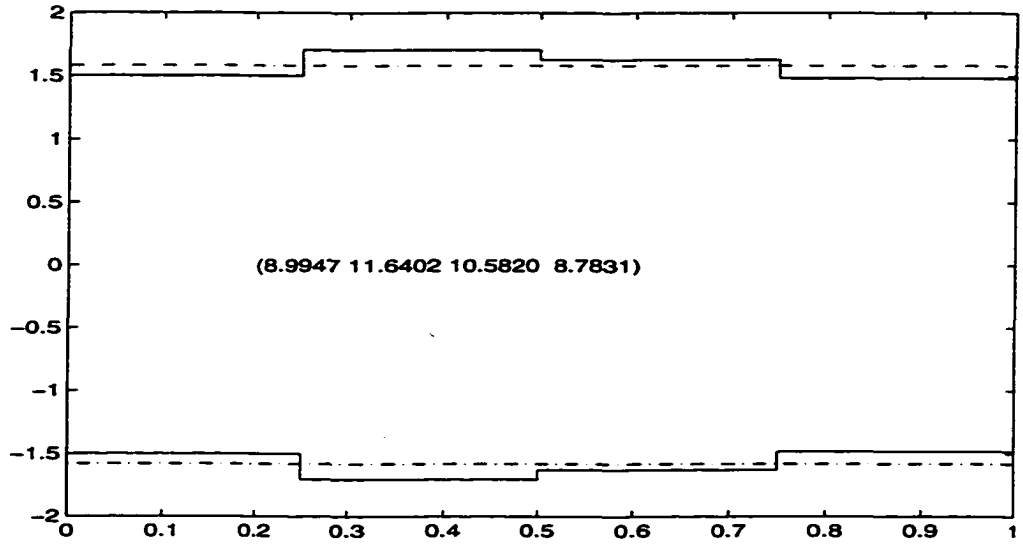

Figure 7.13: Optimal Shapes for w (H_∞) Feedback

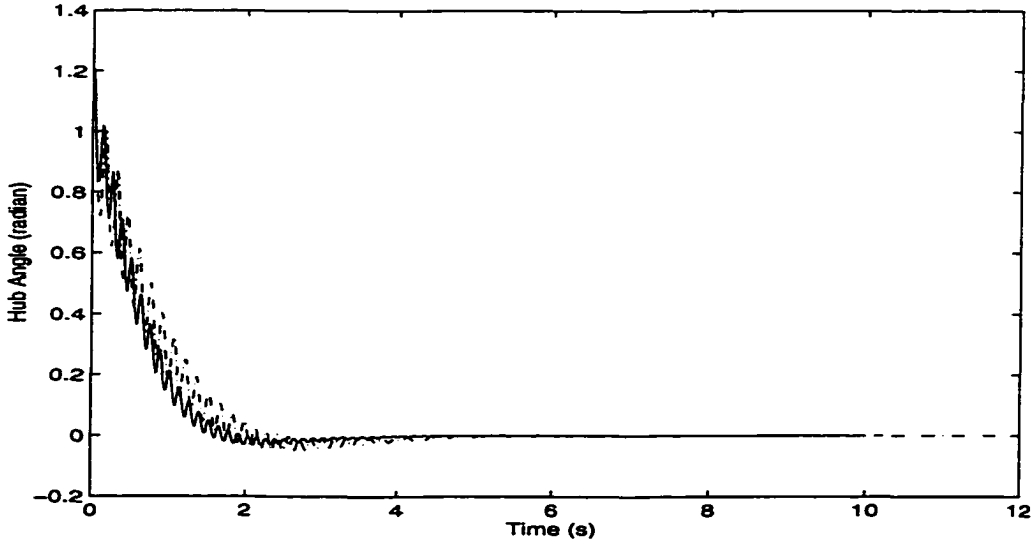

Figure 7.14: Hub Tangent Angle Initial Response of w (H_∞) Feedback

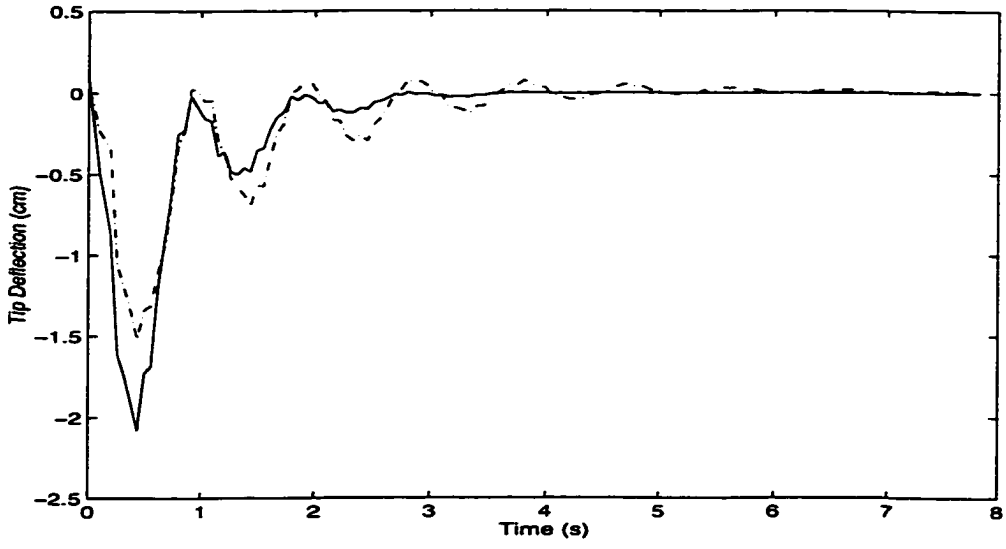

Figure 7.15: Tip Deflection Initial Response of w (H_∞) Feedback

Fig. (7.16) is the w feedback step responses of the hub tangent angle for uniform and associated optimal beam respectively. Fig. (7.17) is the step responses of tip deflection.

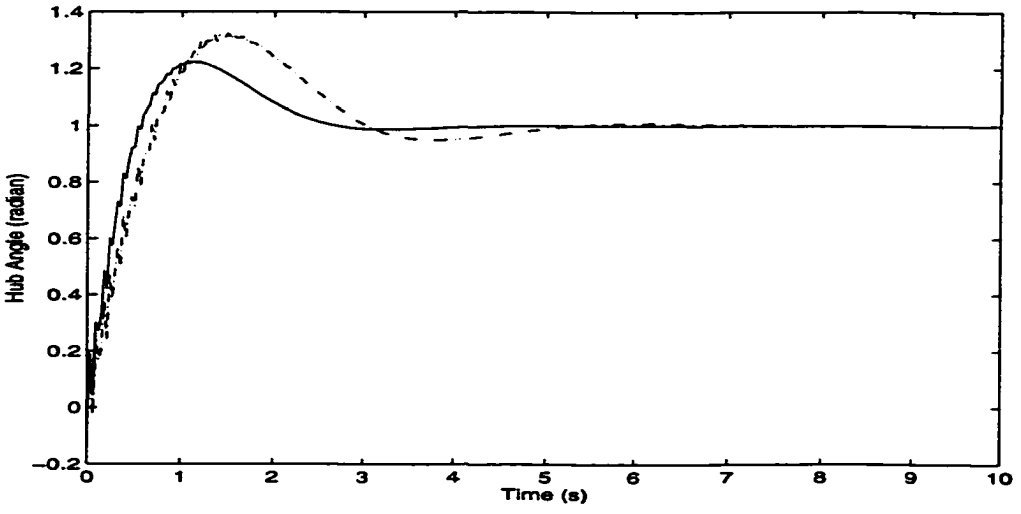

Figure 7.16: Step Response of Hub Angle for w (H_∞) Feedback

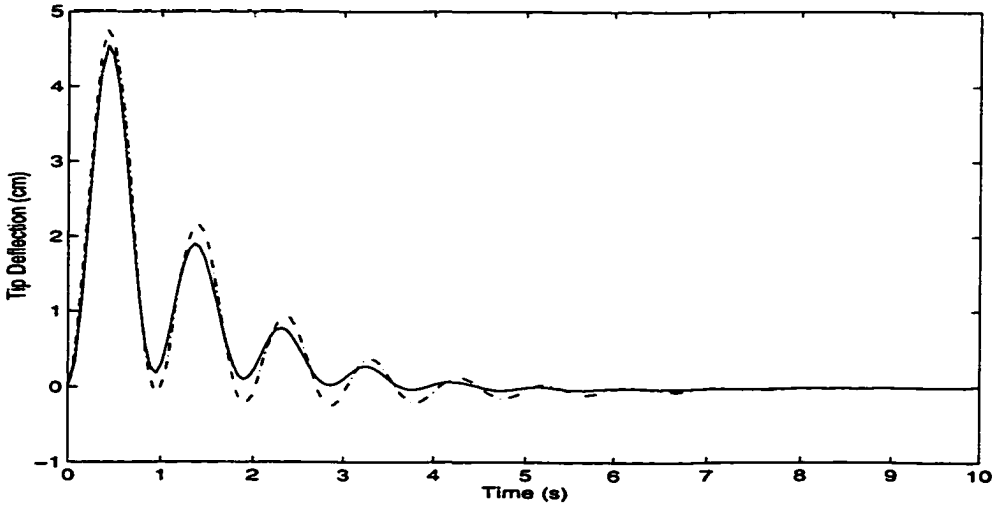

Figure 7.17: Step Response of Tip Deflection for w Feedback

For the tip position v feedback as Eq. (5.20), the optimal shape is as Fig. (7.18) with a $r = 0.8162$. The initial responses of the hub tangent angle is in Fig. (7.19). Fig. (7.20) is the associated initial responses of the tip deflection. Fig. (7.21) is tip position feedback step responses of the hub tangent angle for uniform and associated optimal beam respectively. Fig. (7.22) is the step responses of tip deflection.

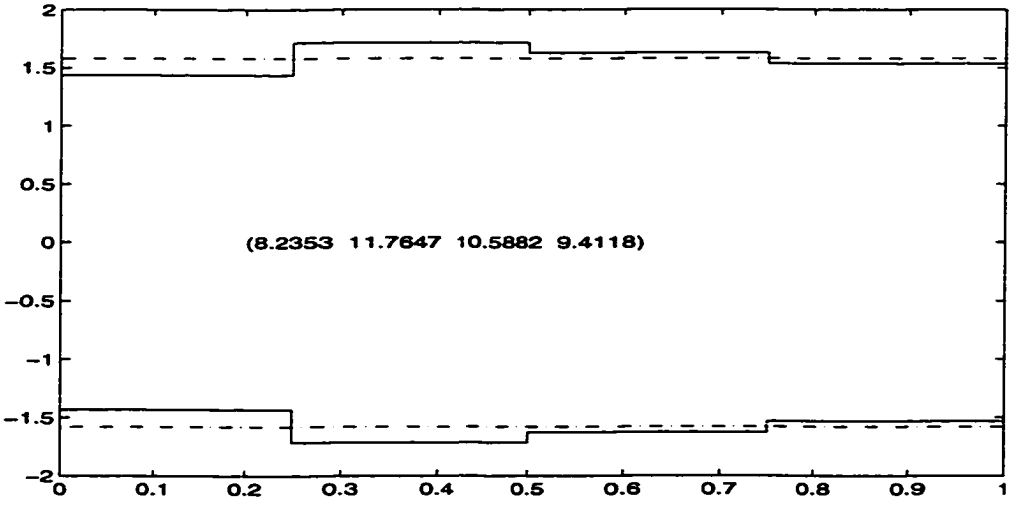

Figure 7.18: Optimal Shapes for v (H_∞) Feedback

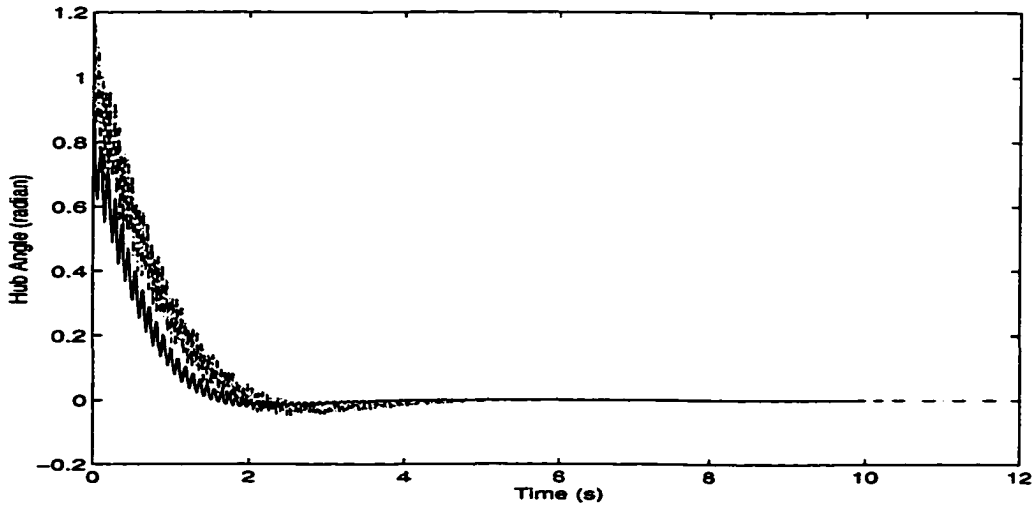

Figure 7.19: Hub Tangent Angle Initial Response of v (H_∞) Feedback

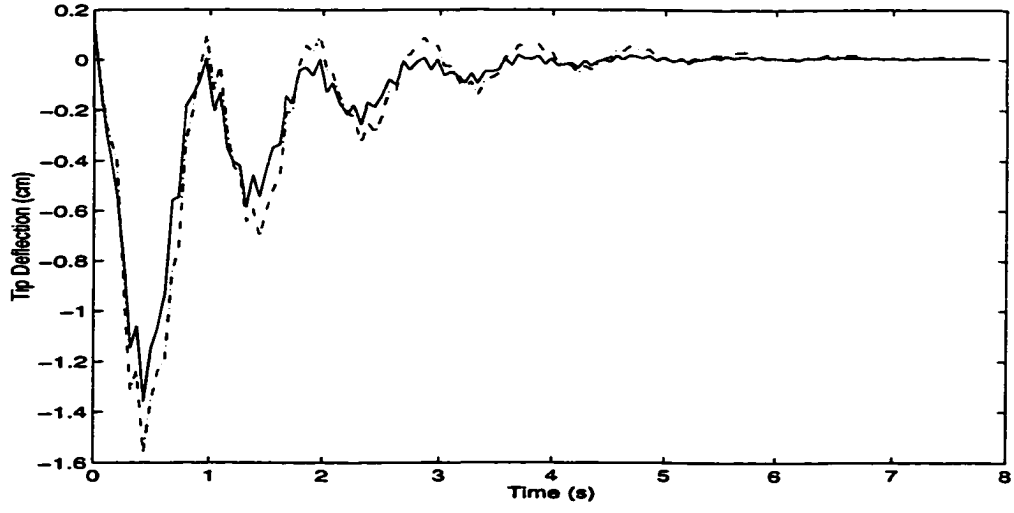

Figure 7.20: Tip Deflection Initial Response of v (H_∞) Feedback

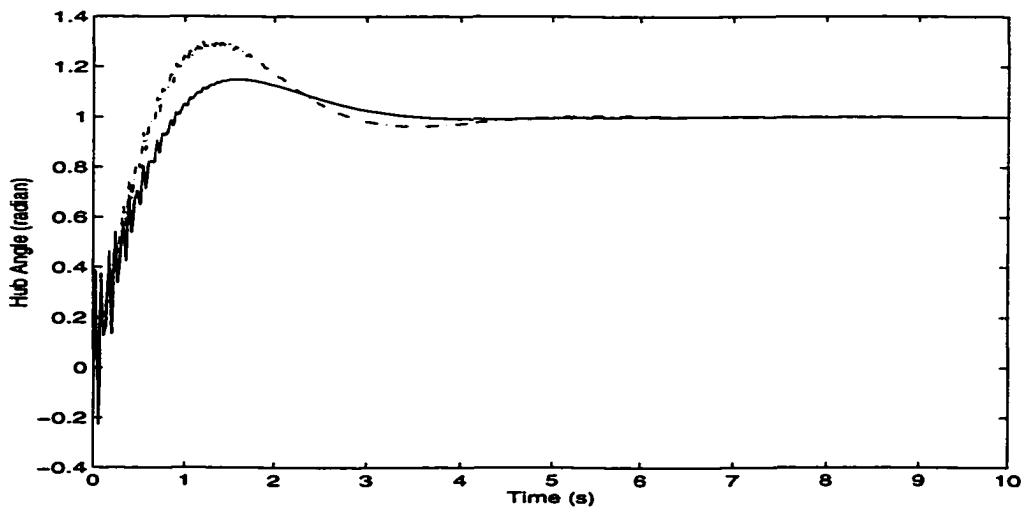

Figure 7.21: Step Response of Hub Angle for v (H_∞) Feedback

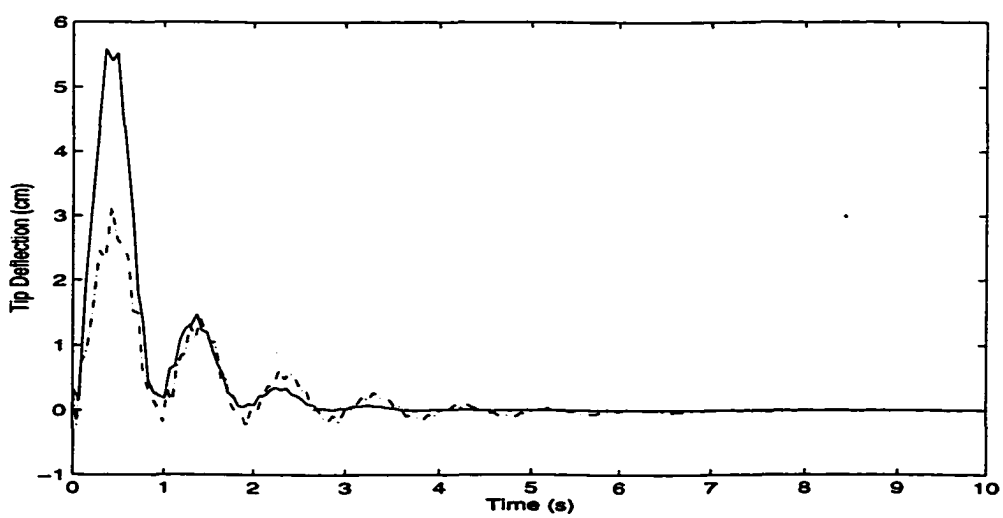

Figure 7.22: Step Response of Tip Deflection for v (H_∞) Feedback

From here, the optimal shape has faster responses less vibration cycles than uniform beam under the Θ feedback. In this chapter, both the generalized state-space model and model uncertainties are developed for H_∞ controller to completely avoid the complexity of frequency domain implementation. The design goal is to internally stablize the close-loop, whiling minimizing the maximum singular value of the transfer function from characterized error inputs to error outputs, so that impacts from disturbances and system uncertainties vanish. All the results show that the H_∞ controller here is stable against system uncertainty and works robustly.

CHAPTER 8

SYSTEM ROBUSTNESS ANALYSIS

8.1 Sensitivity Analysis

In chapter 3, less significant terms of the dynamic model were cut off to get the Euler-Bernoulli dynamic model with rotatory inertia, but this generated modeling error. It is critical to design a controller that has the ability to provide stability in spite of modeling errors. There are many papers ([48] and references therein) addressing such problems. This chapter focuses mainly on the beam parameter variations due to beam manufacture accuracy and DC motor dynamics variations. After the DC motor equation and the beam dynamics were integrated into the system state equation, these two kinds of variations are treated as system disturbance $d(t)$. This is illustrated as the system configuration in Fig. (8.1). The plant is $G(s)$, and the feedback compensator is $K(s)$, which can be designed by various techniques. The system output is $y(t)$, the system control input is $u(t)$. The sensitivity of the overall system is related to the technique employed in the design of the controller. In this case LQR and H_∞ were chosen to demonstrate of the mechatronic methodology, since the system robustness depends on the characteristics of these controllers. For systems with LQR, the classical analysis of robustness is measured in frequency-domain. The notions of singular value, multivariable loop gain, and Bode magnitude plot are

either evaluated for the sensitivity analysis, or they are used directly as design tools. These methods are not readdressed here. Instead, numerical results with these two kinds of parameter variations to show the system robustness are speculated.

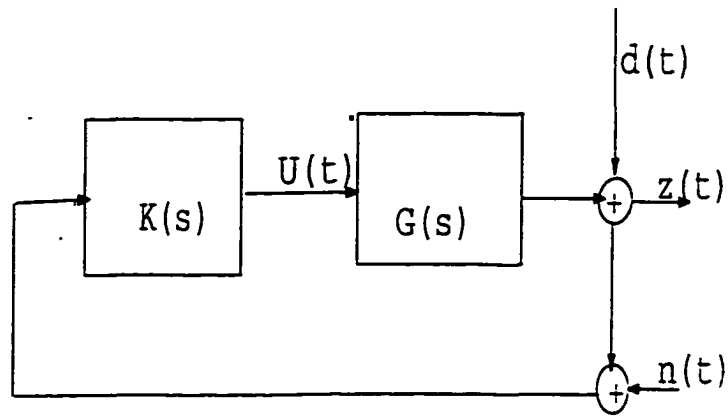

Figure 8.1: Standard LQR Feedback Configuration

8.2 Numerical Results of System Robustness

First the beam shape variations are tested. For the beam with 4 segments, the performance index differences with the three feedbacks are carried out due to a ± 0.1 width variation of the ith segment. The optimal LQR controller is unchanged, $Q = 50$. A_i is the width of the ith segment from the hub end. The results are as in Table 8.1. All data in the following tables are the PI difference due to the variation of the segment width or motor parameter.

Table 8.1: Robustness Analysis with ($q_1(0)$, 4, 50).

	$\{\Theta\}$	$\{\Theta, w\}$	$\{\Theta, v\}$
Optimal shape ($A_1A_2A_3A_4$)	(11.2031 10.7338 9.2351 8.8080)	(5.9555 12.4597 12.027 9.5578)	(9.8623 6.1054 11.4927 12.5595)
Optimal PI	2540.470	2098.374	2388.850
$A_1 \pm 0.1$	±9.7	±3.3	±3.0
$A_2 \pm 0.1$	±9.7	±3.4	±8.0
$A_3 \pm 0.1$	±9.3	±3.4	±7.7
$A_4 \pm 0.1$	±9.7	±3.5	±6.5

In order to explore the PI with different variations of each segment separately, the beam with 4 segments, feedback $\{\Theta, w\}$, $Q = 50$ is chosen. Table 8.2 summarizes the results.

Table 8.2: Robustness Analysis with ($q_1(0)$, $\{\Theta, w\}$, 4, 50).

	$A_i - 0.3$	$A_i - 0.2$	$A_i - 0.1$	$A_i + 0.1$	$A_i + 0.2$	$A_i + 0.3$
A_1	-8.1	-2.8	-2.5	-3.3	9.9	16.5
A_2	9.7	-2.6	3.4	-2.5	-6.2	10.9
A_3	-10.0	6.8	-3.4	2.5	6.5	-10.6
A_4	10.1	-6.7	3.4	3.5	6.4	10.5

From a beam with 12 segments, feedback $\{\Theta, w\}$, $Q = 50$ was chosen. Table 8.3 illustrates analyses with only one segment variation at a time.

Table 8.3: Robustness Analysis with $(q_1(0), \{\Theta, w\}, 12, 50)$.

$A_1 + 0.1$	$A_2 + 0.1$	$A_3 + 0.1$	$A_4 + 0.1$	$A_5 + 0.1$	$A_6 + 0.1$
-3.8	2.8	-5.3	-3.7	-1.1	0.5
$A_7 - 0.1$	$A_8 - 0.1$	$A_9 - 0.1$	$A_{10} - 0.1$	$A_{11} - 0.1$	$A_{12} - 0.1$
1.1	-0.7	0.8	1.2	-1.7	1.9

For motor parameter uncertainties, J_m with -0.1 variation was attempted. The results are listed in Table 8.4.

Table 8.4: Robustness Analysis with Motor Coefficient J_m Variations $(q_1(0), Q = 100 * I, 50 * I, 10 * I)$.

	$\{\Theta\}$	$\{\Theta, w\}$	$\{\Theta, v\}$
$Q = 100 * I$	-23.0453	-54.3013	-15.1548
$Q = 50 * I$	-5.4908	-14.3455	-5.7012
$Q = 10 * I$	-2.3543	-9.6067	-5.4134

As results in above tables, show a small beam geometric variation changes the associated PI a little when compared with the original optimal PI. Note however

that the larger the variation of the beam dimension, the larger the offset of the PI. Motor parameter J_m is shown to have larger impacts on PI then does.

For the H_∞ controller, the beam shape (13.8813 12.6027 8.4932 **4.5228**) instead of the optimal shape (13.8813 12.6027 8.4932 5.0228) was tested, comparing with the uniform beam with the first segment near the tip was 9, instead 10. The tip deflection responses for the initial condition, step input and step-type disturbance are as in Fig. (8.2)- Fig. (8.4). They are not much different between the optimal shape and the uniform beam.

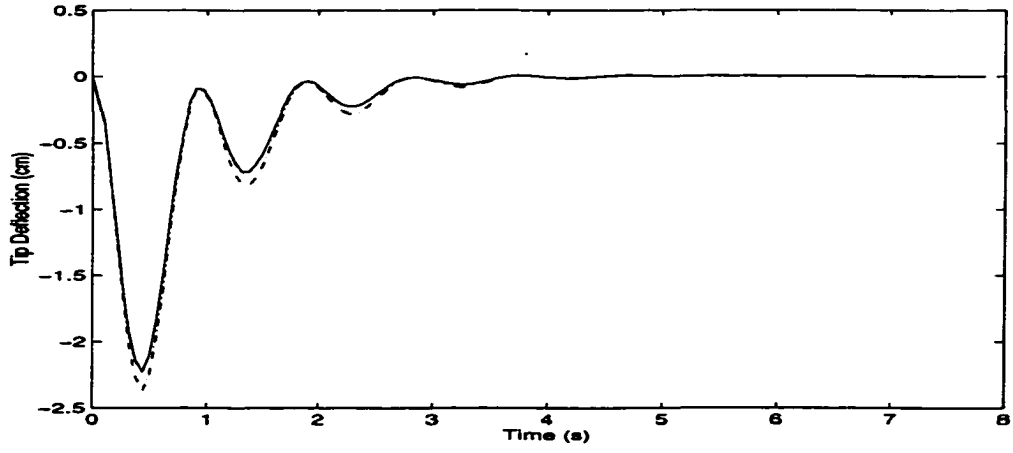

Figure 8.2: Initial Input Response (Tip Deflection) for H_∞

As these results show, both LQR and H_∞ controllers for flexible manipulators have very good robustness to parameter variations and disturbance. H_∞ has stronger stability against system uncertainties.

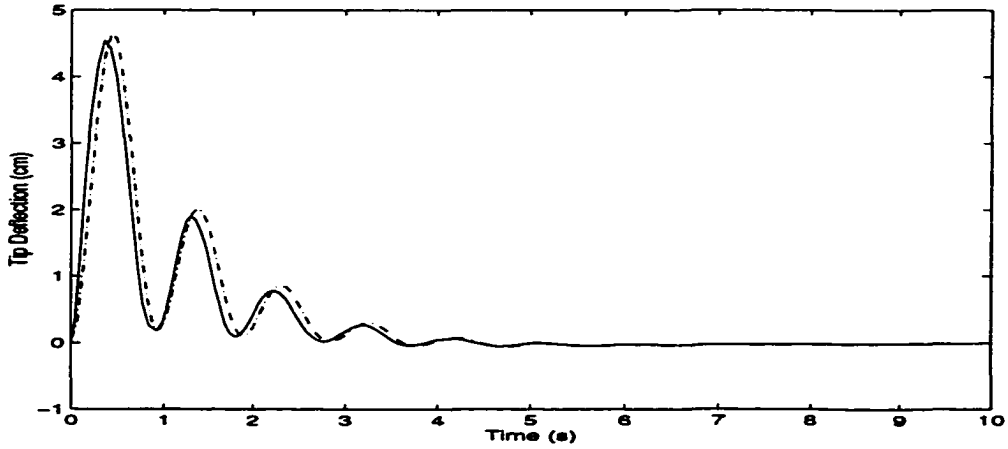

Figure 8.3: Step Input Response (Tip Deflection) for H_∞

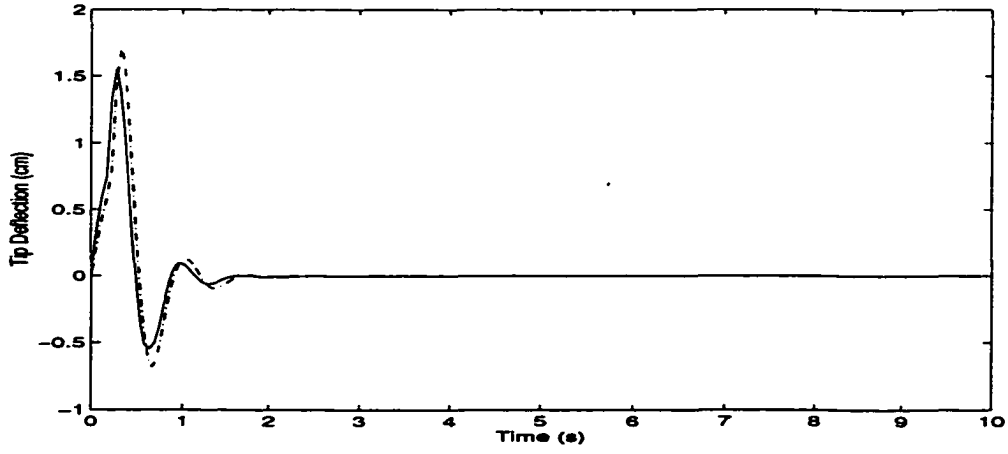

Figure 8.4: Step Type Disturbance Response (Tip Deflection) for H_∞

CHAPTER 9

CONCLUSIONS AND FUTURE RESEARCH

9.1 Conclusions

The mechatronic approach as a significant and valid design for the global optimization of a flexible manipulator is the highlight of this research. The critical point of this design is global integration and optimization, which treats all the subsystems in a system as a whole and covers the full searching space for system parameters, including the beam parameters (material and geometric), coefficients in motor dynamics and controller parameters, and controller structure. Compared to traditional optimal design, which relies on a local optimization by assigning a controller to a given plant, the mechatronic mechanism achieves a better solution by regarding the plant and the controller concurrently. Each parameter in the system equation or their combination could be the optimized variable. From this perspective, the boundaries of mechatronic design expansion into other field is limited only by the imagination. The LQR standard output feedback is the only one used here to illustrate this basic idea. H_∞ control is used to obtain more robust system resistant to disturbances.

In this research, the search space is limited only with regard to the beam physical dimension; all other parameters are supposed to be constant. There are two options for the mechatronic simulation, the first being what was addressed in this

dissertation. From a uniform link, the most significant modes and associated natural frequencies were calculated and these modes were used as universal space base. Thus, all elements in those coefficients of the state space equation are the only functions of the geometric link. Since the mechatronic method as outlined in Chapters 7, and 8 searches the beam geometric distribution through the whole space to find an optimal solution, this 'base' approach can save a lot of computation time.

The other option for mechatronic simulation is, what is referred to as 'segmentized-method'. Based on segmentized beams, and their interfacial conditions, a set of constraints is achieved. To solve these equations with beam boundary conditions, the most significant natural frequencies from the determinant equal to zero were obtained. Furthermore a series of eigenfunctions to each segment was found. In this approach, even if one segment of the beam shape changes, all these frequencies and eigenfunctions will be changed. Because of the searching process in the mechatronic design, this approach will take a longer time to reach the optimal point. So the first option is better for mechatronic design and why it was employed in this research. The other main topics addressed so far are listed next.

In the previous chapters,

1. The flexible beam dynamics were formulated with a tip load, taking rotatory inertia into account.

2. With beam natural frequencies and modal shapes, based on separability property, the beam state space equations were derived.

3. The beam state space equation was integrated with motor torque dynamics in order to obtain overall state space formulae for the system.

4. To explore this new method, the standard LQR with output feedbacks was employed, giving results under different conditions.

5. The model uncertainties were obtained, the H_∞ controller was developed to attenuate the effects of model uncertainties and system noise.

6. Finally the system sensitivity was tested with variations of beam dimension and motor coefficient.

Several combinations with different output feedbacks, number of segments and weighting matrix as listed in tables of Chapter 6 were tested. The simulation results show that in all cases the performance index (PI) improved to various degree. It was found find that the PI does not change much with varying numbers of segments. The results are better for two outputs feedback than that for single feedback. If the motor parameters are added into the search space, better performance is obtained.

The results in Chapter 7 show that the H_∞ controller gives better performance, but this is a tradeoff for slower computation time because the H_∞ controller is much more complicated than the LQR controller and needs more calculation. The robustness analysis was also conducted numerically. As was pointed out, the controller is responsible for having a robust feature for parameter uncertainties or variations, as

well as disturbance. The numerical responses to different kinds of parameter variations were illustrated, showing, that the system designed by the mechatronic method displays good robustness against parameter variations.

9.2 Future Research

Due to the limited scope of this dissertation, many issues were not able to be addressed. Instead, they can serve to point to future research considerations. they include, but not limited to:

- Considering unmodeled dynamics such as the damping term, further exploring the effects on beam dynamics and PI.
- Choosing frequency weighting functions and scalar factors effectively in H_∞ controller design.
- Minimizing the inaccurate measurement of the system parameters, including tip payload.
- Improving the IHR algorithm. If search space is expanded by introducing more parameters as variables, it will dramatically slow down the search process, causing a need for more and better priors input to start searching and to find better searching direction.
- Comparing different control strategies to ascertain their efficiency in choosing the best suitable controller for flexible manipulators.

- Introducing power consumption into the design objective, which will expand the design application to some area with power limitation, such as conditions in outer space.

- Building a real system to verify this design method.

- Developing an analog mechatronic mechanism for multi-link flexible manipulators to meet real application requirements, including the modeling and algorithm improvement.

- Extending this approach to other system designs.

APPENDIX A

MECHATRONIC DESIGN PROGRAMS

This appendix contains an alphabetical listing of all *Matlab* programs.

Codes in mechatronic design with the LQR Controller are:

1. CALB.M
2. CALC.M
3. EIPPSI.M
4. GAMMA1.M
5. GAMMA2.M
6. GAMMA3.M
7. JIHR.M
8. LAMBDA1.M
9. LAMBDA2.M
10. LAMBDA3.M
11. MAR.M
12. OMEGA31.M

13. OPTK.M

14. POTENT.M

15. PPSI.M

16. SEGDIR.M

17. SEGSELECT.M

18. SEGSTEP.M

19. XPSI.M

20. XS.M

Codes in mechatronic design with the H_∞ controller are:

1. ASSEM.M

2. ASSEMB1.M

3. ASSEMB2.M

4. ASSEMCD1.M

5. ASSEMCD2.M

6. ASSEMQ.M

7. DAMPING.M

8. HINF.M

9. W1.M

10. W2.M

REFERENCES

[1] H. Asada, J. Solotine, *Robot Analysis and Control* (John Wiley and Sons).

[2] H. Asada, J.-H. Park, and S. Rai, "A Control-Configured Flexible Arm: Integrated Structure/Control Design," *IEEE Conf. on Robotics and Automation* (Sacramento, CA, 1991), Vol. 3, pp. 2356-2362.

[3] Y. Aoustin, et al, "The singular Perturbation Control of a Two-Flexible-Lnk Robot," in *IEEE Conf. Rob. Auto.*, Atlanta, GA, pp. 737-742, 1993.

[4] S. Bailey, *A Common Lunar Lander for the Space Exploration Initiative*, (NASA Johnson Space Center, Houston, TX, 1991).

[5] G. Balas, *Robust Control of Flexible Structure; Theory abd Experiments*, (Ph.D. thesis, California Institute of Technology).

[6] J. P. Karidis, et al, "The hummingbird Minipositioner" *Proc. IEEE Conf. Robotics and Automation*, nice, France.

[7] P. R. Beesack, "Isoperimetric Inequalities for the Nonhomogeneous Clamped Rod and Plate," *Journal of Mathematics and Mechanics*, Vol. 8 (1959), pp. 471.

[8] F. Bellezze, L. Lanari, and G. Ulivi, "Exact Modeling of the Flexible Slewing Link," *Proceedings of IEEE Int. Conference on Robotics and Automation* (Cincinnati, OH, 1989), Vol. 2, pp. 734-739.

[9] W. K. Belvin and K. C. Park, "Structural Tailoring and Feedback Control Synthesis: An Interdisciplinary Approach," *Journal of Guidance and Control*, Vol. 13, No. 3 (1990), pp. 424-429.

[10] W. J. Book, "Recursive Lagrangian Dynamics of Flexible Manipulator Arms," *International Journal of Robotics Research*, Vol. 3, No. 3 (1984), pp. 87-101.

[11] W. J. Book, "Structural Flexibility of Motion Systems in the Space Environment," *IEEE Transactions on Robotics and Automation*, Vol. 9, No. 5 (1993), pp. 524–538.

[12] R. M. Brach, "On the Extremal Fundamental Frequencies of Vibrating Beams," *International Journal of Solids Structures*, Vol. 4 (1968), pp. 667-674.

[13] R. M. Brach, "On Optimal Design of Vibrating Structures", *Journal of Optimization Theory and Applications*, (1973), pp. 662-667.

[14] H. Bremer, "On the Dynamics of Flexible Manipulators," *IEEE 1987 International Conference on Robotics and Automation*, Vol. 3 (1987).

[15] R. H. Cannon, Jr. and E. Schmitz, "Precise Control of Flexible Manipulators," *Robotics Research: The First Intl. Symposium*, MIT Press, Cambridge, MA (1984), pp. 841-861.

[16] G. Cetinkunt and W. J. Book, "Symbolic Modeling of Flexible Manipulators". *IEEE 1987 International Conference on Robotics and Automation*, Vol. 2 (1987).

[17] N. G. Chalhoub, et al "Control of a Flexible Robot Arm: Experiments and Theoretical Results," *J. Dynam. Sys. Measurement Control*, 109, (1987), pp. 299-309.

[18] D. S. Chehil, R. Jategaonkar, "Determination of natural frequencies of a beam with varying section properties", *Journal of Sound and Vibration*, Vol. 115, pp. 423-436, (1987).

[19] S. B. Choi, B. S. Thompson, and M. V. Gandhi, "Modeling and Control of a Single-Link Flexible Manipulator featuring a Graphite-Epoxy Composite Arm," *IEEE 1987 International Conference on Robotics and Automation*, Vol. 2, pp. 1450-1455.

[20] S. K. Clark, *Dynamics of Continuous Elements*, (Prentice-Hall, Englewood Cliffs, N. J.).

[21] J. Doyle, K. Glover "State-Space Solution to Standard H_2 and H_∞ Control Problem", *IEEE AC*, Vol. 34, No. 8 (1989), pp. 831-847.

[22] M. H. S. Elwany, A. D. S. Barr, "Optimal Design of Beams under flexural Vibration," *Journal of Sound and Vibration*, Vol. 88 (1983), pp. 175-195.

[23] C. Foias, H. Özbay, A. Tannenbaum, *Robust Control of Infinite Dimensional System-Frequency Domain Method*, (Springer-Verlag London Limited, 1996).

[24] B. Francis, *A Course in H_∞ Control Theory*, (Springer-Verlag, Berlin-New York, 1998).

[25] M. Fujita, et al, "Experimental Evaluation of H_∞ Control for a Flexible Beam Magnetic Suspension System," S. Hosoe (ed) *Robust Control, Pro of a workshop held in Toyko*, June 23-24, 1991.

[26] S. D. Eppinger and W. Seering, "Modeling Robot Flexibility for Endpoint Force Control," *IEEE 1988 International Conference on Robotics and Automation*, Vol. 1 (1988), pp. 165-170.

[27] Frank, Paul M., *Introduction to System Sensitivity Theory* (Academic Press, NY, 1978).

[28] T. Fukuda, "Control of Flexible Robot Arm," *Bull. JSME*, 29(250), pp. 1269-1273.

[29] H. Geniele, et al, "End-Point Control of a Flexible-Link Manipulator: Theory and Experiments", *IEEE Trans. Control System Technology* , Vol. 5, No. 6, 1997.

[30] M. Ghanekar et al "Scaling Laws for Linear Controller of Flexible Link Manipulators Characterized by Nondimensional Groups', *IEEE Trans. Rob. Auto.*, Vol. 13, No. 1, 1997 .

[31] D. L. Girven and Wayne J. Book, "Numerical Analysis of Nonminimum Phase Zero for Nonuniform Link Design," in *Dynamics of Flexible Multibody Systems: Theory and Experiment*, ASME Winter Annual Meeting (Anaheim, CA, 1992), pp. 5-16.

[32] K. Glover, J. Doyle, "State-Space Formulae for All Stabilizing Controller that satisfy an H_∞-norm Bound and Relations to Risk Sensitivity," *System and Control Letter*, Vol. 11 (1988), pp. 167-172.

[33] L. B. Gutiérrez, F. L. Lewis, J. A. Lowe "Implementation of a Neural Network tracking Controller for a Single Flexible link: Comparison with PD and PID Controller," in *IEEE Trans. on Industrial Electronics*, Vol. 45, No. 2, 1998.

[34] R. T. Haftka, Z. Gurdal, and M. P. Kamat, *Elements of Structural Optimization* (Kluwer Academic Publishers, Boston, 1990).

[35] A. Hale, et al, "Optimal Simultaneous Structural and Control Design of Maneuvering Flexible Spacecraft", *J. Guidance* VOl. 8, N0. 1, 1983.

[36] G. G. Hastings, W. J. Book, "A linear dynamic model for flexible Robotic Manipulators," *IEEE Control Magazine*, pp. 61-64.

[37] P. C. Hughes, "Space Structure Vibration Mode: How Many Exit? Which Ones Are Important?", *IEEE Control System Magazine*, Vol. 7, No. 1, pp. 22-28.

[38] R. Jategaonkar, D. S. Chehil, "Natural frequencies of a beam with varying section properties", *Journal of Sound and Vibration*, Vol. 133, pp. 303-322, (1989).

[39] A. Jnifene, A. Fahim "A Computed Torque/Time Delay Approach to the End-Point Control of a One-Link Flexible Manipulator", *Dynamics and Control*, Vol. 7, pp. 177-189, (1997.

[40] R. Karel, *Variational Methods in Mathematics, Science, and Engineering*, (D. Reidel Publishing Co., Dordrecht, Holland, 1980).

[41] B. L. Karihaloo and F. I. Niordson, "Optimum Design of Vibrating Cantilevers," *Journal of Optimization Theory and Applications*, Vol. 11, No. 6 (1973), pp. 638-654.

[42] F. Khorrami and S. Jain, "Experimental Results on an Inner/Outer Loop Controller for a Two-Link Flexible Manipulator," *IEEE 1992 International Conference on Robotics and Automation*, Vol. 1, pp. 742-747.

[43] F. Khorrami and Ümit Özgöner, "Perturbation Method in Control of Flexible Link Manipulators," *IEEE 1988 International Conference on Robotics and Automation* (Philadelphia, PA, 1988), Vol. 1, pp. 310-315.

[44] L. Lanari and J. Wen, "Asymptotically Stable Set Point Control Laws for Flexible Robots," *Systems and Control Letters*, Vol. 19 (1992), pp. 119-129.

[45] P. A. A. Laura, et al, "Dynamic Stiffness of Structural Element", *shock and Vibration Digest*, Vol. 41 (1991), pp. 13-7.

[46] A. Leissa, *Vibration of Plate*, (NASA SP-160, Washington, D. C. 1969).

[47] K. Lezn, H. Özbay, et al, "Frequency Domain Analysis and Robust Control Design for an Ideal Flexible Beam," *Automatica*, Vol. 27, 1991, pp. 947-961.

[48] F. L. Lewis, V. L. Syrmos, "Optimal Control", *John Wiley and Sons, Inc., Second Edition, 1995.*

[49] B. Liang, Y. Xu, M. Bergerman, "Mapping a Space Manipulator to a Dynamically Equivalent Manipulator," *Journal of Dynamic Systems, Measurement, and Control*, Vol. 120, No. 3 (1989), pp. 1-7.

[50] Y. S. Liao, "A Generalized Methods for the Optimal Design of Beam Under Flexural Vibration," *Journal of Sound and Vibration*, Vol. 167, No. 2 (1993), pp. 193-202

[51] K. B. Lim and J. L. Junkins, "Robustness Optimization of Structural and Controller Parameters," *Journal of Guidance and Control*, Vol. 12, No. 1 (1989), pp. 89-96.

[52] J. Lin, F. L. Lewis, "Improvement Measurement / Estimation Technique For Flexible Link Robot Arm Control," *Proc. of 32nd Conf. on Decision and Control*, San Antonio, Texas, 1993, pp. 627-632.

[53] D. Luca, B. Siciliano, "Trajectory Control of A Nonlinear One-Link Flexible Arm", *Int. J. Control*, Vol. 50, No. 5 1989, pp. 1699-1715 .

[54] Z. -H. Luo, "Direct Strain Feedback Control of Flexible Robot Arms: New Theoretical and Experimental Results," *IEEE Trans. on Automatic Control*, Vol. 38, No. 11 (1993), pp. 1610-1622.

[55] K. J. Ma, M. S. We, "The Study and Application of Place-Grids Structure From Composite Materials," *The FIC on Lightweight Structure in Architecture*, Vol. 2, No. 1 (1986), Sydney, Australia.

[56] S. K. Madhavan, S. N. Singh, "Inverse Trajectory Control and Zero Dynamic Sensitivity of an Elastic Manipulator", *Int. J. Robot. Auto.* , Vol 6, No. 4, pp. 179-192, 1991 .

[57] S. K. Madhavan, S. N. Singh, "Sliding Mode End Point Trajectory Control of a Two Link Elastic Manipulator", *Proc. 31th Conf. Decision Contr.*, Tucson, AZ, 1992 pp. 305-310.

[58] D. Miller, J. shim "Gradient-Based Combined Structural and Control optimization", *J. Guidance* , Vol 10, no. 3, 1987.

[59] M. Moallem, K. Khorasani, R. Patel, "An Integral Manifold Approach for Tip-Position Tracking of Flexible Multi-Link Manipulators", *IEEE Trans On Rob. Auto.*, Vol 13, no. 6, 1997.

[60] M. Moallem, R. Patel, K. Khorasani, "Geometric Shape Design of Flexible-Link Manipulators using Multi-objective optimization", *CDC*, 1998.

[61] Z. S. Makowski, "Analysis, Design and Construction of Double-Layer Grids," *Applied Science Publishers Ltd*, London.

[62] F. I. Niordson, "On the Optimal Design of a Vibrating Beam," *Quarterly of Applied Mathematics*, Vol. 23, No. 1 (1965), pp. 47-53.

[63] P. K. Nguyen, R. Ravindran, R. Carr, D. M. Gossain, and K. H. Doetsch, "Structural Flexibility of the Shuttle Remote Manipulator System Mechanical Arm," *SPAR AeroSpace Ltd., Tech. Info. AIAA* (1982).

[64] C. M. Oakley and R. H. Cannon, Jr., "End-Point Control of a Two-Link Manipulator with a Very Flexible Forearm: Issues and Experiments," *Proc. 1989 American Control Conference* (Pittsburgh, PA, 1989), pp. 1381-1388.

[65] J.-H. Park and H. Asada, "Design and Control of Minimum-Phase Flexible Arms with Torque Transmission Mechanisms," *IEEE 1990 International Conference on Robotics and Automation*, Vol. 3 (1990), pp. 1790-1795.

[66] J.-H. Park and H. Asada, "Integrated Structure/Control Design of Two-Link Nonrigid Robot Arm for High Speed Positioning," *IEEE Conf. on Robotics and Automation* (Nice, France, 1992), pp. 2356-2362.

[67] Pars, L. A., *A Treatise on Analytical Dynamics*, (John Wiley and Sons, New York, 1965).

[68] Pestel and Leckie, *Matrix Methods in Elastomechanics*, McGraw-Hill, New York (1963).

[69] A. Pil and H. Asada, "A Computer Integrated Development System for High Speed Robot Design Incorporating Structural Reconfiguration," *IEEE Conf. on Robotics and Automation* (Atlanta, GA, 1993), pp. 677-683.

[70] E. P. Polak, "Basics of Minimax Algorithms," *Proceedings of the Summer School on Nonsmooth Optimization and Related Topics*, Erice, Italy (1988).

[71] W. Prager and J. E. Taylor, "Problems of Optimal Structural Design," *ASME Trans. Journal of Applied Mechanics* (1968), pp. 102-106.

[72] J. N. Reddy, *Energy and Variational Methods in Applied Mechanics*, (John Wiley and Sons, New York, 1984).

[73] R. Karel, *Variational Methods in Mathematics, Science, and Engineering*, (D. Reidel Publishing Co., Dordrecht, Holland, 1980).

[74] S. Rao, "Mechanical Vibrations," *Addison-Wesley Publishing Company*, 1986.

[75] E. I. Rivin, "A chatter-resistant cantilever boring bar", *Proc. of NAMRC-XI*, pp. 403-407, 1983.

[76] E. I. Rivin, Y. H. Kang, "Improving Dynamic Performance of cantilever Boring Bars", *Annals CIRP* , Vol. 38, No. 1, pp. 377-380, 1983.

[77] S. M. Roberts, J. S. Shipman, "Two-Point Boundary Value Problem: Shooting Methods," *American Elsevier*, New York 1972.

[78] P. K. Roy, N. Ganesan, "Studies on the Dynamic Behaviour of a Cantilever Beam with Varying Thickness" *Journal of Sound and Vibration*, 177(1), pp. 1-13, 1994.

[79] J. L. Russell, "Optimum Shape Design of Flexible Manipulators with Tip Loads," in *Advanced Studies in Robotic Flexible Manipulators: Modeling, Design, Control, and Application*, edited by Fei-Yue Wang, World Scientific Pub., N. J., 1995.

[80] J. L. Russell, "Optimization Model for Flexible Manipulators", *Ph. D. Dissertation*, University of Arizona, Tucson, Arizona, 1995.

[81] T. Sakawa, F. Matsuno, and S. Fukushima, "Modeling and Feedback Control of a Flexible Arm," *Journal of Robotic Systems*, Vol. 2 (1985), pp. 453-472.

[82] B. Schwarz, "On the extrema of Frequencies of Nonhomogeneous Strings with Equimeasurable Density," *Journal of Mathematics and Mechanics*, Vol. 10 (1961), pp. 401.

[83] B. Schwarz, "Some Results on the Frequencies of Nonhomogeneous Rods," *Journal of Mathematical Analysis and Applications*, Vol. 5 (1962), pp. 169.

[84] C. Y. Sheu, "Elastic Minimum-Weight Design for Specified Fundamental Frequency," *International Journal of Solids Structures*, Vol. 4 (1968), pp. 953-958.

[85] B. Siciliano and W. J. Book, "A Singular Perturbation Approach to Control of Lightweight Flexible Manipulators," *International Journal of Robotics Research*, Vol. 7, No. 4 (1988), pp. 79-90.

[86] B. Siciliano, J. V. R. Prasad, and A. J. Calise, "Output Feedback Two-Time Scale Control of Multilink Flexible Arms," *ASME Journal of Dynamic Systems, Measurement, and Control*, Vol. 114 (1992), pp. 70–77.

[87] A. Sideris, H. Rotstein, "Singel-Input Single-Output H_∞ Control with Time Domain Constrains," *Automatica*, Vol. 29, No. 4.

[88] N. Sundararajan, et al, "Experiments using lattice filters to identify the dynamics of a Flexible Beam," *J. Dyna. Sys. Measurement Control*, 107, pp. 187-191.

[89] J. Swevers, et al "Fast and Accurate Tracking Control of a Flexible One-Link Robot BAsed on Real-Time link Deflection Measurements," *Mechatronics*, Vol. 2, No. 1 (1992), pp. 29-41.

[90] H. Takeyama, et al, "Improvement of dynamic rigidity of tool holder by applying high-damping material," *Annals CIRP*, Vol. 39, No. 1, pp. 249-252, 1984.

[91] A. Tchernychev, A. Sideris, J. Yu, "Constrained H_∞ Control of an Experimental Flexible Link", *Trans. o fthe ASME*, VOl. 199 June, 1997.

[92] S. Timoshenko and G. H. MacCullough, *Elements of Strength of Materials, third edition* (D. Van Nostrand Company, Inc., New York, 1949).

[93] S. Timoshenko, D. H. Young, and W. Weaver, Jr., *Vibration Problems in Engineering, third edition*, (D. Van Nostrand Company, Inc., New York, 1957).

[94] P. Tang, S. Lu "A Video Signal Processing Technique for Vibration Measurement of a Flexible Beam," *The International journal of robotics Research*, Vol. 11, No. 6 (1992), pp. 1610-1622.

[95] A. Tchernychev, A. Sideris, J. Yu, "Constrained H_∞ Control of an Experimental Flexible Link," *J. of ASME*, Vol. 119, No. 6 (1997), pp. 206-211.

[96] W. J. Wang, et al "Experiments on Position Control of a One-Link Flexible Robot Arm," *IEEE int. J. Robot. Auto.*, Vol. 5, No. 3 (1989), pp. 373-377.

[97] Fei-Yue Wang, "Optimum Design of Vibrating Cantilevers: A Classical Problem Revisited," *J. of Optimization Theory and Applications*, Vol. 84, No. 3 (1995).

[98] Fei-Yue Wang, "On the Extremal Fundamental Frequencies of One-Link Flexible Manipulators," *International Journal of Robotics Research*, Vol. 13, No. 2 (1994), pp. 162-170.

[99] Fei-Yue Wang and G. G. Guan, "Influence of Rotatory Inertia, Shear Deformation and Loading on Vibration Behaviors of Flexible Manipulators," *Journal of Sound and Vibrations*, Vol. 171, No. 4 (1994), pp. 433-452.

[100] Fei-Yue Wang and J. L. Russell, "Optimum Shape Construction of Flexible Manipulators with Tip Loads," *Proceedings of IEEE Intl. Conf. on Decision and Control* (Tucson, Arizona, 1992), Vol. 1, pp. 311-316.

[101] Fei-Yue Wang, "Optimum Design of Flexible Manipulators: Integration of Control and Construction," Dept. of Systems and Industrial Engineering, University of Arizona, SIE working paper #02-92 (1992).

[102] Fei-Yue Wang and J. L. Russell, "Minimum-Weight Robot Arm for a Specified Fundamental Frequency," *Proceedings of the IEEE Conference on Robotics and Automation*, (Atlanta, Georgia, 1993), Vol. 1, pp. 490-495.

[103] Fei-Yue Wang and J. L. Russell, "Optimum Shape Construction of Flexible Manipulators with Total Weight Constraint," *IEEE Transactions on Systems, Man, and Cybernetics*, Vol. 25, No. 3 (1995).

[104] Fei-Yue Wang and J. L. Russell, "A New Approach to Optimum Flexible Link Design," *Proceedings of IEEE Int. Conf. on Robotics and Automation* (Nagoya, Japan, 1995).

[105] Fei-Yue Wang, P. X. Zhou, Paul Lever, "Dynamic Effects of Rotatory Inertia and Shear Deformation on Flexible Manipulators", *Proc. of IEEE International Conf. on Systems, Man, and Cybernetics*, Beijing, China, Oct. 1996.

[106] Fei-Yue Wang and J. T. Wen, "Nonlinear Dynamical Model and Control for a Flexible Beam," CIRSSE Report #75, Rensselaer Polytechnic Inst., (Troy, New York, 1990).

[107] Fei-Yue Wang, "Optimum Design of Flexible Robot Arms: A Mechatronic Approach," *Proc. of the First Chinese World Congress on Intelligent Control and Intelligent Automation* (Beijing, China, 1993), pp. 1160-1165.

[108] Fei-Yue Wang, "Finding the Maximum Bandwidth of a Flexible Arm," *Proc. of 32nd IEEE Conf. on Decision and Control*, (San Antonio, TX, 1993), Vol. 1, pp. 619-625.

[109] Fei-Yue Wang, "Optimization Formulations for Mechatronic Design of Flexible Robotic Manipulators," RAL Technical Report #45, SIE Dept, University of Arizona, Tucson, Arizona (1994).

[110] Fei-Yue Wang, Pixuan Zhou, "Optimization Formulations for Closed-Loop Design of Flexible Robotic Links" *Proc. of International Conf. on Intelligent Manufacturing*, Wuhan, China, June 1995.

[111] D. Wang and M. Vidyasagar, "Modeling a class of Multilink Manipulators with the Last Link Flexible," *IEEE Transactions on Robotics and Automation*, Vol. 8, No. 1 (1992), pp. 33-41.

[112] E. J. Wiest and E. Polak, "On the Rate of Convergence of Two Minimax Algorithms," *Journal of Optimization Theory and Applications*, Vol. 71, No. 1 (1991), pp. 1-30.

[113] G. B. Yang and M. Donath, "Dynamic Model of a One-Link Manipulator with Both Structural and Joint Flexibility," *IEEE 1988 International Conference on Robotics and Automation*, Vol. 6, No. 3 (1988), pp. 476-481.

[114] Z. B. Zabinsky, R. L. Smith, J. F. McDonald, H. Edwin, "Improving Hit-and-Run for Global Optimization", *Journal of Global Optimization*, Vol. 3, pp. 171-192, 1993.

[115] G. Zames, "Feedback and Optimal Sensitivity: Model Reference Transformations, Multiplicative Seminorms, and Approximate Inverses", *IEEE Trans. Automat. Contr.*, Vol. 26, pp. 301-320, 1981.

[116] P. Zhou, M. Willians, F. Y. Wang, "On the closed-loop Design Of Flexible Robotic links," in *IEEE Conf. on Systems, Man, and Cybernetics*, 1996.

[117] P. Zhou, F. Y. Wang, . Lever, "Mechatronic-Based Integrated Construction and Control of Flexible Manipulators", *IFAC 1999 World Congress, Beijing, China.*

[118] G. Zhu, T. Lee, S. Ge "tip Tracking Control of a Sngle-link Flexible robot: A Backstepping Approach," in *Dynamics and Control*, 7, 341-360, 1997

[119] K. Zuo and D. Wang, "Closed-loop Shaped Input Control of a Class of Manipulators with a Single Flexible Link," *IEEE International Conference on Robotics and Automation*, (Nice, France), Vol. 6, No. 3, pp. 476-481.

[120] W. L. Winston, *Introduction to Mathematical Programming*, (PWS-Kent Publishing Co., Boston, 1991).

IMAGE EVALUATION
TEST TARGET (QA-3)

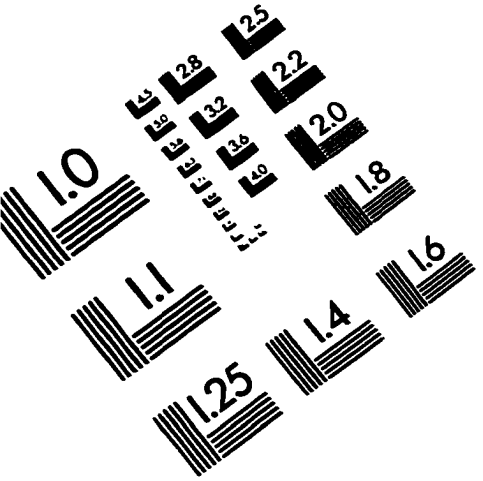

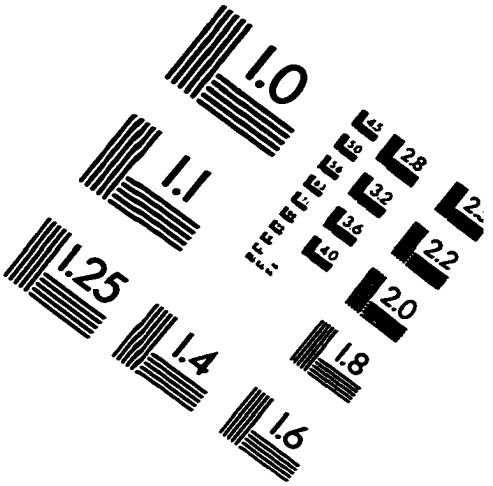

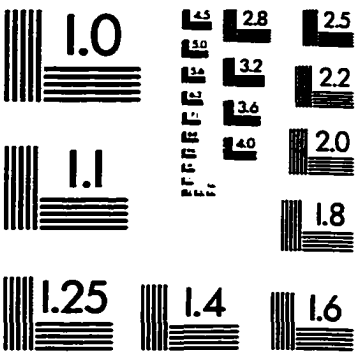

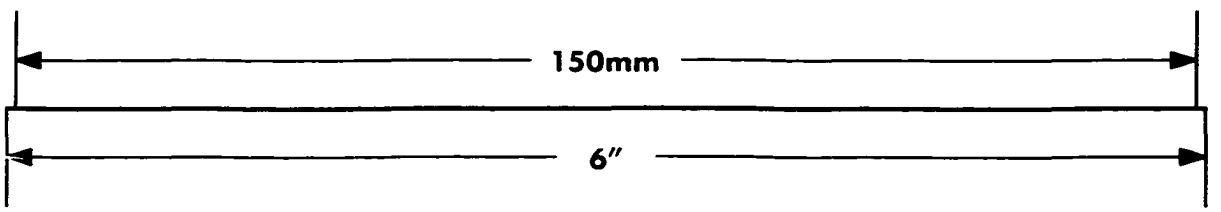

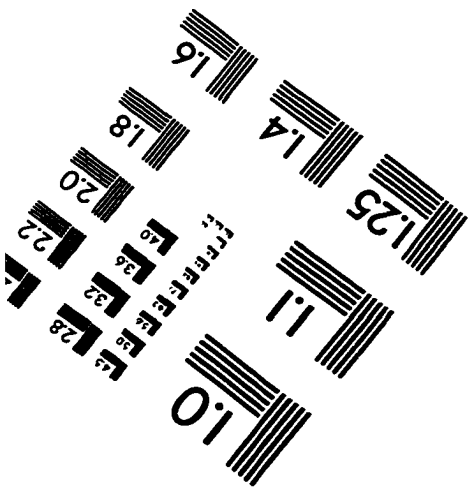

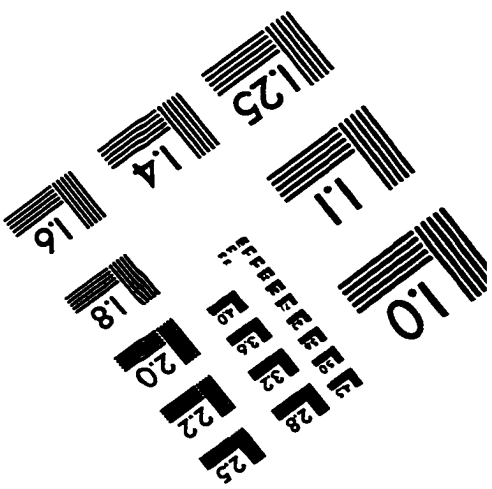

APPLIED IMAGE, Inc
1653 East Main Street
Rochester, NY 14609 USA
Phone: 716/482-0300
Fax: 716/288-5989